1953-08

Some measurements of gamma ray scattering

Bennett, Bradley Frederick.

Cambridge, Massachusetts; Massachusetts Institute of Technology

SOME MEASUREMENTS OF GAMMA RAY SCATTERING

BRADLEY FREDERICK BENNETT

SOME MEASUREMENTS OF GAMMA RAY SCATTERING

by

BRADLEY FREDERICK BENNETT
Commander, U. S. Navy

B. S., U. S. Naval Academy
(1935)

S. M. in Naval Construction,
Mass. Institute of Technology
(1940)

SUBMITTED IN PARTIAL FULFILLMENT OF THE

REQUIREMENTS FOR THE DEGREE OF

MASTER OF SCIENCE IN PHYSICS

at the

MASSACHUSETTS INSTITUTE OF TECHNOLOGY
(1953)

ABSTRACT

Title: "Some Measurements of Gamma Ray Scattering"

Author: Bradley Frederick Bennett, Commander, U. S. Navy
B. S., U. S. Naval Academy (1935)
S. M. in Naval Construction, Mass. Institute of Technology (1940)

Submitted to the Department of Physics on August 24, 1953 in partial fulfillment of the requirements for the degree of Master of Science in Physics.

This paper reports an investigation of the distribution of the energy, E, of the secondary electrons released in an organic scintillator by secondary gamma radiation measured on the same side of a scattering medium as that on which the source is located. The investigation was conducted by scintillation spectrometry using stilbene on an RCA 6199 photomultiplier, and employing the technique of Dr. G.J. Hine. The amplified detector output is analyzed by a differential discriminator of constant window width whose base line is continuously varied mechanically so as to scan the energy spectrum. The output is recorded by a counting rate meter and recording milliammeter.

Effectively semi-infinite scatterers of wood, aluminum, iron, tin, and lead were used. The surface of the scatterer was always horizontal with its centerline always parallel to the source-detector line. The source-detector distance was kept at 40 cm while their distance, y, above the scatterer surface was varied from 0.5 cm to 90 cm. Essentially all of the secondary gammas originated in the scatterers because collimation was avoided. The primary beam was not excluded from the detector; the energy spectrum of the primary obtained with no scatterer was subtracted from that obtained with the scatterer in place. The difference was plotted. These data were presented in various ways to show the counting rate as

a function of the other three prime variables, E, y, and Z (atomic number of the scatterer).

Auxiliary experiments were run in the same manner measuring effects of reducing the surface area of a scatterer, changing the primary gamma-ray energy from the mean of 1.25 Mev from Co^{60} to 0.663 Mev from Cs^{137}, and changing the thickness of one of the scatterers.

A qualitative discussion is presented for each part of the investigation, explaining as far as possible the significant features of the data such as maxima and variations in intensity observed, and attempting to correlate them with the prime variables. A relation to the density of the scatterers is also inferred.

By consideration of the angular distribution shown in Compton-Rayleigh scattering, and by taking into account the absorption of the scattered gammas by photoelectric effect in high Z materials, satisfactory explanations are found for most of the observed phenomena on the basis of existing knowledge. A few features, however, require further observations for verification and clarification.

Thesis Supervisor: Robley D. Evans

Title: Professor of Physics

ACKNOWLEDGMENTS

The author is especially grateful to Professor Robley D. Evans for his assistance, understanding, and guidance inside and outside the laboratory which made possible the undertaking and completion of this thesis, and to Dr. Gerald J. Hine for suggesting the problem and for continued instruction and guidance throughout both the experimental and the writing phases.

He is also very grateful to so many of the members of the Radioactivity Center who have contributed their time and their knowledge, especially to Miss Virginia K. White for suggestions on the taking and handling of data and the month she spent in averaging raw data without which help the completion date could not have been met.

The support of the Laboratory for Nuclear Science was an important aid throughout the problem, esepcially that of Mrs. Charles Rowe, Jr. who did such a fast and neat job of tracing the curves used to present the data.

The Supply Department of the U. S. Naval Shipyard, Boston, especially the Material Control Office, Cdr. Clark, was particularly cooperative in expediting and facilitating the loan of the 940 pounds of tin used for one scatterer.

Profound and enduring thanks are due to Miss Mary-Margaret Shanahan for getting the typing done in spite of the way the author missed his dates.

TABLE OF CONTENTS

TABLE OF CONTENTS

LIST OF FIGURES

I. INTRODUCTION

A. The interaction with matter of gamma rays and hard x-rays is inclined to be rather complicated. It is also involved in important ways with applications of x-rays and nuclear processes, both natural and artificial. Probably the greatest practical importance is due to their effect on biological tissue, apparently always harmful to any directly affected cell but not always harmful to the organism as a whole, of which the cell is a part.[B5, L2, N1]

The resulting interest in such interaction has been very fruitful, particularly in determining the mechanisms and coefficients for absorption, primarily narrow beam absorption.[D1, D2, F1, H12, W2] In broad beam attenuation experiments the loss in a given direction by scattering of some primaries away from this direction is partly compensated for by the scattering of other primaries into the given direction. The ratio of primary plus secondary to primary is known as the "build-up factor". This also has recently come in for considerable attention.[D4, H10, F8, P4, S4, V2, V4] Complications arise here because the scattered radiation has different energies than the primary and hence different attenuation coefficients.

These difficulties are aggravated in the area of investigation which has received a little less attention, namely the components of scattered radiation emerging from a scatterer in a direction other than that at which the primary enters it. This back-scattered or side-scattered radiation can be an important factor when making measurements near the ground, shielding, or other heavy structure. It can result in increased exposure to patients undergoing extensive radiography or therapy or to personnel working with or near x-ray equipment, accelerators, reactors, or radioactive materials. The exposure problem is normally aggravated by the greater susceptibility of biological tissue to damage by the lower energy scattered radiation. Thus the energy spectrum of the scattered radiation becomes of considerable interest.

As will be shown in Section II, the calculation of this spectrum is exceedingly difficult. In fact, U. Fano[F11] says in part, "The presence of ground near a source-detector system complicates the problem greatly and puts it, in the main, beyond the reach of present-day theory". And approximations which are suitable for many problems involving ground or concrete, are more restricted when the scatterer is of considerably higher atomic number, e.g., steel (Z_{Fe} = 26).

The energy spectrum of back-scattered radiation from an uncollimated source has been investigated by G. Hine.[H13] That of radiation scattered at various angles from a collimated source has been reported by E. Hayward and J. H. Hubbell.[H12] And experiments have been reported which gave the total scattered radiation but not its spectrum.[V2, W3]

B. It is the purpose of this thesis to measure the energies of the secondary electrons created in a detector practically equivalent to soft biological tissue by the secondary gamma radiation resulting from the proximity of various scatterers to the source-detector system. Other scattering agents were reduced as far as practicable and kept essentially constant. For simplification the source-detector distance (r) was kept constant and the line between them was kept parallel to the long edge of the scatterer with its center vertically above the center of the horizontal scatterer. The atomic number of the scatterer was varied, and for each scatterer the vertical distance (y) of the source and detector was varied. For each geometry the energy spectrum with Co^{60} source (1.25 Mev average) was taken using as small a stilbene crystal as practicable mounted on an RCA 6199 photomultiplier tube. The photomultiplier output was amplified and its spectrum analyzed

by a differential discriminator with power-driven scanner. The discriminator output was recorded by a counting rate meter and an Esterline-Angus recorder. Runs were repeated and these were averaged. From each of these averaged spectra there was subtracted the average spectrum obtained with no scatterer in place. The energy scale was calibrated with internal conversion electrons of Cs^{137}. An effort has been made to analyze qualitatively these energy spectra of the build-up as a function of the atomic number of the scatterer and the distance of source and detector above the scatterer. Some data have also been similarly obtained and treated using a Cs^{137} source (663 Kev) to examine the effect of changing the energy of the primaries.

II. THEORETICAL ANALYSIS OF THE PROBLEM: INTERACTION OF RADIATION WITH MATTER[D2, E1, F2, F8, H1]

A. GENERAL.

Gamma rays, and of course x-rays, interact in one or more of several ways with the matter they pass through. Fano[F1] discusses the various modes of interaction particularly effectively by dividing them into absorption (A), coherent scattering (B), and incoherent scattering (C), any of which may occur with atomic electrons (I), nucleons(II), or the electric field surrounding charged particles, either nuclei or orbital electrons (III). Interactions with meson fields (also discussed by Fano) occur only at photon energies considerably greater than those with which this investigation is concerned. Of the nine remaining processes, photo-absorption in the nucleus (IIA), nuclear elastic scattering (IIB) and Delbruck scattering (IIIB) are also insignificant, and (IIC) and (IIIC) are unobserved.

B. PHOTOELECTRIC EFFECT (IA)[D2, E1, H1]

In the photoelectric effect (IA) all the energy of the photon is absorbed. A free electron cannot do this because momentum would not be conserved; an almost free (outer) electron does not do it for the same reason. Most of the photoelectric absorption is by the most tightly bound electrons, i.e., in the K shell. Because of the binding

energy the atom as a whole is able to participate and we have 100% absorption. The electron is emitted with the full energy of the photon less its binding energy in accordance with the Einstein equation

$$T = h\nu - I \qquad \text{(II-1)}$$

This process is most probable when $h\nu$ is slightly greater than the energy of the K-absorption edge. The empirical value which is quoted herein is[H11]

$$\frac{\tau}{\rho} = K_1 N \frac{Z^{4.1}}{A} f_1(h\nu) \qquad \text{(II-2)}$$

where K_1 is a constant signifying proportionality, N is Avogadro's number, Z is the atomic number, A is the atomic weight, and $f_1(h\nu)$ is a function of the photon energy. For a detailed discussion which breaks the problem up into several ranges of energy defining K_1 and $f_1(h\nu)$ for each, see particularly Davisson and Evans[D2], Heitler[H1](second edition - not the first edition which contains errors), and the references quoted by these authors.[H2, H3, H4, H5, S1,S2,S3]

C. THOMSON SCATTERING[C4]

Classical, or Thomson, scattering is usually discussed on the basis of the effect of an electromagnetic field on an electron; the oscillations of the electron in this field cause the emission of radiation of the same frequency and phase as the incoming radiation. The same frequency means

the same energy, i.e., no energy is transferred. Because the phase is the same, this type of scattering is known also as coherent scattering. The Thomson scattering coefficient, calculated by classical electrodynamics is 0.666×10^{-24} cm^2. For $1 < Z < 17$, $Z/A = 0.5$; for $Z \geq 17$, $0.4 \leq Z/A < 0.5$. For $Z/A = 0.5$, the mass scattering coefficient for Thomson scattering ≈ 0.2. Angular dependence of intensity is as $1 + \cos^2 \theta$ i.e., maximum variation is 2 to 1 and preferential directions are 0° and 180°. For high Z materials constructive interference effects modify this; for high energies ionization takes place and the process is no longer coherent. Thomson scattering itself is of no importance in this investigation but a discussion of it is included as an appropriate preliminary to discussion of Rayleigh and Compton scattering.

D. RAYLEIGH SCATTERING (IB)[F1, H1, R3]

Rayleigh scattering will be discussed first from a classical analogy and the particulate point of view. If a relatively high energy photon strikes an orbital electron squarely it will eject it, but if it strikes it a glancing blow so that the momentum transfer results in less kinetic energy for the electron than its binding energy, we get a completely elastic collision of type IB, called by Fano[F1] "Rayleigh scattering". The momentum transferred to the electron is taken up by the entire atom. The higher the

atomic number of the atom the more momentum can be transferred without ejecting the electron and hence the greater the possible angle of scattering of the photon. Conversely, the greater the energy of the photon, the less the angle for a given Z. See Table 4.3 for a few representative values.

Within the restriction of momentum transfer, Rayleigh scattering behaves like Thomson scattering, being coherent. At high Z there is constructive interference. The effect is strong at low energies and high Z. In this investigation with relatively high energy it is of importance only at high Z and very small angles.

E. COMPTON SCATTERING (IC)[D2, E1, F8, H1, H11, K4, R3]

With photons of the energy encountered in gamma rays, interaction with a free electron is not elastic and a valence electron in an atom has so much less binding energy than the gamma ray that for any but the most oblique collisions the electron is essentially free. This may be spoken of as the relativistic range below $2m_oc^2$; relativistic because the conservation of momentum in the interaction involves the relativistic mass of the photon, and below $2m_oc^2$ because above this, although the Compton effect still exists, there is competition from pair production which soon exceeds it in importance.

Compton's equations are obtained by applying conservation of energy and conservation of momentum in two orthogonal

directions in the plane determined by the paths of the scattered photon and the secondary electron. This yields

$$h\nu' = \frac{h\nu}{1 + \frac{h\nu}{m_0c^2}(1 - \cos\theta)} \qquad \text{(II-3)}$$

and

$$E_e = h\nu\left(1 - \frac{1}{1 + \frac{h\nu}{m_0c^2}(1 - \cos\theta)}\right) = \frac{(h\nu)^2(1 - \cos\theta)}{m_0c^2 + h\nu(1 - \cos\theta)} \qquad \text{(II-4)}$$

where $h\nu$ is the energy of the incident photon and $h\nu'$ that of the photon scattered at θ. Equation II-3 gives the energy of scattered photons as a function of scattering angle; to get the distribution of the intensity of scattering it is necessary to treat the problem quantum-mechanically, as done by Klein and Nishina[H1, K4] who get as the differential cross section per electron per unit solid angle

$$\frac{d({}_e\sigma)}{d\Omega} = \frac{r_0^{\,2}}{2}\left(\frac{\nu'}{\nu}\right)^2\left(\frac{\nu}{\nu'} + \frac{\nu'}{\nu} - \sin^2\theta\right) \qquad \text{(II-5)}$$

where r_0 is the classical radius of the electron ($r_0^{\,2} = 7.94 \times 10^{-26}$ cm^2) and $d\Omega$ is the differential solid angle $= 2\pi \sin\theta \, d\theta$. Results in the form of tables and curves are available, particularly due to Davisson and Evans[D2] and White[W2]. Qualitatively these results indicate preferential forward scattering, particularly at higher energies. Consideration of the Compton formula (II-3) and the behaviour

of cos θ at large angles will point out that there is surprisingly little variation in energy over very considerable changes in angle. Thus there is a relatively nearly monoenergetic component of scattered radiation in this range which is of particular importance both in back-scattering experiments and in scintillation spectrometry, particularly with organic scintillators. For gamma-ray energies encountered in radio-active isotopes, the Klein-Nishina relation does not indicate such extreme small-angle preference that a great many photons are not scattered between 135° and 180°. Approximately this range gives a sufficiently constant energy to give a back-scattering peak and to give in a scintillator a secondary electron energy peak commonly referred to as the Compton peak. This is of great assistance in analyzing data, especially when using an organic scintillator which has no photoelectric peak for such energies.

F. PAIR PRODUCTION (IIIA)

When the photon energy exceeds $2m_0c^2 = 1.02$ Mev in the center of mass system, it can interact with the atomic nucleus and create a positron-negatron pair which carry away the excess energy over 1.02 Mev. This process has a low cross section until hv appreciably exceeds 1.02 Mev and hence it is of no importance in this investigation.

G. FLUORESCENCE.

When, due to the photoelectric effect (IA) an atom is ionized in an inner shell (usually the K shell), the electrons dropping in to fill the vacancy emit the characteristic x-rays of the element. K x-rays usually predominate at higher Z. Fano[F1] gives for tin a fluorescent yield in the K series of 0.85, and for lead 0.95. Except in elements of high Z these x-rays are rather soft to be measured in gamma-ray experiments but for lead they are 75 Kev and must be reckoned with; for tin they are ~25 Kev and of minor importance in this investigation.

H. BREMSSTRAHLUNG.

Secondary electrons travel at relativistic velocities and are decelerated as they pass through matter. They radiate the continuous x-ray spectrum of their energy which has a maximum equal to their entire kinetic energy. For thick enough matter to stop them, I, the average energy radiated per electron is[E1]

$$I = (7 \pm 3)ZE^2 \times 10^{-4} \text{ Mev} \qquad \text{(II-6)}$$

where E is the electron energy in Mev. Evans[E1] has provided a curve for the relationship between the radiation loss and the ionization loss for electrons of various energies. For a 1 Mev secondary electron in lead the radiation loss is approximately 15 percent of the ionization loss, and the mean energy will be about 100 Kev.

III. EXPERIMENTAL EQUIPMENT AND PROCEDURE

A. EQUIPMENT.

The original intention was to use the equipment assembled by Prestwich and Colvin[P3] for familiarization with the technique of gamma-ray scintillation spectroscopy, and on receipt of the RCA 6199 photomultipliers then on order, substitute one of them for the RCA 5819 and proceed with the experiment. While the electronic components were being reassembled, a framework to support source, detector, and scatterer was designed. This framework, called a "scattering table" for want of a better term, was constructed by the Physics Department Machine Shop. It consists of a 3' × 8' sheet of 3/4" plywood stiffened on the under side with steel angles and channels. Two sockets on the center-line, spaced 4' apart and equally spaced from the ends of the table, each take a 4' aluminum tube, 7/8" O.D. with 1/16" wall thickness. These tubes were guyed with 0.054" steel music wire tightened by turnbuckles as can be seen in Fig. 1. By the time the scattering experiments were actually started, work by Dr. G.J. Hine on backscattering[H13] pointed out the advisability of using a scattering area several times as large as originally intended. This forced considerable modification of technique so that in many ways the scattering table was not used as planned but it proved adaptable and

served the purpose well. The final arrangements provided for (1) a stationary scatterer resting on the table top; (2) an extremely compact photomultiplier assembly, constructed at the Naval Research Laboratory, supported by an aluminum ring adjustable in height by a clamp on one of the aluminum tubes; and (3) a wire "padeye" secured to the horizontal longitudinal guy wire and another below it taped or otherwise secured to the scatterer through both of which passed a nylon thread on which was mounted the point source.

The original electronic equipment consisted of a positive regulated high voltage supply, a selected RCA 5819 photomultiplier with conventional circuitry, a Model 100 preamplifier, an Atomic Instrument Co. Model 204-B linear amplifier, a Model 210 single channel differential discriminator with a motor-driven potentiometer unit which we call a "scanner", a Model Huber 2 counting rate meter, and an Esterline-Angus recorder. Suitable energy spectra were obtained with Co^{60} gammas using an anthracene crystal 10 cm thick and 20 cm square, mounted with mineral oil on a short lucite light pipe. The light pipe was necessary to adapt the plane surface of the crystal to the curved end window of the 5819.

Energy calibration was successfully made with Cs^{137} internal conversion electrons, but discriminator window width calibration and stability gave difficulty. Spurious sharp changes appeared in spectra, which were eventually identified positively as being due to change of discriminator window width with change in temperature. Opening the door of the laboratory on a summer's night gave changes of the order of magnitude of 20 percent; blowing a fan on the discriminator closed its window altogether. After several months of trying to eliminate this difficulty it was decided to replace the equipment with one of more modern design. The Atomic Instrument Co. Model 510 pulse height analyzer, a single channel differential discriminator with expander amplifier gain of 10, was decided upon and procured. The design of this instrument is due to Higinbotham and Chase.[V3] Fed from the 204-B linear amplifier operating on 0.8 μsec rise time, it has given excellent service. Variations of window width, or channel width, have been certainly less than 0.1 volt out of 2 volts during a week of steady full-time operation, probably considerably less. Base line control on this instrument is obtained with a 10 turn helipot; this necessitated the provision of a new scanner which was constructed for the purpose by A. Maselli of the Radioactivity Center. In this

scanner, a 10 turn helipot is driven by a 1 rpm motor with gear ratio chosen so as to run the complete spectrum from 0 volts to 100 volts in approximately 2 1/2 hours. This time was chosen from previous experiments which indicated that this was a good compromise between accuracy of data and the need for collecting the data in a reasonable time with a source of strength compatible with other work and with personnel safety in the laboratory. Automatic cutoff of the scanner was provided by inserting a pin in the front of the helipot dial which operated a microswitch at the end of the run. Cutoff was usually set in excess of 98 volts, and when set remained constant within 0.1 volt for several months. A clutch operable from the front of the panel was provided. Spring pressure normally kept this clutch engaged but a pivoted spacer was provided to hold it disengaged when so desired. This clutch was not sufficiently positive; it wore so that it disengaged for half a revolution at a time during some runs, spoiling them. Marking (manually) of the discriminator base line at beginning and end of every run, and usually at several points in between, spotted all the defective runs and gave the necessary clue as to the cause. As soon as such a jump was actually witnessed, the clutch was reworked by squaring up the slotted end of the pin, which served as the female, and replacing the round pin, seconds, - 10 turn helipot is driven by a 1 rpm motor with gear ratio chosen so as to run the complete spectrum from 0 volts to 100 volts in approximately 1 1/2 hours. This time was chosen from previous experiments which indicated that this was a good compromise between accuracy of data and the need for collecting the data in a reasonable time with a source of strength compatible with other work and with personnel safety in the laboratory. Automatic cutoff of the scanner was provided by inserting a pin in the track of the helipot dial which operated a microswitch at the end of the run. Cutoff was usually set in excess of 68 volts, and once set remained constant within 0.1 volt for several months. A clutch operable from the front of the panel was provided. Spring pressure normally kept this clutch engaged but a pivoted keeper was provided to hold it disengaged when so desired. This clutch was not sufficiently positive; it wore so that it disengaged for half a revolution at a time during some runs, spoiling them. Marking (manually) of the discriminator bias line at beginning and end of every run, and usually at several points in between, spotted all the defective runs and gave the necessary clue as to the cause. As soon as such a jump was actually observed, the clutch was reworked by squaring up the slotted end of the pin, which served as the female, and replacing the round pin, which had acted as the male, with a flattened one. No further difficulties with the scanner were encountered.

On receipt of the RCA 6199 photomultiplier, rough tests of possible circuits were made with the anthracene scintillator. The circuit selected was that due to Hoover[H14] as modified by Faust[F12]; this involved elimination of the preamplifier and converting the high voltage power supply to negative. Tests of tubes and crystals were conducted using NaI(Tl) scintillators. This work and the circuit are discussed in Appendix A, but it may be stated here that excellent resolution was obtained, better than that of the best 5819's.

Evidence presented by Faust's group at NRL[F12] led to consideration of shifting from anthracene to stilbene because of the apparent greater availability of good crystals of the latter. On the basis of the relative quality of crystals which they and other workers had obtained from various sources, it was decided to try stilbene crystals from Larco Nuclear Instrument Co. These were quite satisfactory and an assortment of four sizes in all was obtained, all cylindrical. The sizes were as follows: 2 1/2 cm diam., 2 1/2 cm long; 2 1/2 cm diam., 1/3 cm long; 1 cm diam., 1 cm long; 1 cm diam., 1/3 cm long. The second of these gave the best resolution and would have permitted the closest measurements to the surface of the scatterer, but its assymetrical geometry

was considered likely to introduce excessive angular discrimination. The 1 cm diam., 1/3 cm long crystal would have required sources of strength not compatible with other work in the Radioactivity Center. The 1 cm diam., 1 cm long stilbene crystal was chosen as the smallest suitable organic scintillator at hand,[89] and all the scattering experiments were conducted with it mounted with Dow Corning 200 fluid at 6 × 10^5 centistokes viscosity on the best available RCA 6199 (designated 61-B).

After numerous experiments with reflectors, principally Al foil and MgO, 0.00025" aluminum foil, cemented by a minimum quantity of Dow Corning 200 fluid of 2 × 10^5 centistokes viscosity, was used with its bright side to the crystal. The scintillator covered such a small portion of the photocathode that an additional reflector of 0.0007" Al foil covering both the crystal and the end of the 6199 was also used; this was placed outside the source when making energy calibrations with the internal conversion electrons of Cs^{137}. For a light shield, a black rubber glove was found to be adequate and convenient to use. It had the particular advantage of facilitating measurements of crystal position. The total absorbers around the crystal were approximately: (a) when measuring gammas and fluorescence, 0.024" black rubber, 0-0.014" black electrical tape, 0.001" aluminum, and air; (b) when calibrating with

internal conversion electrons, 0.00025" aluminum and 0.04" air. With the flat end of the 6199 a light pipe was no longer needed. After considering the arguments of other workers some of whom claim a lightpipe gives improved light collection while others claim it reduces resolution, and my own measurements which, while not exhaustive, indicated little effect for light pipes up to 3", I decided to work without one (just eliminating one or two more possible sources of error or other trouble).

As indicated in Appendix A the 6199 showed considerable sensitivity to angular orientation. The small change in resolution was not particularly significant to the scattering experiments, but the 14 percent change in gain was critical. Although this was apparently eliminated by the use of a 0.062" μ-metal shield and nearly so by a 0.020" μ-metal shield, it was decided not to use them. The former did not fit properly and was furthermore considered an undesirable source of scattering so close to the crystal. The latter caused noise if in electrical contact with the aluminum reflector; this noise filled the entire spectrum if contact was also made with the grounded aluminum socket mounting. Consequently the tube was operated in only one orientation for all the scattering experiments, and it is considered that any variations in the cause of the observed effects would be corrected

for in normalizing the curves. Because of the effect of the μ-metal shield, and because the critical orientations for all tubes tested were the same or 180° apart, it has been presumed that the cause was the terrestrial magnetic field, known to cause somewhat similar effects with the 5819.[M3]

The high voltage supply used for the photomultiplier was so unstable as to greatly hamper the work. Its difficulty has been blamed on the low and extremely variable line voltage, but was not eliminated by placing it on a Sola constant voltage transformer. It is inherently less stable than appropriate for this use but has performed well below the standard to be expected of its design. The error is not known as precisely as desired because the meter is entirely too coarse for the purpose, but by adopting Prof. R. D. Evans' suggestion of cementing a mirror to the glass and aligning the image of the eye pupil in the mirror with the pointer tip, readings can probably be obtained within ±2 volts, and relative readings within ±1 volt. Relative deviations of 5 volts in a few hours and 10 volts in about two days were encountered. Inasmuch as a 1 volt change produces a 1 percent change in gain at the normal operating level of a 6199 (1080 volts in this case), one of the new power supplies designed for the purpose would be recommended. The above

difficulties did not harm the data used but resulted in throwing out many runs.

There was also another gain change, the cause of which was never determined. That it was due to some other cause than the high voltage was evident in that the effect was sometimes concurrent with a change in high voltage, but with the net effect in the opposite direction. The worst net change observed during a 2 1/2 hour run was 1.5 percent. It could have been caused only in the photomultiplier (as by a change of magnetic field), the linear amplifier, the expander amplifier of the discriminator, or the baseline of the discriminator. Time did not permit concentrating on the cause and its correction; it was quicker to normalize all runs before starting by adjusting the gain of the linear amplifier to compensate, and checking at the end to see that it had not shifted appreciably during the run. Normalization was accomplished by a steady run at 71 volts (corresponding to 1 Mev - on the high energy side of the "Compton peak"). The counting rate of this energy should be independent of the scatterer unless Rayleigh scattering becomes appreciable; each run was therefore normalized to give a counting rate of 600 cpm at this energy. The maximum Compton scattered intensity which could yield, in the stilbene, secondary difficulties did not harm the data used but resulted in throwing out many runs.

There was also another gain change, the cause of which was never determined. That it was due to some other cause than the high voltage was evident in that the effect was sometimes concurrent with a change in high voltage, but with the net effect in the opposite direction. The worst net change observed during a 2 1/2 hour run was 1.5 percent. It could have been caused only in the photomultiplier (as by a change of magnetic field), the linear amplifier, the expander amplifier of the discriminator, or the baseline of the discriminator. Time did not permit concentrating on the cause and its correction; it was easier to normalize all runs before starting by adjusting the gain of the linear amplifier to compensate, and checking at the end to see that it had not shifted appreciably during the run. Normalization was accomplished by a steady run at 72 volts (corresponding to 1 Mev — on the high energy side of the "Compton peak"). The counting rate of this energy should be independent of the scatterer unless Rayleigh scattering becomes appreciable; each run was therefore normalized to give a counting rate of 200 cpm at this energy. The maximum Compton scattered intensity which could yield, in the vicinity, resulting electrons of this energy, is an order of magnitude below a readable quantity.

Unless it was responsible for the above gain shift, the Model 204-B linear amplifier was highly satisfactory. Long runs were made with no noise at a discriminator base line of 1 volt operating it as an integral discriminator.

The counting rate meter, on the other hand, gave a great deal of difficulty. Changes in line voltage, which occur many times an hour, make the zero shift momentarily, after which it drifts back. The sensitivity also varies occasionally and required completely re-running eight of the wood scattering experiments. The zero changes are believed to be the largest single source of error in the scattering experiments; they are usually of the order of 20 counts per minute and sometimes as high as 40 counts per minute. These appear suddenly as positive errors; negative errors due to this cause appear only slowly and only when a recent positive change leads to setting the zero too high at the beginning of a run. Under-compensation is thus indicated, but requires a "feel" for the instrument. Another failing of this counting rate meter is in the integration circuits which cause a sufficient lag to require considerable care (a wait of 3 to 5 minutes) at the beginning of a run and at each change of counting rate. Furthermore, there is some

indication that on steep portions of the curve there is a little lag. On runs with a great deal of scattering this lag makes the 2 volt (28 Kev) reading a little high but the percentage error is small ($\sim$ 2 percent); the 3 volt (42 Kev) reading is relatively unaffected on those curves where a precise check was made.

The data are recorded by an Esterline-Angus recording milliammeter. The curved scale of its chart is not optimum. Errors in printing the tapes result in errors of data of the order of $\pm$ 0.2 volts ($\pm$3 Kev) and, in the ordinate, of $\pm$10 cpm. These errors are obviously inherent in the use of this instrument. The particular instrument is badly worn and should be overhauled but its defects in this respect lead primarily to inconvenience. There is one exception however: wear and corrosion of the knife edge render the pen balance sufficiently unreliable so that the pen must be kept a little heavy or it will be found off the paper and the record gone; a heavy pen gives an error of up to 40 cpm due to paper drag, but there is no such error near the middle of the chart and the violent oscillations due to statistical variations eliminate its effect at good counting rates. It has more tendency to give errors in calibrations and zero setting than anything else.

The Esterline-Angus is plugged into the scanner so that when the latter is cut off at the end of the run, so is the recorder. This marks the end of the run and saves chart footage. A block diagram of the entire setup is shown in Fig. 2.

B. EXPERIMENTS.

The experiments consist of measuring the total spectrum with various scatterers parallel to and at various distances from the line between source and detector, keeping these latter two always 40 cm apart on a horizontal line of constant orientation. From these spectra are subtracted the spectrum of the same source and detector at the same separation (r = 40 cm) taken with them both 90 cm above the table top with no other scatterers than the table, the pipes 90 cm above, air, and with heavy concrete floor, walls, and ceiling each at approximately 180 cm. The difference, known as the build-up, n, is to be related to the distance above the scatterer, y, the atomic number of the scatterer, Z, the primary gamma energy, E_o, the energy at which the reading is taken, E, and the area of the scatterer, A. The thickness of the scatterer is to be such that it can be considered to be a semi-infinite medium. It is desired that the data yield, qualitatively at least:

$$n = f_1(E, y)_{Z, E_o, A} \quad \text{(for 2 values of } E_o\text{)}$$

$$n = f_2(Z, y)_{E, E_o, A}$$

$$n = f_3(E, Z)_{y, E_o, A}$$

$$n = f_{3a}(E, Z)_{y, E_o, A, \rho}$$

$$n = f_4(E, Z)_{y, E_o, Z}$$

C. SOURCES.

Three sources were used. The first was composed of three pieces of Co^{60} wire totalling approximately 2 mc in activity wrapped in a 1 cm square of black scotch electrical tape No. 33, with a nylon thread through the tape for handling and positioning. The reasons for nylon are: (1) strong, (2) slides easily through wire "padeyes", (3) elasticity facilitates accurate positioning, (4) sticks to tape enough for securing and not too much for repositioning. The largest piece of Co wire was approximately 2 mm long. The second source was made by damming off a piece of filter paper with Duco cement and beeswax and adding drops of a high activity Cs^{137} source, allowing each to evaporate. This was done until the counting rate of the "Compton peak" was the same height as that of the Co^{60} source at the same gain. The estimated

source strength is 3 mc. The impregnated portion of the filter paper was wrapped in a small square of scotch cellophane tape with a nylon thread through it. For energy calibration a small Cs^{137} source was used. The Cs was bare, evaporated from solution on aluminum foil. A piece of cardboard with a square hole was cemented to the foil with the hole over the active spot. A 3 mm sheet of lucite with 1 cm hole was taped to the cardboard to act as a guide to position the source on the crystal.

D. SCATTERERS.

Five scatterers were used, giving the best practicable spread in Z: wood ($Z \approx 7$), Al ($Z = 13$), Fe ($Z = 26$), Sn ($Z = 50$), Pb ($Z = 82$). Were we dealing with energies such that photoelectric effect or pair production were important, we would have to give separate values for Z_{eff} for each process in wood, but in these experiments the primaries interact essentially completely by Compton effect. The effective Z for the Compton process can be calculated[H11] from the approximately known composition of wood.[N2, S12] The method just gives double weight to the electrons of hydrogen because its $Z/A = 1$. A representative estimate of the composition yielded a $Z_{eff} = 7.06$. Wood was chosen instead of water for convenience and economy (the large tank required to use water would have been expensive).

The effect of area on backscattering[H13] indicated that the largest scattering area practicable should be used. The maximum area which would fit on the scattering table without modification involved weights of the order of magnitude of 1500 lbs. unless special lead shapes were poured; this was as great as considered appropriate. Accordingly the area of scatterers was 36" × 47" for wood and iron, and approximately 36" × 48" for the others. A thickness of two mean free paths was considered effectively infinite where deep scattering into the detector becomes effectively back scattering. This criterion indicated 24" wood, 5 3/8" Al, 1 7/8" Fe, 2" Sn, and 1 1/4" Pb. These thicknesses were used except for lead where economy dictated the use of available 2" bricks. In the case of the wood, the pile became too high for some other experimental work not included herein. Runs were made of several values of "y" from 0.5 cm to 45 cm using first 24" thickness and then 18" thickness. No difference was detectable and where convenient the thickness was reduced to 18".

The value of r = 40 cm between source and detector approximately divided the total length of the scatterer into thirds and placed each of them about 40 cm from the nearest aluminum tube of the scattering table. This also satisfied the criterion of counting rate vs source strength.

The effect of area on backscattering[11] indicated that the largest scattering area practicable should be used. The maximum area which would fit on the scattering table without modification involved weights of the order of magnitude of 1500 lbs. unless special lead bricks were used; this was as great as considered appropriate. Accordingly the area of scatterers was 30" x 27" for wood and iron, and approximately 30" x 28" for the others. A thickness of two mean free paths was considered effectively infinite where deep scattering into the detector becomes effectively back scattering. This criterion indicated 10" wood, 3 3/8" Al, 1 7/8" Fe, 2" Cu, and 1 1/4" Pb. These thicknesses were used except for lead where economy dictated the use of available 2" bricks. In the case of the wood, the pile became too high for some other experimental work not included herein. Runs were made at several values of "r" from 0.5 cm to 45 cm using first 10" thickness and then 12" thickness. No difference was detectable and where convenient the thickness was reduced to 12".

The value of r = 20 cm between source and detector approximately divided the total length of the detector into thirds and placed each of them about 40 cm from the nearest aluminum tube of the scattering table. This also satisfied the criterion of counting rate vs source strength.

E. EXPERIMENTAL PROCEDURE.

The first step in running an experiment was to set up the required geometry. Measuring rods cut to length facilitated this. Ten values of "y" were first chosen at random to cover the possible range, with the intention of eliminating a few as soon as data indicated the feasibility of doing so. All 10 were kept except for wood for which the thickness was so great that a special rig would have had to have been prepared to get a run at y = 90 cm. For other scatterers, 90 cm was the maximum and placed the source and detector also 90 cm from iron pipes overhead. For all, the 1 cm length of the crystal set 1/2 cm as the closest approach possible for its center, to which all measurements were taken.

The counting rate zero was checked. Occasionally its sensitivity was checked with 60 cycle, there being an internal arrangement to make this possible. The integration rate was set as low as possible, at 2 for all these experiments. Counting range was set at 4 (2000 cpm full scale). The discriminator base line was set at 71 volts (1000 Kev) with the scanner clutch disengaged, and the channel width was checked for its setting at 2.00 volts (28 Kev). The high voltage was checked and recorded, but seldom adjusted; all experiments were run at approximately 1080 volts. The gain of the linear amplifier was adjusted until the Esterline-Angus read 30

(600 cpm). Due to statistical variation in the curve, 5 minutes or more is required at each setting to determine the value. When the normalization was satisfactory, the discriminator base line was changed to 1.0 volt (14 Kev), the counting rate adjusted to keep the Esterline-Angus on scale, and all the above information was written on the tape. Once the need for doing so became apparent, the base line was left set long enough to determine quite accurately the counting rate at 1.0 volt. The clutch was then engaged and reset until the base line reached 1.0 volt at the same time as the Esterline-Angus pen reached one of the printed curved lines on the chart, at which time the scanner was stopped. This particular ritual was found to have many advantages in checking the progress near the beginning of the run, in checking the normalization at the end, and in averaging the data later. If successful in matching the discriminator and recorder, the tape was marked accordingly and the scanner restarted, the recorder stopping and starting with it. Usually 2 volts (28 Kev) and 3 volts (42 Kev), and other points as convenient, were marked. To change counting ranges, the scanner was stopped and the equipment left at least 5 minutes at the new range before restarting. The shift was marked. Before this much time was allowed, the data on the two ranges frequently failed to check, in which case the former range was the one trusted.

Several runs were made with the same geometry. An effort was made to set it up more than once, taking at least two runs one time and at least one the other. If only one setting was used, it was remeasured at least once.

Numerous runs were made with the calibration source described above. Comparison of the position of the 663 Kev peak with the gain normalization of preceding or succeeding Co^{60} runs gave, as the result of about 20 measurements, a value of 47.1 volts for a properly normalized peak, or a conversion factor of 14.08 Kev per discriminator volt.

Cs^{137} curves were taken at the same gain. Sources were repeatedly switched on successive short runs of only the appropriate part of the spectra and the normalization values for Cs^{137} were found to be 600 cpm at 36.2 volts (510 Kev).

When the equipment was not otherwise in use it was kept running on a single setting to check stability of one or another component. Shutting it down was found to be detrimental rather than beneficial and the information gained on stability was either useful or comforting.

Runs of the same geometry were averaged by taping them to glass above a fluorescent light. When all were carefully aligned, an average spectrum was drawn on a separate strip of Esterline-Angus tape. The control run, at 90 cm with no scattering, was subtracted from the average spectrum, also

on the lighted glass, differences less than 200 cpm being measured graphically and greater ones by use of a calibration chart of the various counting ranges of the counting rate meter. The values of the difference were recorded on a clean strip of Esterline-Angus chart taped on top of the other two, and from this was plotted a build-up curve (Figs. 4-8 incl.) and from them were plotted cross curves (Figs. 9-16 incl.).

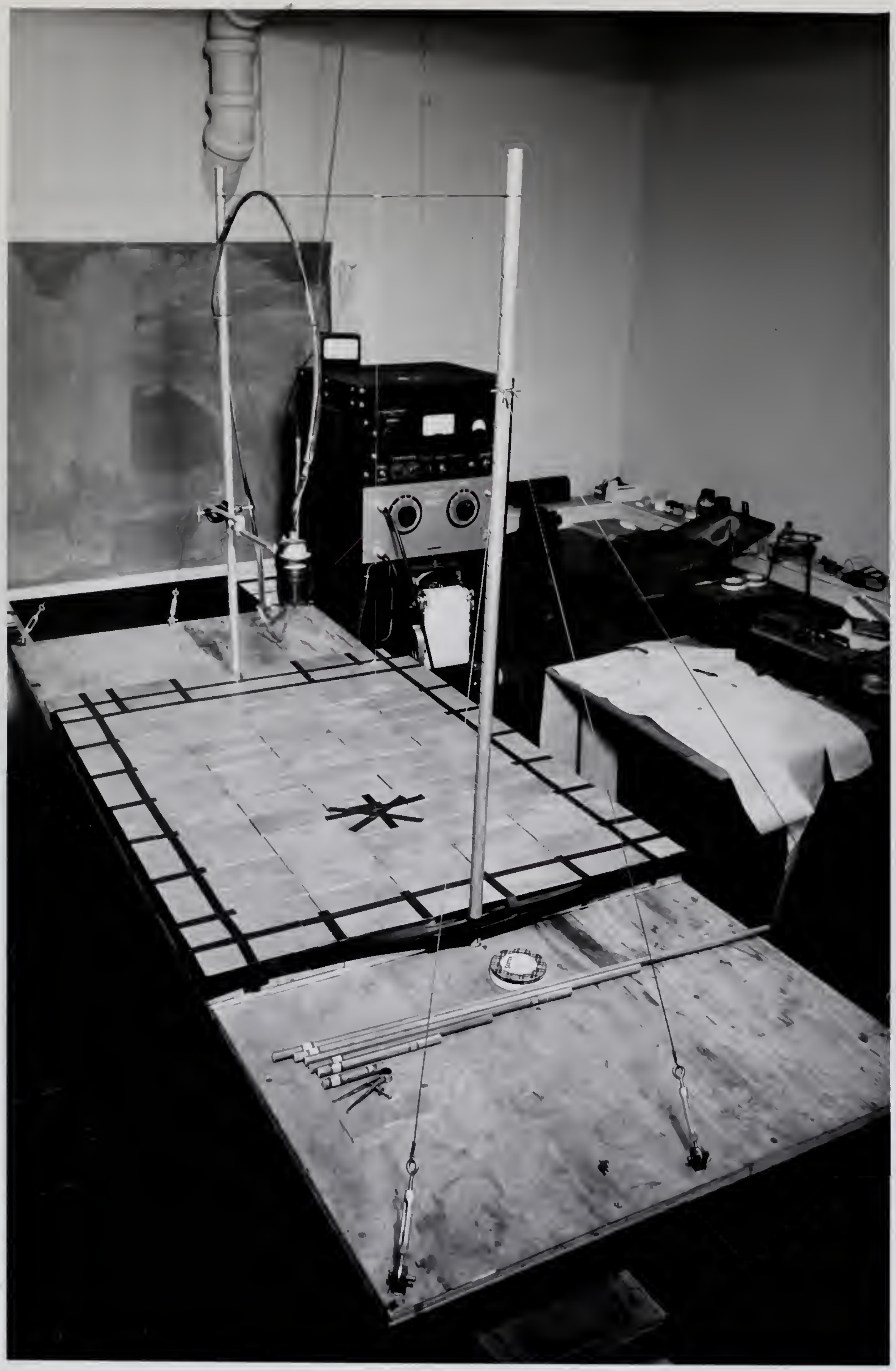

FIGURE 1

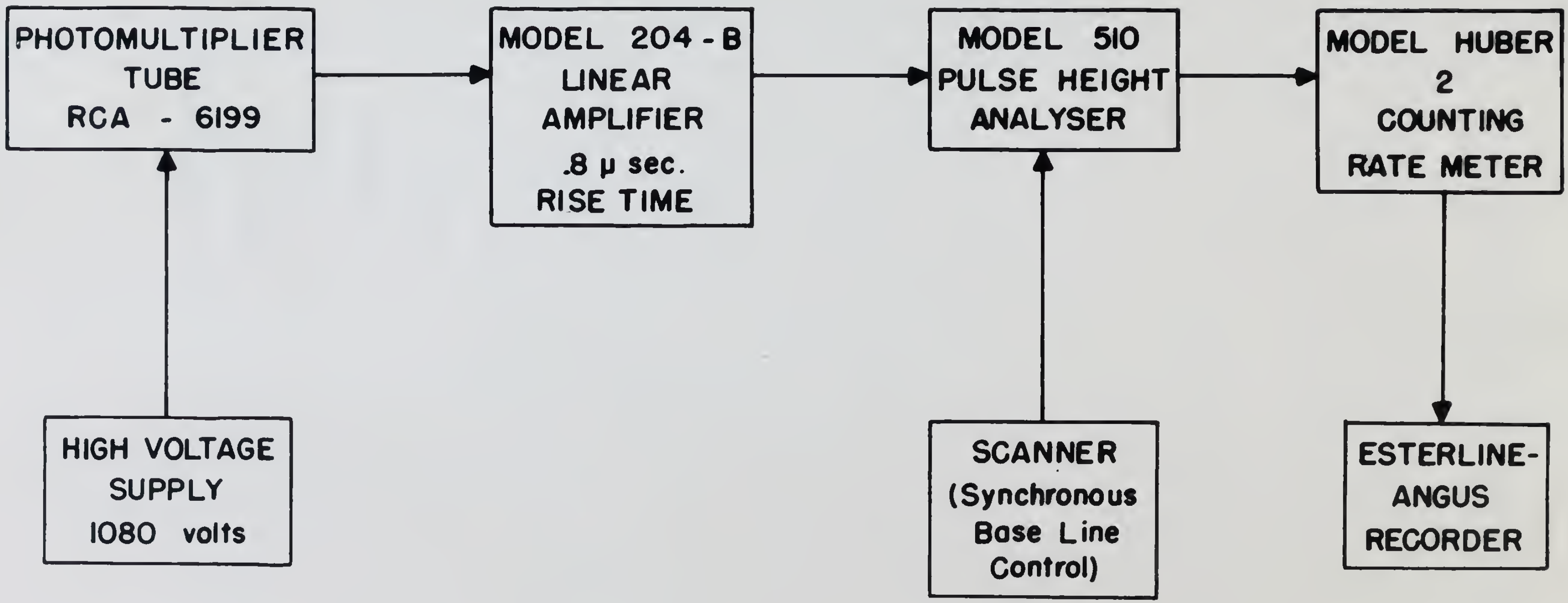
PHOTOMULTIPLIER TUBE RCA - 6199
MODEL 204 - B LINEAR AMPLIFIER .8 μ sec. RISE TIME
MODEL 510 PULSE HEIGHT ANALYSER
MODEL HUBER 2 COUNTING RATE METER
HIGH VOLTAGE SUPPLY 1080 volts
SCANNER (Synchronous Base Line Control)
ESTERLINE-ANGUS RECORDER

Figure 2

IV. RESULTS AND INTERPRETATION

A. VARIABLES AND THEIR EFFECT.

1. The controllable variables introduced into the investigation were:

a. Z, the atomic number of the scatterer

b. y, the distance of source and detector above the top surface of the scatterer

c. E_o, the energy of the primary radiation.

Two measurements were also made to give a rough idea of the effect of changing A, the surface area of the scatterer, and a few to determine whether or not there was some freedom in the choice of t, the thickness of the scatterer. In general a change of Z was accompanied by a change in ρ, the density of the scatterer; this was essentially not the case however in changing between iron and tin. No experiments were conducted with a single Z at more than one value of ρ.[H12] Also, the system of measurement gives data on the dependent variable E, the energy of the secondary electrons created in the stilbene detector by the detected radiation. Let us consider the effects of these variables.

2.a. The mass attenuation coefficients are proportional to Avogadro's number, N; inversely proportional to

the atomic weight, A; and proportional to some power of the atomic number, Z. The Compton process goes as Z, the photoelectric process as $Z^{4.1}$, the pair production as Z^2, Rayleigh scattering as Z. For this reason we find for the 1.25 Mev average energy of Co^{60} that the photoelectric effect is appreciable only for tin and lead of the scatterers investigated. And this energy, measured of course in laboratory coordinates, is too low to give any appreciable pair production, for which process 1.02 Mev in center of mass coordinates is necessary just to create the positron-negatron pair. Compton and Rayleigh scattering per unit volume depend on the number of electrons in that volume. Therefore the linear Compton coefficients depend on Z while the corresponding mass attenuation coefficients depend on Z/A which equals 0.5 or close thereto for all light and medium elements except hydrogen. For hydrogen Z/A = 1; for lead Z/A $\approx$ 0.4. This information is best summarized by a table of attenuation coefficients.[D2, W2]

Table 4.1

Linear attenuation coefficients for 1.25 Mev gammas in cm^{-1}

Medium	Z*	ρ gm/cm³	σ_a	σ_s	τ	κ	μ_o	$\mu_o-\sigma_s$
Air	7.3	0.001205	3.3×10^{-5}	3.6×10^{-5}	0	0	6.9×10^{-5}	3.3×10^{-5}
Water	8	1	0.029	0.034	0	0	0.063	0.03
Wood	7	0.5	0.015	0.017	0	0	0.032	0.015
Al	13	2.7	0.07	0.08	0	0	0.15	0.07
Fe	26	7.85	0.20	0.22	0	0	0.42	0.20
Sn	50	7.31	0.17	0.195	0.015	0	0.38	0.19
Pb	82	11.35	0.24	0.28	0.14	0	0.66	0.38

*For the first three this is $\overline{Z}_{Compton}$, the effective Z for the Compton process.[H11, S11]

Table 4.2

Mass attenuation coefficients for 1.25 Mev gammas in cm^2/gm

Medium	σ_a/ρ	σ_s/ρ*	τ/ρ	κ/ρ	μ_o/ρ	$(\mu_o-\sigma_s)/\rho$	Rayleigh / ρ
Air	0.027	0.030	0	0	0.057	0.027	0
Water	0.029	0.034	0	0	0.063	0.030	0
Wood	0.029	0.034	0	0	0.063	0.030	0
Al	0.026	0.030	0	0	0.056	0.026	0
Fe	0.025	0.029	0	0	0.054	0.025	0
Sn	0.022	0.025	0.002	0	0.052	0.025	
Pb	0.022	0.025	0.013	0	0.061	0.035	0.0014

*Rayleigh not included.

Table 4.3

Rayleigh scattering angle (in degrees)
to include 60-70 percent[F1]

Energy (Mev)	0.1	1	10
Al	15	2	0.5
Fe	20	3	0.8
Pb	30	4	1

Table 4.4

Representative mean free paths

	Pb	Air	Water
1 mfp in cm for 1.25 Mev	1.5 cm	$\sim 10^4$ cm	15.9 cm
1 mfp in cm for 1 Mev	1.25 cm	$\sim 10^4$ cm	14.2 cm
1 mfp in cm for 0.08 Mev	0.052 cm	$\sim 10^4$ cm	5.6 cm

2. b. Variation of y changes the <u>source to scatterer distance</u> and the <u>detector to scatterer distance</u> equally. For an area small enough in relation to its distance from a point source so that it does not differ appreciably from a portion of a spherical surface about that point, the intensity varies as $1/R^2$. These conditions are not met for the geometry of this experiment. The surface to which measurements should be referred is actually not the top surface of the scatterer because of the penetrating nature of the radiation. It will be shown that this effect is so pronounced for the wood with its low density that the data is markedly affected, while it is so slight for the lead with its high density that the data are probably relatively unaffected. For practical reasons the measurements have to be made to the top surface of the scatterer; the solid angle it subtends at the source (or detector) has been calculated. For the variation in y from 0.5 to 90 cm this solid angle varies by a factor of 6, while y^2 varies by a factor of 32,000. If the scattering were isotropic, the variation in solid angle would be the measure but throughout the investigation the scattering is primarily Compton and highly anisotropic;[D2] therefore both considerations enter. The cross sectional area of the 3/8" diameter × 3" long cylinder of stilbene will in general be small compared to its distance from a detected scattering event. Hence for

the detector the distance alone will have an effect as $1/R^2$. The contribution by these criteria will <u>decrease</u> as y is increased.

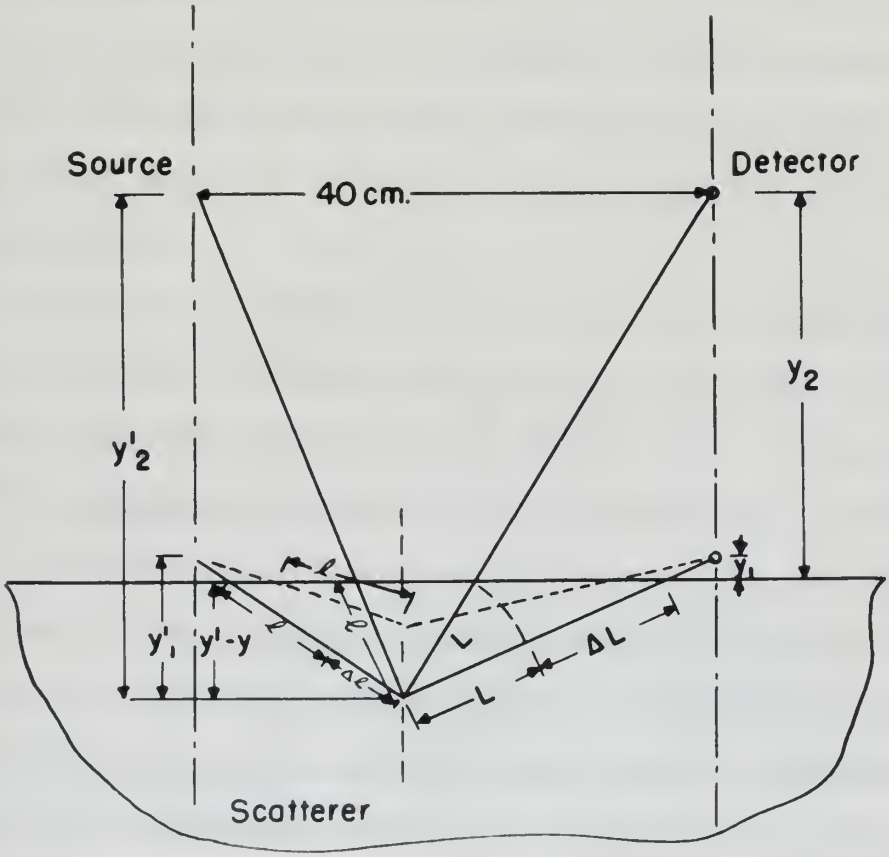

At small y, the path length in the scatterer of the primary radiation to reach a given depth, except directly under the source, will be greater than for large y as can be readily seen in the following sketch, the given depth being $y' - y$ and the difference in path length $\Delta \ell$. In general, therefore, the scattering events will occur closer to the surface for smaller y, by the amount shown as $\Delta y'$.

Conversely, the path length in the scatterer for scattered radiation from a given point within its volume to the detector will be correspondingly longer for smaller y, by the amount ΔL. The average value of ΔL will equal the average value of $\Delta \ell$ and for the same distance primary radiation of the energies involved in these experiments will be attenuated less than will the lower energy scattered radiation. The net of these effects will be to give increased build-up as y is increased.

As mentioned before, the Compton process is highly anisotropic, strongly favoring small angle scattering which can reach the detector only at small values of y, giving markedly decreased build-up as y is increased. But this effect will be modified in the case of lead where on one hand the atomic weight and electron binding energy are great enough to allow Rayleigh scattering which is distinctly a small angle phenomenon, while on the other hand an appreciable part of the scattering should be isotropic fluorescence, or bremsstrahlung which while not isotropic will not on the other hand favor the small angles. Not only is the lead K-fluorescence the only one of sufficient energy to reach the detector readily (75 Kev as compared to ~ 25 Kev for Sn)[C4] but it will accompany only the photoelectric effect and this will be appreciable only in the lead. Likewise

Conversely, the path length in the scatterer for scattered radiation from a given point within its volume to the detector will be correspondingly longer for smaller γ, to the amount Δl. The average value of Δl will equal the average value of $\Delta \ell$ and for the same distance primary radiation of the energies involved in these experiments will be attenuated less than will the lower energy scattered radiation. The net of these effects will be to give increased build-up as γ is increased.

As mentioned before, the Compton process is highly anisotropic, strongly favoring small angle scattering which can reach the detector only at small values of γ, giving markedly decreased build-up as γ is increased. But this effect will be modified in the case of lead where on one hand the atomic weight and electron binding energy are great enough to allow Rayleigh scattering which is distinctly a small angle phenomenon, while on the other hand an appreciable part of the scattering should be isotropic fluorescence, or bremsstrahlung which while not isotropic will not on the other hand favor the small angles. Not only is the lead K-fluorescence the only one of sufficient energy to reach the detector readily (75 kev as compared to $\sim$ 25 kev for Sn)[64] but it will accompany only the photoelectric effect and this will be appreciable only in the lead. Likewise the bremsstrahlung energy will take roughly a Gaussian distribution about the mean, which in the case of a lead photoelectron ejected by Co^{60} radiation will be $\sim$ 100 Kev as compared to that, from the low probability 0° (maximum energy) Compton electron, in Sn which would be $\sim$ 50 Kev.

Small angle scattering by the Compton process gives scattered radiation of almost as much energy as the primary, and for very small angles Rayleigh scattering, with no decrease in energy, sets in. The attenuation is less for these higher energy components, and this factor tends to decrease the build-up as y increases.

Actually these factors, particularly the latter two which are really sensitive to angle, depend not on y so much as they do on y', the distance of source and scatterer above an unknown surface inside the scatterer which may be said to be its mean effective position for the observed scattering. For lead this position must lie near the top surface because of the high attenuation. For lead then we may say $y \approx y'$. Therefore with lead we would expect to observe some of the small angle effects. But for wood this is not true; perhaps y' exceeds y by 1/2 mfp, and 1/2 mfp in wood for 1.25 Mev gamma rays is of the order of magnitude of 15 cm (based on a ρ of 0.5 gm/cm^3). Small variations in the magnitude of y should have very little effect on the scattering, and the small angle effects should be undetectable. It is obvious

that this feature is primarily a function of ρ because the mass absorption coefficient, $\mu-\sigma/\rho$, is practically independent of Z except for hydrogen.

Very low energy scattered radiation, even if it escapes the scatterer, will be only partly detected if at all, due to <u>attenuation in air and in the lightshield</u>. The 0.031" water equivalent lightshielding plus 0.001" aluminum reflector are equivalent to about 70 cm air so that the attenuation of the soft radiation will not be markedly affected by changing y. What effect there is will be a <u>decrease</u> of build-up with increase of y, and will be only at the very low energy end of the spectrum.

Except for this last factor, and the fluorescence and bremsstrahlung mentioned above, all these effects will cover a considerable portion of the spectrum because the equipment gives the energy only of the secondary electrons produced in the stilbene. Thus a scattered component cannot affect any of the spectrum above its own energy, but it can affect any portion below its own energy.

c. The value of E_o determines the values of the coefficients for the various interactions, thus affecting both the total attenuation and the relative distribution among the processes. This effect continues because the energy of the

singly scattered radiation depends on that of the primary and it in turn has its appropriate coefficients which determine the probability of absorption, transmission, or multiple scattering. The following are the coefficients for the only other value of E_o used.[D2, W2]

Table 4.5

Mass attenuation coefficients for 663 Kev gammas in cm^2/gm

Medium	σ_a/ρ	σ_s/ρ*	τ/ρ	κ/ρ	μ_o/ρ	$\frac{\mu_o-\sigma_s}{\rho}$	$\frac{\text{Rayleigh}}{\rho}$
Wood	0.0328	0.0530	0	0	0.0858	0.0328	0
Aluminum	0.0285	0.0461	0	0	0.0747	0.0285	0.0001
Iron	0.0279	0.0450	0	0	0.0735	0.0280	0.0006
Tin	0.0244	0.0400	0.008	0	0.0751	0.033	0.0029
Lead	0.0234	0.0378	0.0427	0	0.1082	0.0677	0.0043

* Rayleigh not included.

d. As for the others, it is obvious that reducing the scattering area, A will reduce the build-up. What is desired is to see how much the build-up is reduced by

removing the outer two-thirds of the scatterer. Much more than this would have been of interest had time permitted.

The experiments relative to the depth of the scatterer, t, were to determine the appropriateness, or lack thereof, of reducing the thickness of the wood scatterer from 24" to 18". The density being slightly greater than the estimated 0.5 cm/cm^3, this represented a reduction from a little over 2 mfp to between 1 1/2 and 2 mfp. No variation in buildup was found and henceforth the 18" thickness was used for convenience.

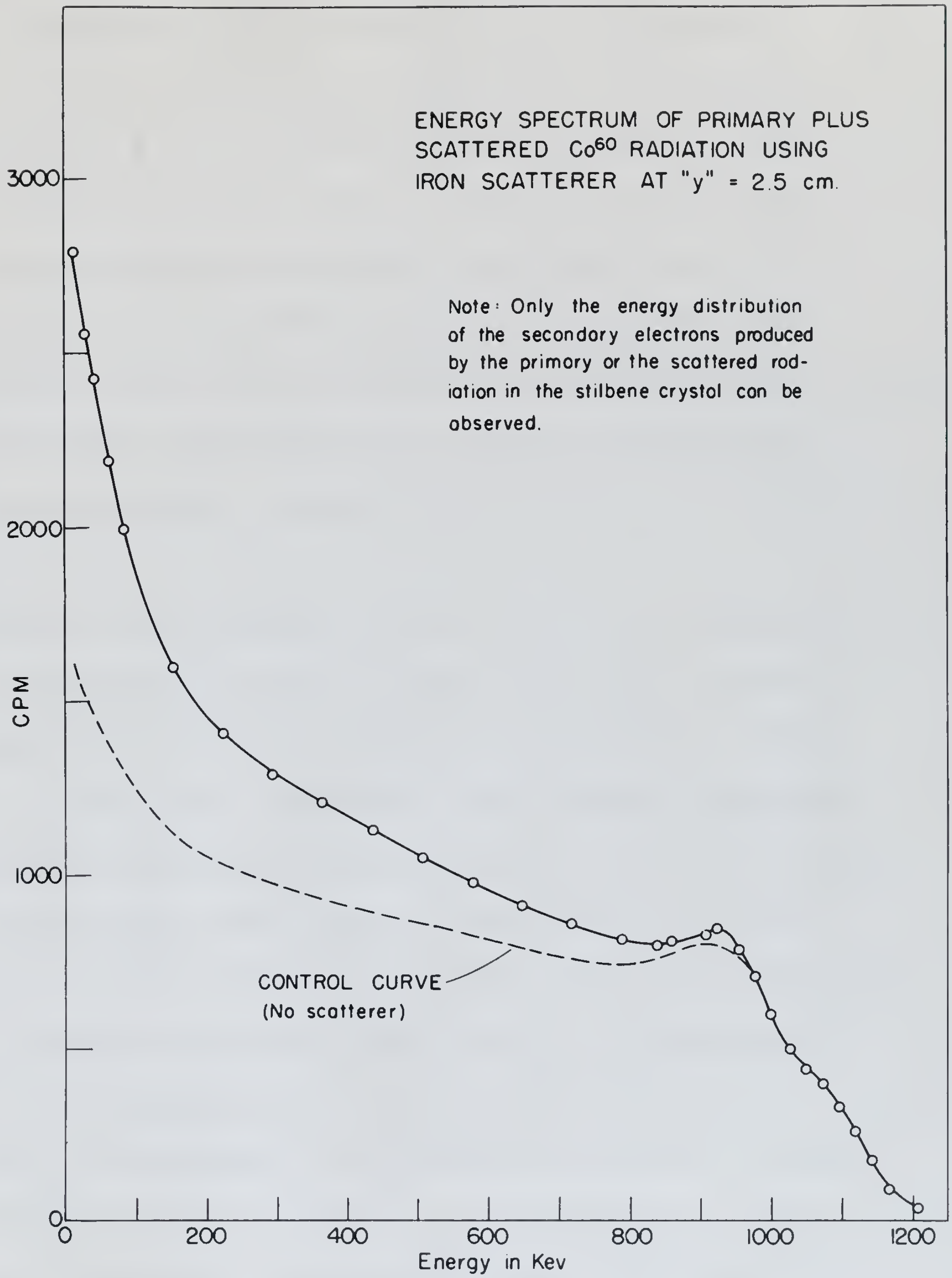

ENERGY SPECTRUM OF PRIMARY PLUS SCATTERED Co60 RADIATION USING IRON SCATTERER AT "y" = 2.5 cm.
Note: Only the energy distribution of the secondory electrons produced by the primory or the scattered rodiation in the stilbene crystol con be observed.
CONTROL CURVE
(No scatterer)
CPM
3000
2000
1000
0
0
200
400
600
800
1000
1200
Energy in Kev

Figure 3

B. EXPERIMENTAL DETERMINATION OF BUILD-UP.

The experimental setup consisted of the following:

36" × 47" iron plates totalling 1 7/8" in thickness, laid horizontally, at y = 0.5 cm below the source (2 mc Co^{60}) and the detector (3/8" dia. × 3/8" long cylindrical stilbene crystal mounted on RCA 6199 photomultiplier tube). Source and detector separated by distance r = 40 cm along horizontal line parallel to 47" dimension of scatterer; center of this line vertically above center of scatterer. See sketch on Fig. 17 for somewhat similar setup with wood 18" thick.

The spectrum obtained was generally similar in appearance to the one shown in Fig. 3 as can been seen from the relative appearance of the two pertinent difference curves in Fig. 6. Figure 3 also shows the control curve which is the "no scatterer" spectrum; subtraction of the control curve from the spectrum gives the build-up curve plotted in Fig. 6. Use of this control curve is somewhat subject to criticism in that it includes some scattering from the table which is shielded by the scatterer when a scattering experiment is run. This effect is small, as demonstrated by the following fact. When the table was covered by lead, which is a poor scatterer, no difference could be detected. Other even less

important limitations to the correctness of the control curve are that it was obtained at 90 cm from two large iron pipes and approximately 180 cm from the concrete ceiling and floor, while the scattering runs are at (180 - y) cm from the pipes, (270 - y) cm from the ceiling, and (90 + y) cm from the floor from which it receives varying amounts of shielding from the scatterer.

<u>IRON</u>. The discussion of results is being opened with a report on the iron scattering experiment at the smallest value of y for simplification, and in order to facilitate later comparisons with other data. Although the specific gravity of iron is relatively high (7.85) its atomic number is low (26) so that τ and κ are essentially zero, and Rayleigh scattering can also be neglected.[W2] This leaves only Compton scattering. The mean free path in iron for 1.25 Mev gammas is 2.4 cm. A glance at the geometry, with a point source 0.5 cm. above the scatterer and the detector touching the surface of the scatterer and extending to 1 cm above it, shows immediately that the preferential forward scattering for the Compton process should yield mostly high energy scattered radiation at the detector. The detector can measure only the energy of the secondary electrons produced in the stilbene crystal by the radiation interacting with it and as stated above this interaction is also almost completely Compton scattering. All the build-up curves

should therefore be highest at the lowest energies. But compared with experiments at greater values of y, this particular build-up curve should be relatively higher at the high energy end. Examination of Fig. 6 shows that as expected, the counting rate for 14 Kev secondary electrons is less for 0.5 cm than for any other value of y up to 30 cm, but the 0.5 cm curve crosses the 30 cm curve at 100 Kev, the 20 cm at 155 Kev, the 10 cm at 350 Kev, and even the 5 cm, 2 1/2 cm, and 1 cm curves between 500 Kev and 700 Kev.

The strong attenuation for such a relatively high density scatterer cuts out most of the scattered radiation having a long path length in the iron. Thus, although the solid angle subtended by the scatterer is a maximum, the total amount of scattered radiation detected may be expected to be rather small. In Fig. 6 the area under this curve is obviously less than that taken at 1, 2 1/2, 5, or 10 cm and nearly equal to that at 20 cm. But at 20 cm the high energy build-up has disappeared showing that the small angle scattering is practically undetectable. The solid angle reduction however has a pronounced effect and we see the total scattering dropping sharply with further increase of distance. Looking at the build-up at each distance shown on Fig. 6, the following features are of interest:

1. The maximum number of the low energy secondary electrons is produced by the scattering at 10 cm.

2. All curves show rapid rise at low energies, extremely so for all values of y less than 45 cm.

3. For values of y up to and including 10 cm there are secondary electrons formed up to the maximum energy attainable by the Compton process from incident photons of 1.10 to 1.20 Mev. This may be presumed to be due to small angle scattering, primarily of the 1.33 Mev component of the primary. At 20 and 30 cm the maximum energy is sharply reduced. At 45 cm, the value of y at which the sharp low-energy rise begins to fall off, the counting rate has dropped to zero by the plotted value of 155 Kev. At y = 45 cm the scattering angle for scattering at the top surface directly under source or detector is calculated to be 138.4° and that for the midpoint between is 132°. The maximum energy of scattered photons should then be

$$h\nu' = \frac{1.33}{1 + \frac{1.33}{0.51}(1 - \cos 132^{\circ})} = 248 \text{ Kev}$$

which would give for the maximum energy Compton recoil electrons in the stilbene

$$E = 248\left(1 - \frac{1}{1 + \frac{0.248 \times 2}{0.51}}\right) = 123 \text{ Kev.}$$

Going back to the original data, at 123 Kev there are less than 20 cpm which is within experimental accuracy of zero.

The minimum energy scattered photons are those back-scattered at 180°

$$h\nu' = \frac{1.17}{1 + \frac{1.17 \times 2}{0.51}} = 209 \text{ Kev}$$

Then all single scattered photons incident on the detector lie in the range from 209-248 Kev. This is, broadly speaking, a monoenergetic source of 228 ± 19 Kev. Hence the build-up curve already commences to take on the aspects of a spectrum like that of Fig. 3, and this is even more true at 60 cm, explaining the change of shape away from the extremely sharp low energy rise. Comparison with the Hg^{203} (280 Kev) spectrum reported by Prestwich and Colvin[P3] shows very similar proportions, and this has been verified with the equipment used for those scattering experiments but too late for inclusion of the spectrum.

TIN. Consideration should next be extended to scattering from other materials. First a comparison with tin is interesting because tin has almost the same density as iron. To facilitate this comparison Figs. 15 and 16 have been prepared showing the situation at y = 0.5, 1, and 10 cm. At 0.5 cm the iron curve is considerably higher than the tin; at 1 cm they are almost equal in the intermediate

range but the tin is lower at the extremes, particularly at low energies where the counting rate of the iron rises to almost twice that of the tin. At 10 cm the iron is higher, especially at low energies where it is more than twice as high; furthermore, the iron scattering appears to include high enough energies to give secondary electrons in the detector of 800 Kev while the tin cuts off at about 650 Kev. Experimental error could possibly account for this however, as the counting rates due to the build-up are low and are only a small fraction of the total counting rate experimentally measured.

The difference at the low energy end is as would be expected from the much higher mass absorption coefficient of tin for low energies. Tin with Z = 50 has much more photoelectric effect than does Fe with Z = 26 and this becomes important with low energies. The total mass absorption coefficient for tin is somewhat less than that for iron because Z/A drops from 0.5 to 0.42 and at 1.25 Mev τ/ρ is not large enough to compensate. For this reason we get somewhat reduced scattering by the tin as evident in Figs. 16 and 17. The 1 cm curves, however, show the expected increase only at the highest energy. For the intermediate energies they are equal. Rayleigh scattering may partly account for this as it is favored for small angles and high

Z. The higher Z of tin will spread the angle beyond that of iron, perhaps explaining the fact that there is compensation at y = 1 cm and not at y = 0.5 cm.

The remainder of the discrepancy is probably due to experimental error, which is composed of errors in averaging original data and in reading the average, occasional distortion of the printed scale of the Esterline-Angus chart paper, minor counting rate meter instability, and small gain changes not corrected in normalizing. A weighted combination of those errors gives a value of ±22.5 cpm random instrumental error. All of the above contributions, except the gain change which is too small to consider, are independent of counting rate. To this must be added the effect of standard deviation due to statistics; this is strictly dependent on counting rate. The scanner requires 3 minutes to traverse the channel width of 2 volts; if the counting rate is 1000 cpm there will be 3000 ± 55 counts in this time. Summing these two deviations we get

$$\pm\sqrt{3000 + 510} = \pm 59 \text{ counts} = \pm 20 \text{ cpm}$$

If we set twice this deviation as the nominal limit of error,[E1] we get ±40 cpm.

Examination of Fig. 7 reveals the same trends as found for iron in Fig. 6. The very small values of y give curves which start low and then cross those representing greater

distances. The maximum at lowest energy is still the 10 cm curve as with iron, but the 5 cm curve crosses it at 62 Kev. Most of the curves also show a tendency toward exhibiting a peak which must have its maximum between 85 Kev and 100 Kev. This must be the "Compton peak" in the stilbene from the radiation scattered out of the tin at or near 180°. As shown above this is nearly monoenergetic for a considerable range of angles, hence the peak. For the mean Co^{60} radiation of 1.25 Mev this peak occurs at 93 Kev. If correctly interpreted, it should be strongest in curves with relatively large y and weak for very small values of y; although not sharply borne out by Fig. 7 this trend is still apparent. The first sharp peak unambiguously delineated by the data is at 30 cm. At values of y greater than 30 cm the peak position shifts slightly to lower energies corresponding to scattering angles closer to 180° as would be expected from the geometry. As mentioned in the case of iron, as the scattered radiation becomes monoenergetic the curve looks more and more like the unscattered spectrum from Hg^{203}.

As discovered by Hayward[H12] and independently by Hine[H13], using NaI(Tl) scintillators, this approximately monoenergetic singly scattered radiation may suffer a second scattering giving a peak of gamma energies about 115 Kev for 180° back-scattering, which in turn would give secondary electrons with

a maximum at 35.6 Kev. It is too much to expect that an organic scintillator would resolve this, and it is not indicated by these data.

The constant secondary electron energy curves for iron and tin, Figs. 11 and 12 respectively, point out clearly that at the lowest energies recorded in the detector, the highest counting rates are at or near 10 cm. The sharp drop-off at shorter distances, explained in detail above, was noticed to a small degree by White and Henderson[W3] but was much less apparent without energy discrimination and with their somewhat larger detector. Also as mentioned and explained above, as the energy increases, the maximum shifts to shorter distances. Quite interestingly, Fig. 12 shows that at 225 Kev there is a double maximum which can be seen developing in the curves at 85 Kev and 155 Kev respectively. At 437 Kev there is only a single maximum but it occurs with the lower of the two found at 225 Kev, while the low energy curves follow the higher of the two at 225 Kev. A similar, but much less clearly defined, phenomenon is observed in Fig. 12 for the tin, but occurring at a somewhat higher energy. This must be taken as a clear indication of two competing processes, one predominating at lower energies and the other at higher energies. Both processes emit radiation well within the range in which the detector is linear. The

higher energy peak which predominates at small values of y is obviously small angle scattering. The value of y is approximately proportional to the sineof half the scattering angle or the scattering angle minus 90°. The energy increases as the angle gets smaller just as predicted by the Klein-Nishina relation. The sharp peak at 910 Kev is believed to be caused largely by Rayleigh scattered radiation; it becomes especially pronounced with the lead scatterer, Fig. 13. The angle to include 60-70 percent of the Rayleigh scattering (Table 4.3) includes more than half the crystal at y = 0.5 cm and some of it at y = 1 cm; none at all at 2.5 cm. The peak at the greater distance, which predominates at the low energies is due, as discussed above, to the increase from shorter path length in the scatterer (and hence less absorption) exceeding the decrease due to greater distance (decreased solid angle and $1/R^2$).

WOOD. This phenomenon is completely lost in the case of wood, In fact the constant secondary electron energy curve for wood, Fig. 9, shows only a slight falling off of counting rate for the smallest values of y; the maximum at low energies occurs at between 1 and 2.5 cm while for aluminum it is about 8 cm, for iron 10 cm, for tin 8 cm, and for lead 5 cm. The situation is obvious except for lead which deserves a later separate discussion. As covered before, the data are higher energy peak which predominates at small values of y is obviously small angle scattering. The value of y is approximately proportional to the sine of half the scattering angle or the scattering angle since 90^0. The energy increases as the angle gets smaller just as predicted by the Klein-Nishina relation. The energy peak at 210 Kev is believed to be caused largely by Rayleigh scattered radiation; it becomes especially pronounced with the lead scatterer, Fig. 12. The angle to include 40-70 percent of the Rayleigh scattering (Table 4.1) includes more than half the crystal at $y = 0.5$ cm and some of it at $y = 1$ cm; none at all at 2.5 cm. The peak at the greater distances, which predominates at the low energies is due, as discussed above, to the increase from shorter path length in the scatterer (and hence less absorption) exceeding the decrease due to greater distance (decreases with angle and $1/R^2$).

Note. This phenomenon is completely lost in the case of wood. In fact the constant secondary electron energy curve for wood, Fig. 9, shows only a slight falling off at counting rate for the smallest values of y; the maximum at low energies occurs at between 1 and 2.1 cm while for aluminum it is about 5 cm, for iron 10 cm, for tin 5 cm, and for lead 4 cm. The situation is obvious except for lead which deserves a later separate discussion. As expected before, the data are plotted against the measured distance y, while the scattering phenomena occur as a function of a relatively unknown distance y' which is the vertical distance between the source-detector plane and a sort of mean-scattering-plane within the scatterer. The difference between y and y' is so pronounced for the low density, lightly absorbing wood, that one would expect little variation in the data taken for 0.5, 1, and 2.5 cm. Figure 4 shows that this is the case, the measured points lying so close to one another that only one curve could be drawn through them.

Wood gave the greatest intensity of low energy scattering as would be expected; its mass scattering coefficient is high because it contains appreciable amounts of hydrogen with Z/A = 1, and its linear absorption coefficient is low because of its low density. And even more important, photoelectric absorption is negligible, even for most of the scattered radiation. The high energy end of the curves is small or zero; any small angle scattering at the depth (y' - y) of the mean-scattering-plane will miss the detector even at the smallest values of y. Therefore the mass of the scatterer which is so disposed as to get high energy scattered radiation into the detector is quite small. The back-scattering peak is defined at y = 30 cm and is indicated at least by all the curves from y = 20 cm on up.

ALUMINUM. Aluminum (Figs. 5 and 10) is so much more dense than wood that its curves more closely resemble those of iron. The low energy scattering is again high; as with wood the photoelectric absorption is low, even for most of the scattered radiation. The high energy build-up is much greater than that of wood and somewhat greater than any of the other scatterers at 600-700 Kev or than any but lead at 910 Kev. This is due to a combination of the effects of relatively strong Compton scattering because Z/A = 0.5, high enough density to get small angle scattered radiation into the detector at small values of y, but low enough density to keep the linear absorption coefficient small, and essentially no photoelectric absorption of primary radiation because of low Z. The back-scattering peak is not well resolved in the case of the aluminum data. Re-examination of the original data yielded very little more indication of it than shown in Fig. 5. No explanation is readily forthcoming.

LEAD. The scattering from lead (Figs. 8 and 13) is interesting because it absorbs strongly the soft scattered radiation, and annoying because the low counting rates obtained under these circumstances are highly subject to the influence of instrumental and statistical errors. The major characteristics of this scattering are:

1. Low intensities at low energies because of very strong photoelectric absorption of energies below 400 Kev.

2. Relatively high intensities at high energies for small and medium values of y because high density and strong photo-absorption of scattered radiation makes $y' \approx y$ and confines detected scattering to a very thin layer near the surface, favoring detection of small angle scattering. The contribution of Rayleigh scattering is certainly significant; its cross section is about 5 percent that of Compton scattering and it is almost entirely confined to a cone of half-apex-angle $\approx 4^{o}$, while the Compton scattering is spread over larger angles; only 0.635 percent of the Compton scattering[D2] is within the cone which contains 60-70 percent of the Rayleigh scattering[F1] making the latter five times as strong within the cone. This cone includes 70 percent of the detector at $y = 0.5$ cm and 20 percent of it at $y = 1$ cm. The 910 Kev peak in Fig. 13 must be due, in a considerable degree, to Rayleigh scattering; the fact that the 1 cm point is higher than the 0.5 cm point seems to be the combined result of the Compton contribution, which is approximately constant per unit solid angle throughout this small range of scattering angles,[D2] and of the strong attenuation of the lead scatterer in the long path lengths at the grazing angles of incidence involved in reaching the detector, particularly at $y = 0.5$ cm.

None of the curves with the lead scatterer show a sharp rise at low energies because of the photo-absorption in lead. That not all of the rise at lower energies is due to the distribution of secondary electrons from the Compton process in the stilbene is shown, however, by the pronounced peak between 50 Kev and 200 Kev for all values of y. These peaks are spread out considerably for y = 2.5 cm, with their highest points at about 120 Kev. This corresponds to a photon energy of 245 Kev and hence is not fluorescence nor bremsstrahlung but scattered gamma radiation. The energy is high and the peak broad because at these small values of y this large angle scattering must come from a considerable range of angles. On the other hand, as shown before, for y = 45 cm the angles are not so widely distributed and the peak should be at the same energy as that obtained with the tin scatterer; they are both in fact at about 90 Kev showing remarkably good agreement. The peaks at intermediate distances lie conveniently between the two values discussed except for that obtained with y = 20 cm. A slightly different plotting within the expected deviation of the 62 Kev and the 85 Kev points would put this one also in line, so no real significance can be attached to any difference it shows.

Fluorescence of 75 Kev and bremsstrahlung with a maximum at 100 Kev are to be expected from the lead scatterer;

either or both may be present but they will merge with the back-scattered peaks and could not be resolved.

Examining the relative liklihood of finding 85 KV secondary electrons in stilbene (or biological tissue) from scattering of Co^{60} gamma radiation, as a function of the atomic number of the scatterer, Fig. 14 was plotted. Wood gives the greatest contribution at distances up to 5 cm, aluminum the most from 5 to 24 cm, and iron for greater than 24 cm. Aluminum, surprisingly enough, cuts down to zero at the smallest value of y of any of the scatterers.

A relatively uninteresting experiment (Fig. 17) with wood showed that removing the outer two-thirds of the scatterer had negligible effect on high energy components at y = 0.5 cm, and caused a 10-30 percent reduction in the secondary electron count at low energies. This is evidence of the familiar workings of the Klein-Nishina relation. This same reduction in area had a much more striking effect on the curves for y = 60 cm whose ordinates decreased by more than 90 percent. Presumably this represents a 67 percent loss due to removal of scatterer and a considerable loss of photons entering the remaining part due to transmission out through its sides.

The only experiment completed to determine the effect of varying E_o was the measurement of the build-up of Cs^{137}

radiation scattered from tin (Figs. 18 and 19). The curves of build-up are a little complicated, resembling in some ways the Co^{60} scattering curves with tin (Fig. 7) and in other ways those with lead (Fig. 8). The build-up is much less than with the higher energy Co^{60}. At low energies the maximum build-up is at y = 10 cm. Curves at small values of y start out lower at the lower energies and wind up higher at the higher energies. The 225 Kev curve of constant secondary electron energy shows the same double peak as a result of this, the peaks for lower energies following the peak with greater y, and the one at higher energy following the peak at lower y.

The build-up curves showed a peak for almost all values of y, a broad one peaked at 90 Kev for y = 0.5 and sharper ones peaked at about 60 Kev for higher values of y. The 180° back-scattered peak is calculated to give secondary electrons of a maximum energy of 63 Kev which is excellent agreement with the above. The higher mean energy of the broader peak at short distances is to be expected from the inclusion of angles considerably less than 180°, in a manner similar to that observed for Pb at y = 2.5 cm.

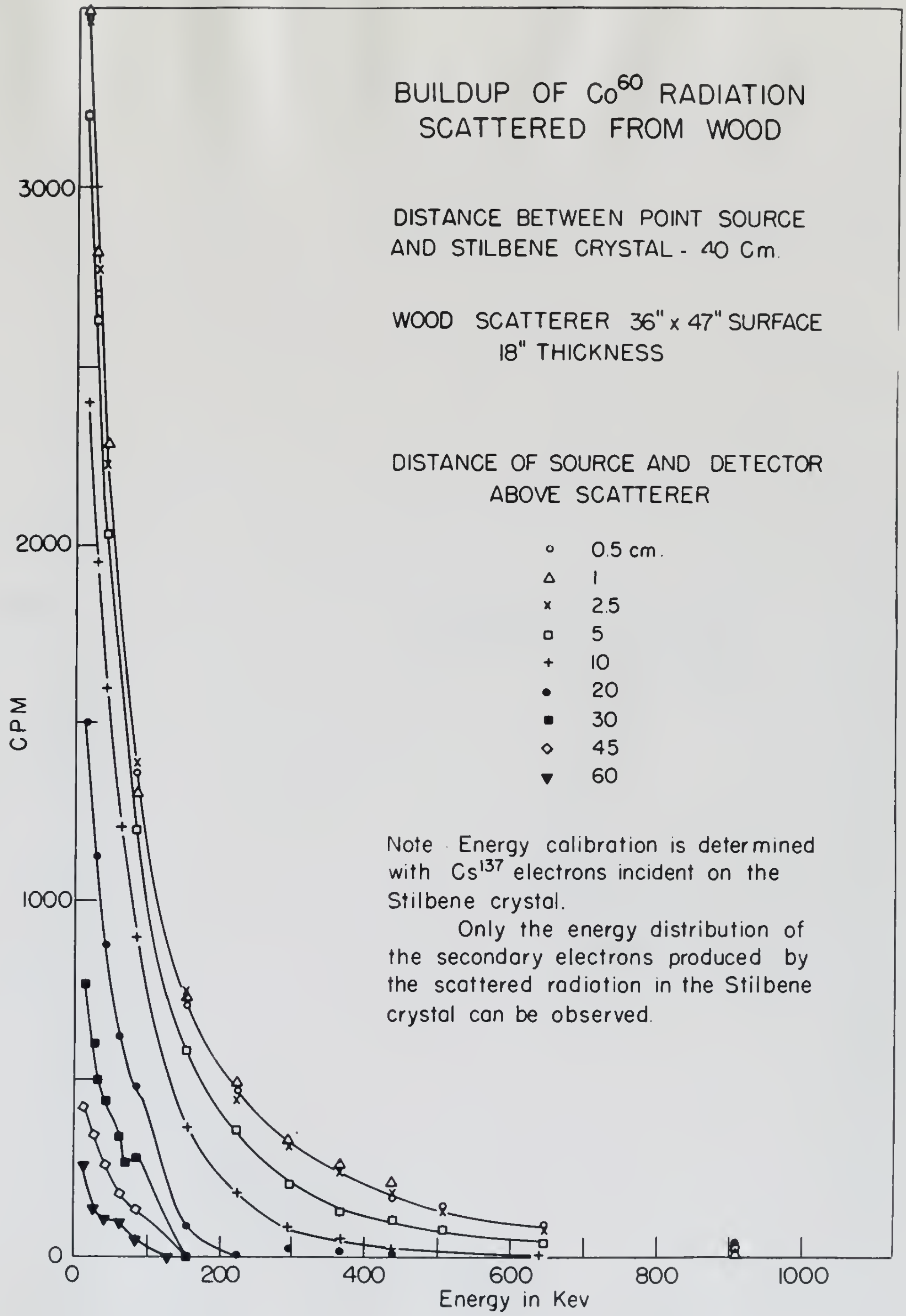
BUILDUP OF Co60 RADIATION SCATTERED FROM WOOD
DISTANCE BETWEEN POINT SOURCE AND STILBENE CRYSTAL - 40 Cm.
WOOD SCATTERER 36" x 47" SURFACE 18" THICKNESS
DISTANCE OF SOURCE AND DETECTOR ABOVE SCATTERER
0.5 cm.
1
2.5
5
10
20
30
45
60
Note Energy calibration is determined with Cs137 electrons incident on the Stilbene crystal.
Only the energy distribution of the secondary electrons produced by the scattered radiation in the Stilbene crystal can be observed.
CPM
3000
2000
1000
0
0
200
400
600
800
1000
Energy in Kev

Figure 4

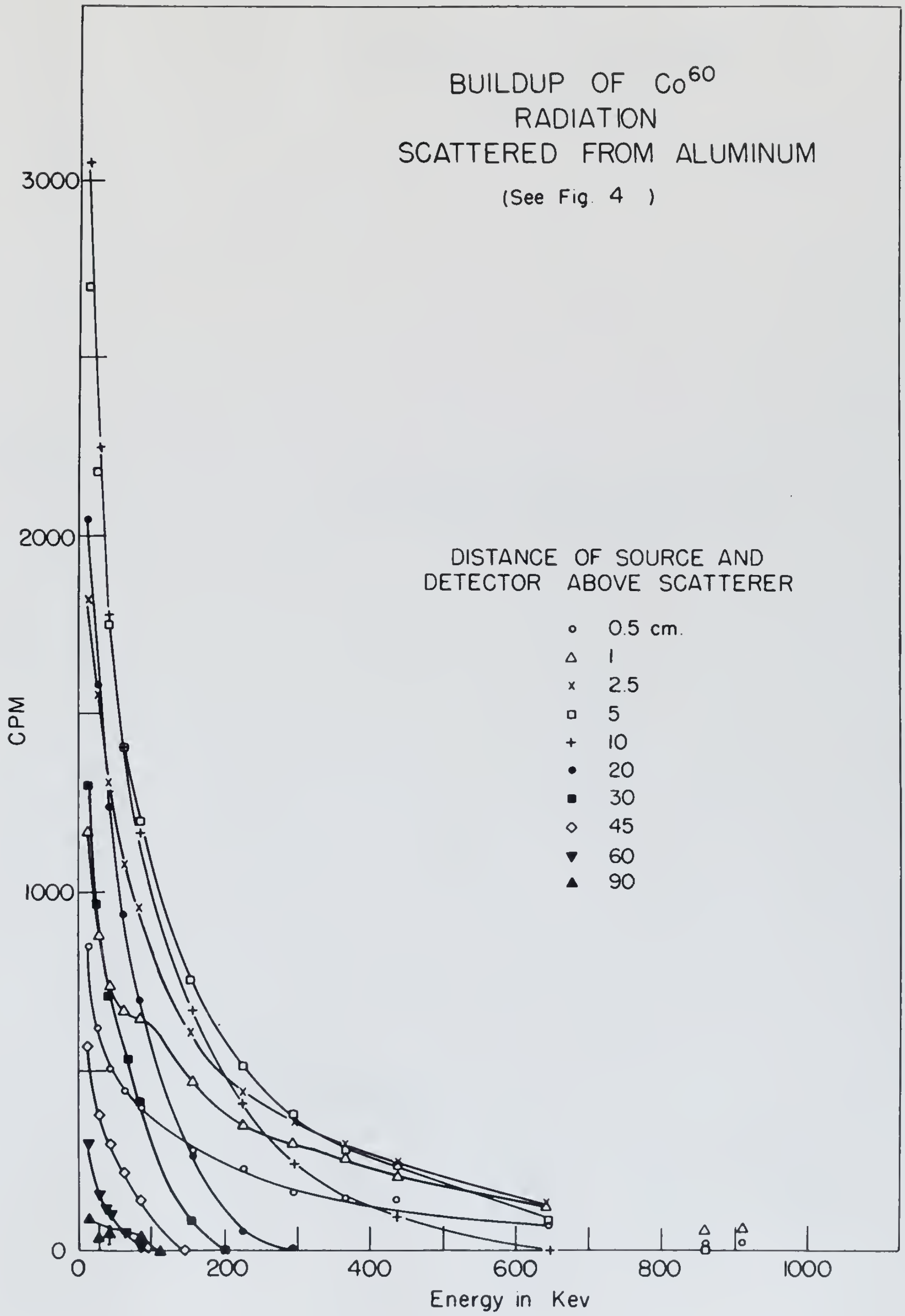
BUILDUP OF Co^{60}
RADIATION
SCATTERED FROM ALUMINUM
(See Fig. 4)
DISTANCE OF SOURCE AND
DETECTOR ABOVE SCATTERER
0.5 cm.
1
2.5
5
10
20
30
45
60
90
CPM
3000
2000
1000
0
0
200
400
600
800
1000
Energy in Kev

Figure 5

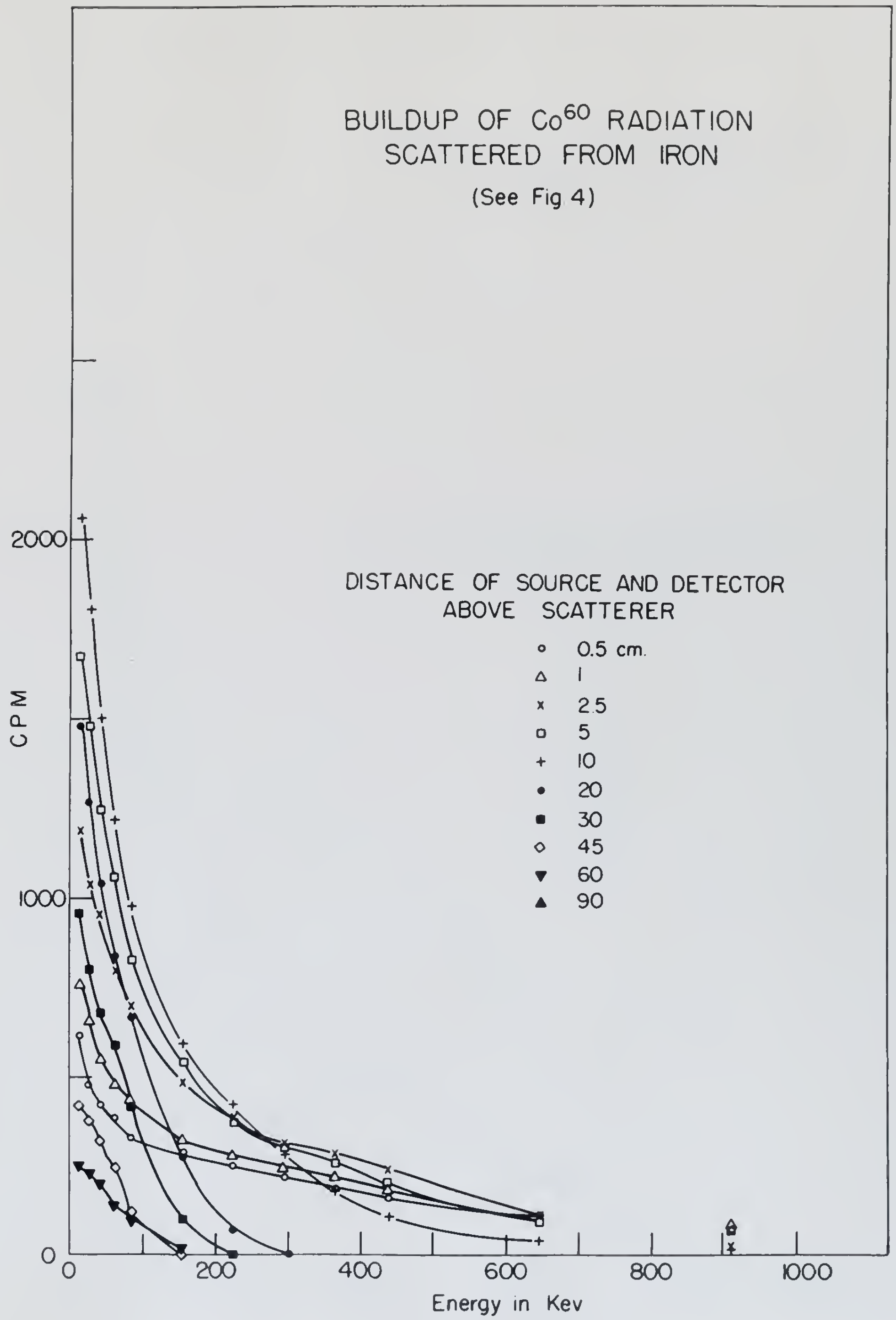
BUILDUP OF Co^{60} RADIATION
SCATTERED FROM IRON
(See Fig 4)
DISTANCE OF SOURCE AND DETECTOR
ABOVE SCATTERER
0.5 cm.
1
2.5
5
10
20
30
45
60
90
CPM
2000
1000
0
0
200
400
600
800
1000
Energy in Kev

Figure 6

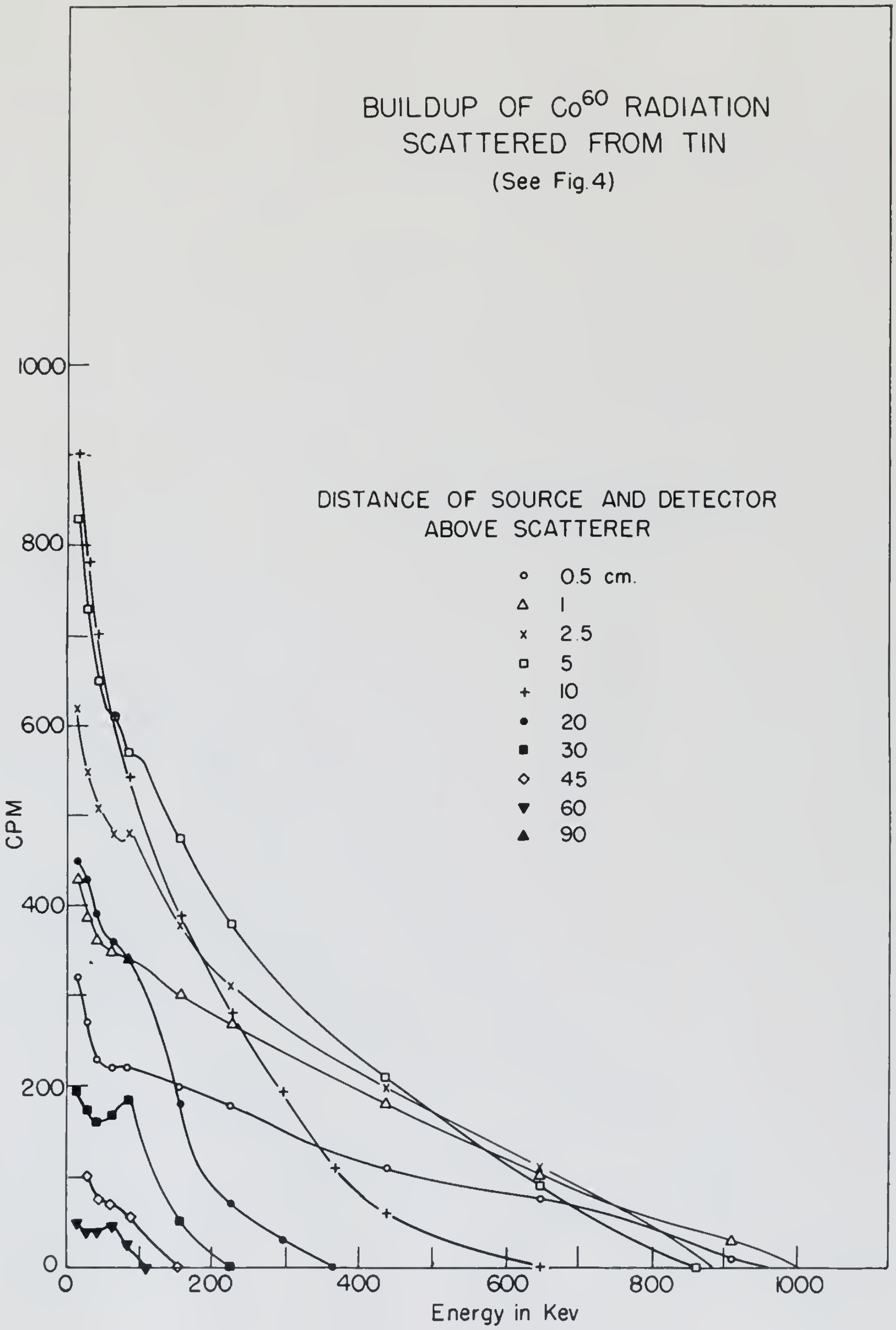
BUILDUP OF Co^{60} RADIATION
SCATTERED FROM TIN
(See Fig. 4)
DISTANCE OF SOURCE AND DETECTOR
ABOVE SCATTERER
0.5 cm.
1
2.5
5
10
20
30
45
60
90
CPM
1000
800
600
400
200
0
0
200
400
600
800
1000
Energy in Kev
Figure 7

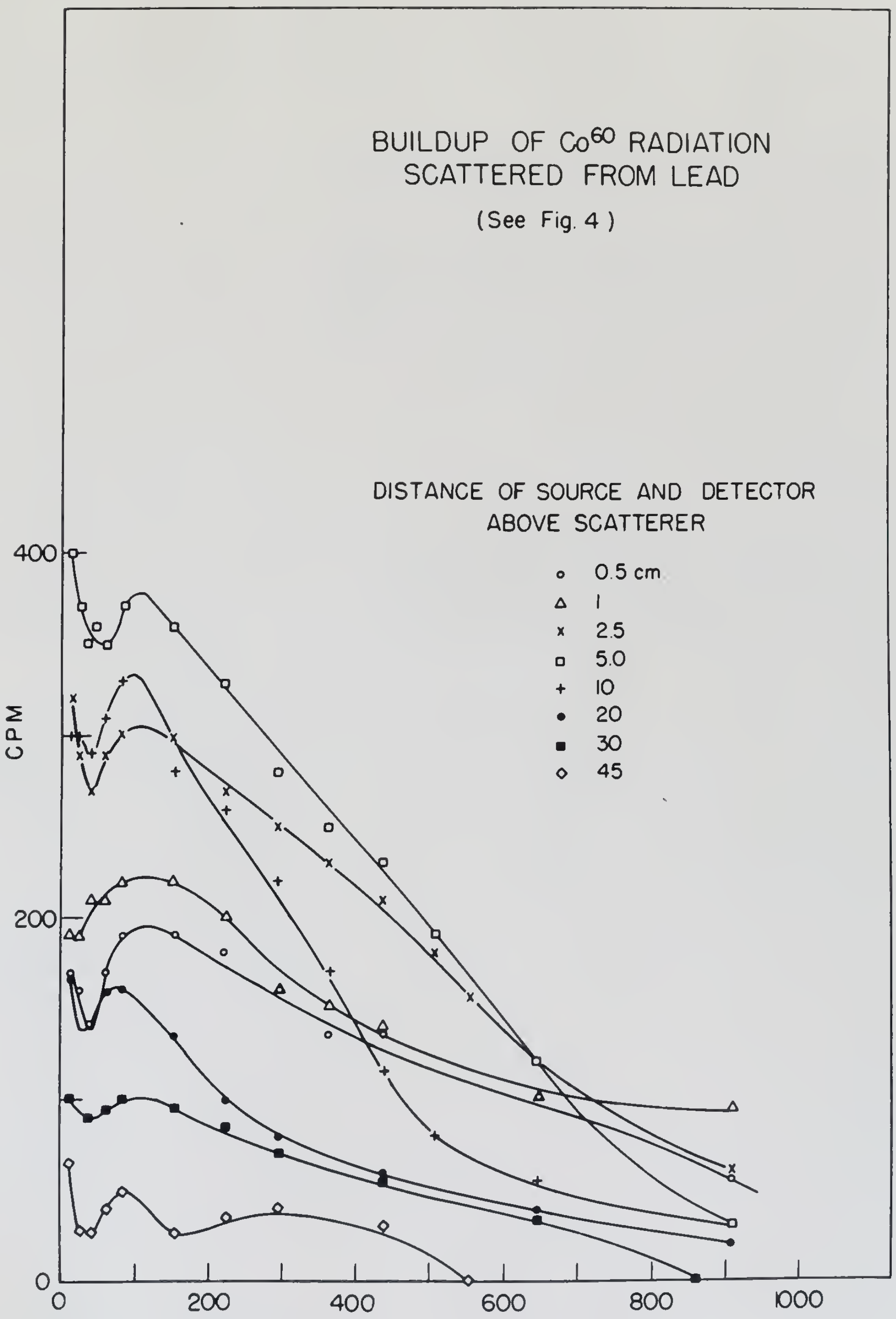

BUILDUP OF Co60 RADIATION SCATTERED FROM LEAD
(See Fig. 4)
DISTANCE OF SOURCE AND DETECTOR ABOVE SCATTERER
0.5 cm
1
2.5
5.0
10
20
30
45
CPM
400
200
0
0
200
400
600
800
1000
Energy in Kev.

Figure 8

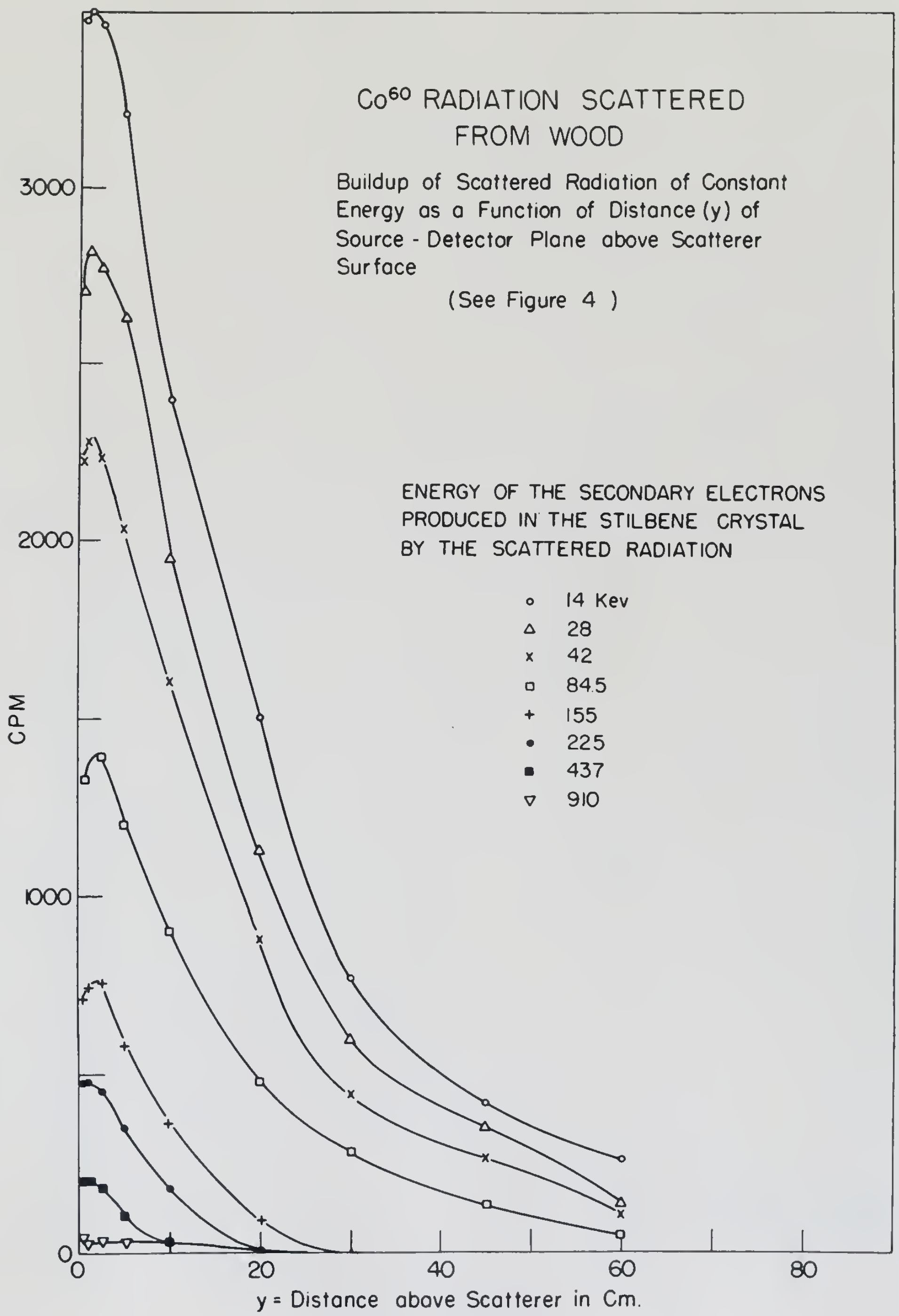
Co^{60} RADIATION SCATTERED FROM WOOD
Buildup of Scattered Radiation of Constant Energy as a Function of Distance (y) of Source - Detector Plane above Scatterer Surface
(See Figure 4)
ENERGY OF THE SECONDARY ELECTRONS PRODUCED IN THE STILBENE CRYSTAL BY THE SCATTERED RADIATION
○ 14 Kev
△ 28
x 42
□ 84.5
+ 155
● 225
■ 437
▽ 910
CPM
3000
2000
1000
0
0
20
40
60
80
y = Distance above Scatterer in Cm.

Figure 9

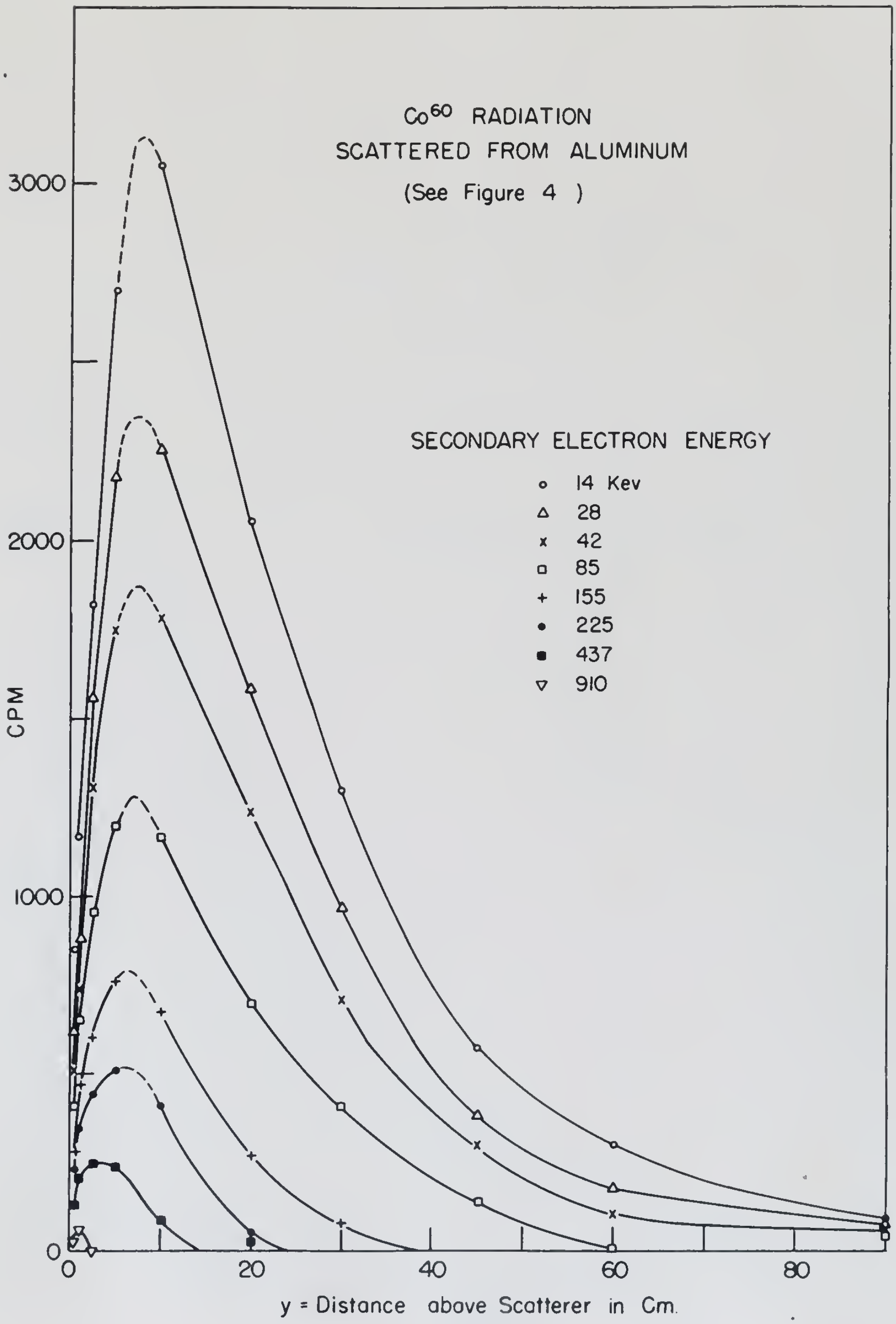

Co60 RADIATION
SCATTERED FROM ALUMINUM
(See Figure 4)
SECONDARY ELECTRON ENERGY
14 Kev
28
42
85
155
225
437
910
3000
2000
1000
0
CPM
0
20
40
60
80
y = Distance above Scatterer in Cm.

Figure 10

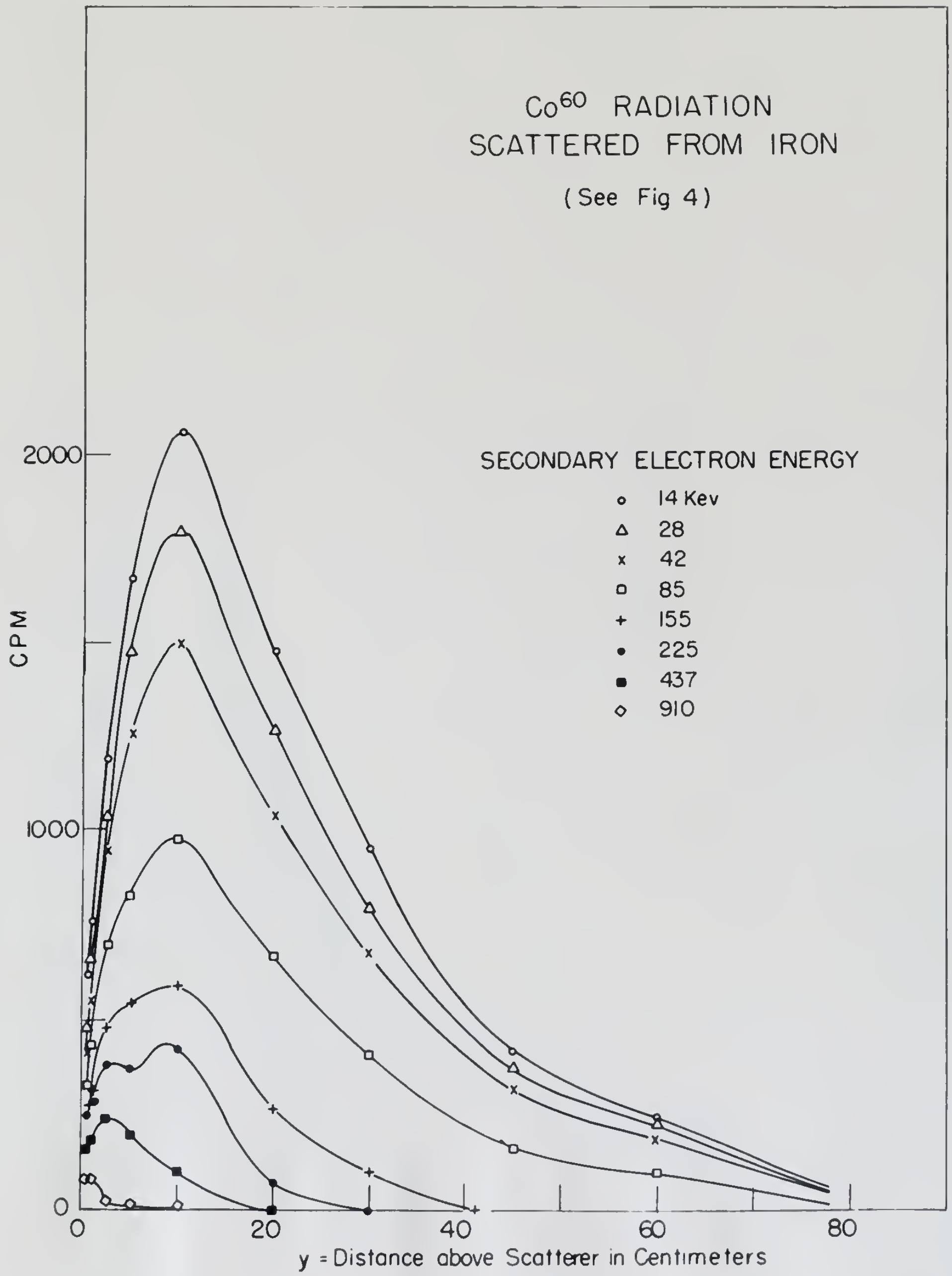

Co^{60} RADIATION
SCATTERED FROM IRON
(See Fig 4)
SECONDARY ELECTRON ENERGY
14 Kev
28
42
85
155
225
437
910
CPM
2000
1000
0
0
20
40
60
80
y = Distance above Scatterer in Centimeters

Figure 11

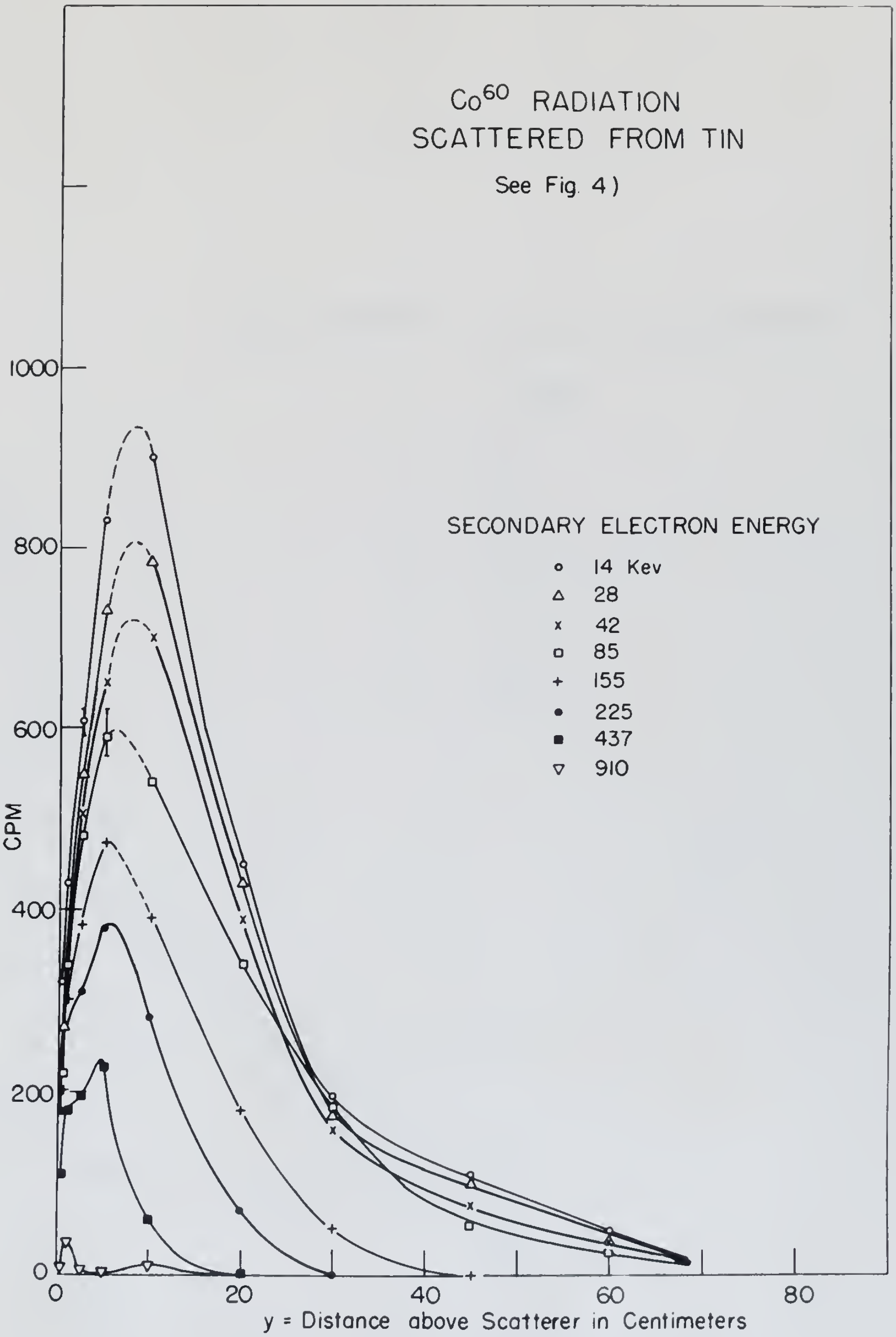

Co^{60} RADIATION
SCATTERED FROM TIN
See Fig. 4)
SECONDARY ELECTRON ENERGY
14 Kev
28
42
85
155
225
437
910
CPM
1000
800
600
400
200
0
0
20
40
60
80
y = Distance above Scatterer in Centimeters

Figure 12

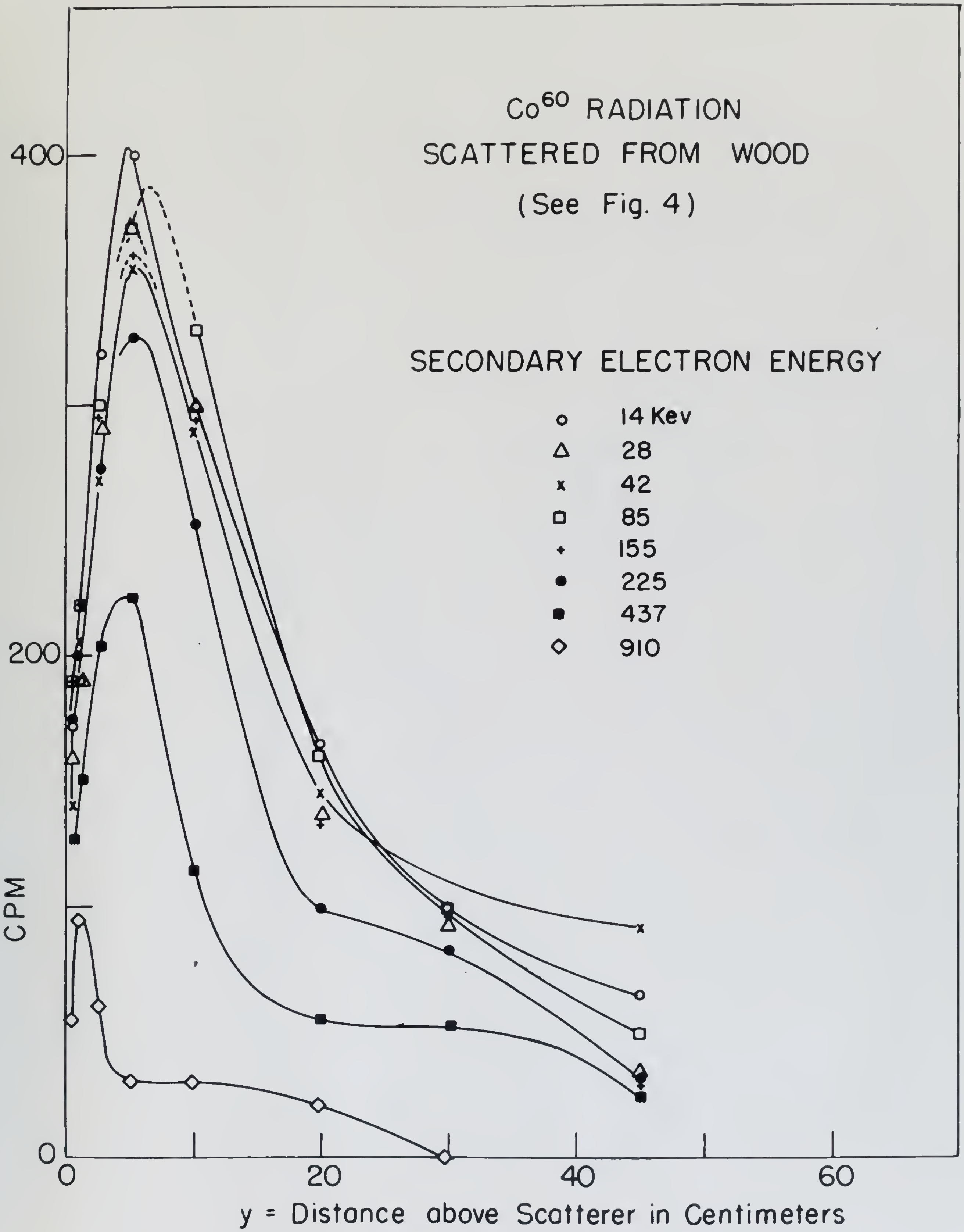
Co^{60} RADIATION
SCATTERED FROM WOOD
(See Fig. 4)
SECONDARY ELECTRON ENERGY
○ 14 Kev
△ 28
x 42
□ 85
+ 155
● 225
■ 437
◇ 910
400
200
0
CPM
0
20
40
60
y = Distance above Scatterer in Centimeters

Figure 13

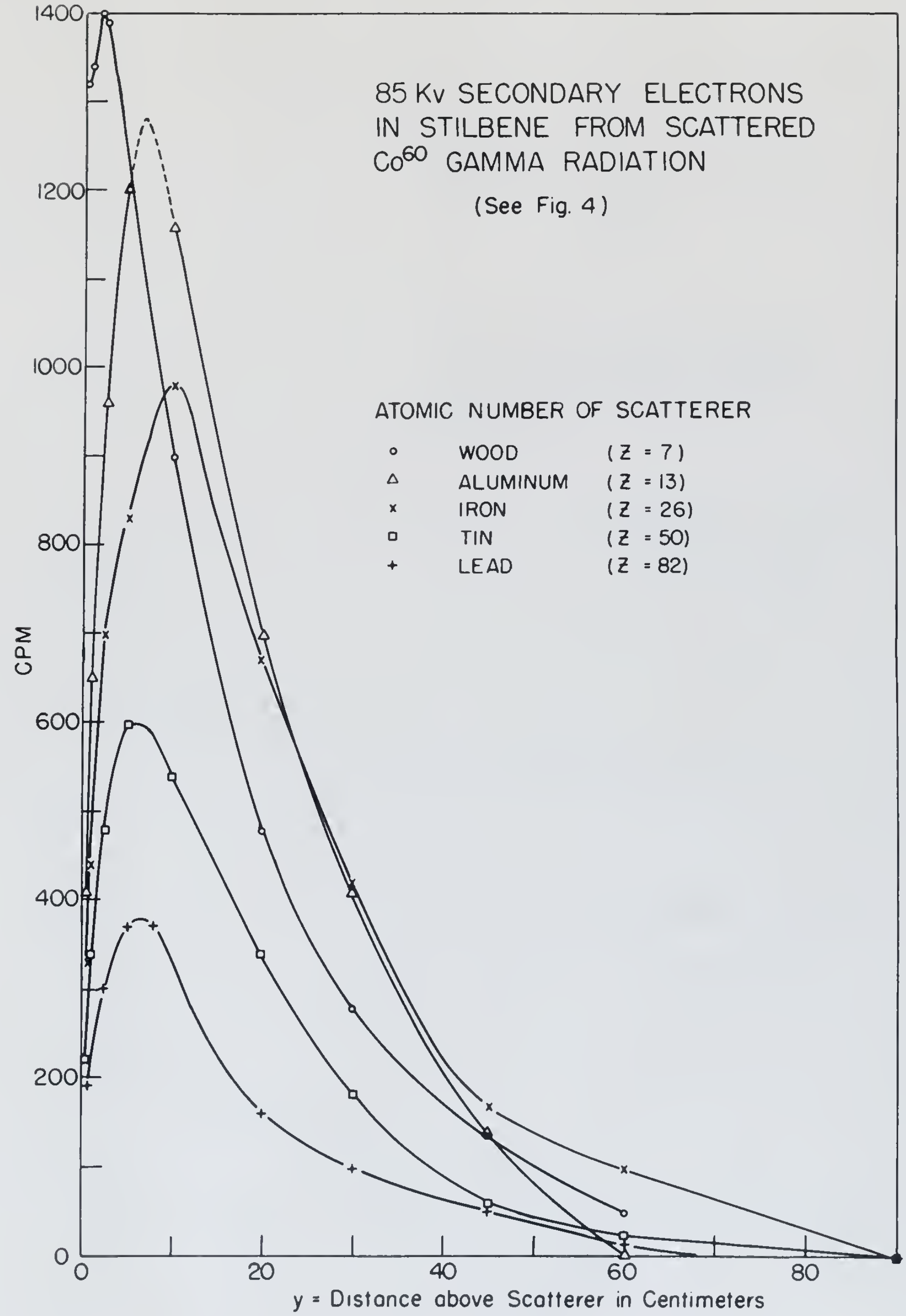

85 Kv SECONDARY ELECTRONS
IN STILBENE FROM SCATTERED
Co60 GAMMA RADIATION
(See Fig. 4)
ATOMIC NUMBER OF SCATTERER
o WOOD (Z = 7)
Δ ALUMINUM (Z = 13)
x IRON (Z = 26)
□ TIN (Z = 50)
+ LEAD (Z = 82)
1400
1200
1000
800
600
400
200
0
CPM
0
20
40
60
80
y = Distance above Scatterer in Centimeters

Figure 14

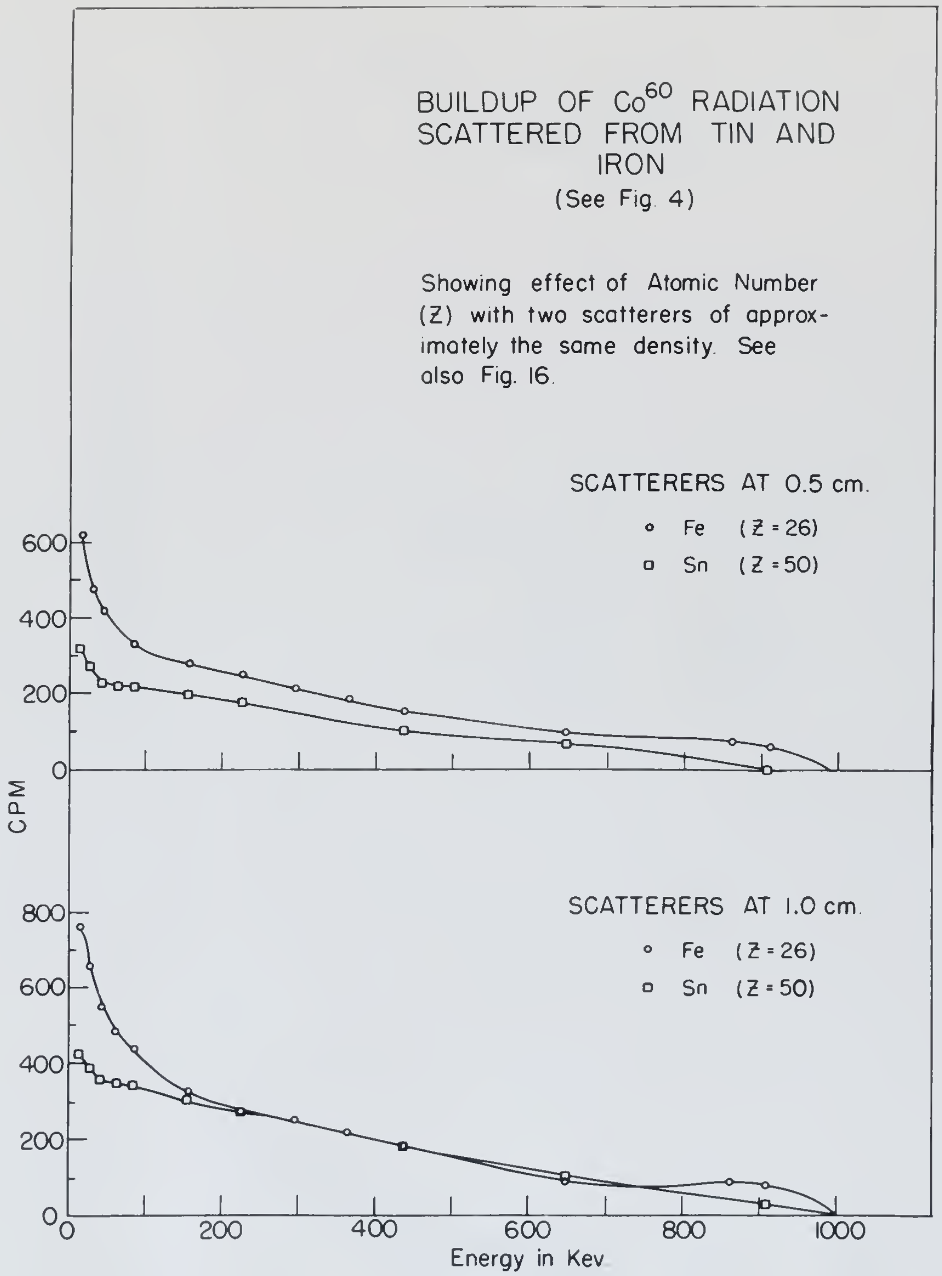

BUILDUP OF Co60 RADIATION SCATTERED FROM TIN AND IRON
(See Fig. 4)
Showing effect of Atomic Number (Z) with two scatterers of approximately the same density. See also Fig. 16.
SCATTERERS AT 0.5 cm.
Fe (Z = 26)
Sn (Z = 50)
SCATTERERS AT 1.0 cm.
Fe (Z = 26)
Sn (Z = 50)
CPM
600
400
200
0
800
600
400
200
0
0
200
400
600
800
1000
Energy in Kev

Figure 15

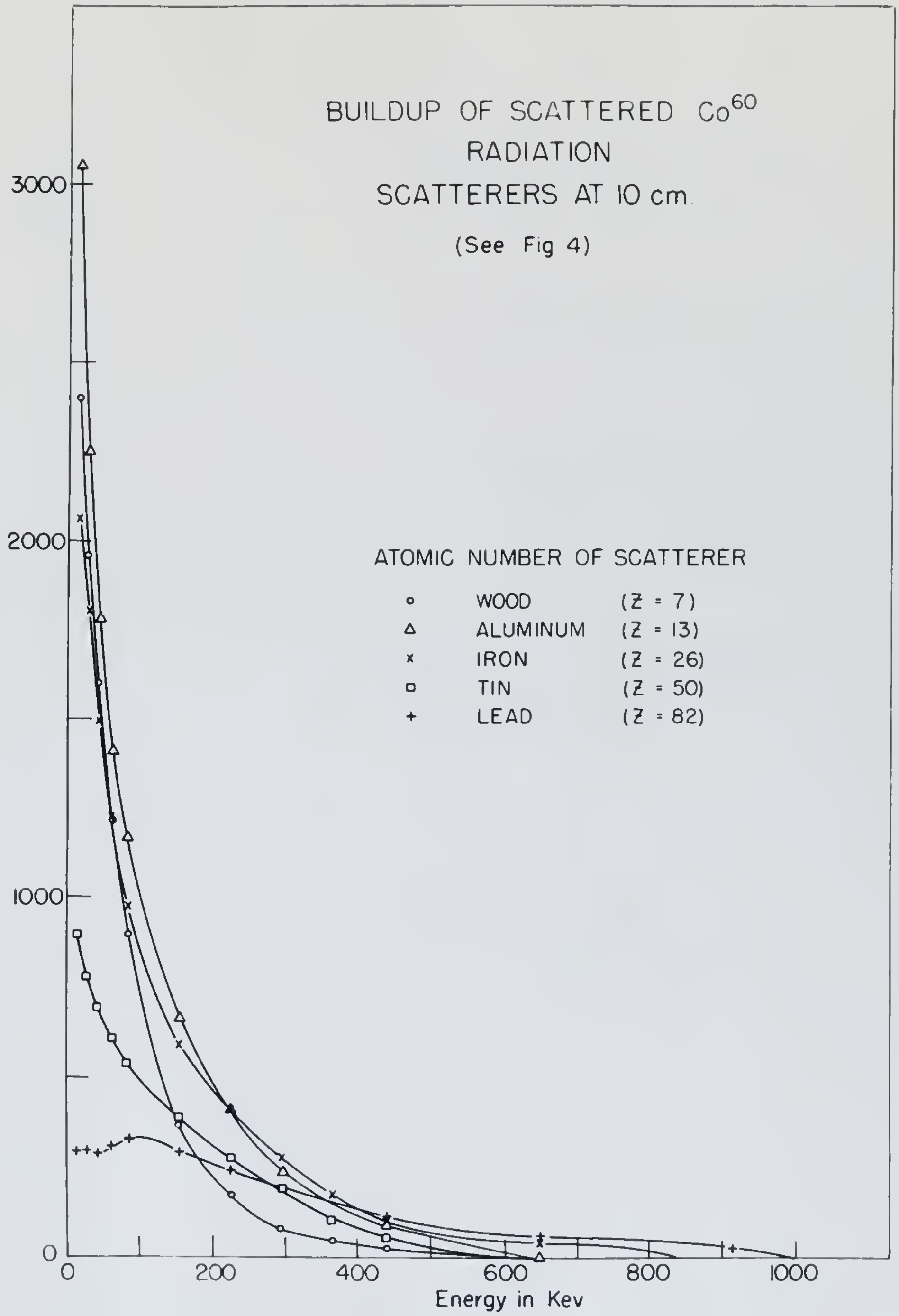

BUILDUP OF SCATTERED Co60
RADIATION
SCATTERERS AT 10 cm.
(See Fig 4)
ATOMIC NUMBER OF SCATTERER
WOOD (Z = 7)
ALUMINUM (Z = 13)
IRON (Z = 26)
TIN (Z = 50)
LEAD (Z = 82)
3000
2000
1000
0
0
200
400
600
800
1000
Energy in Kev

Figure 16

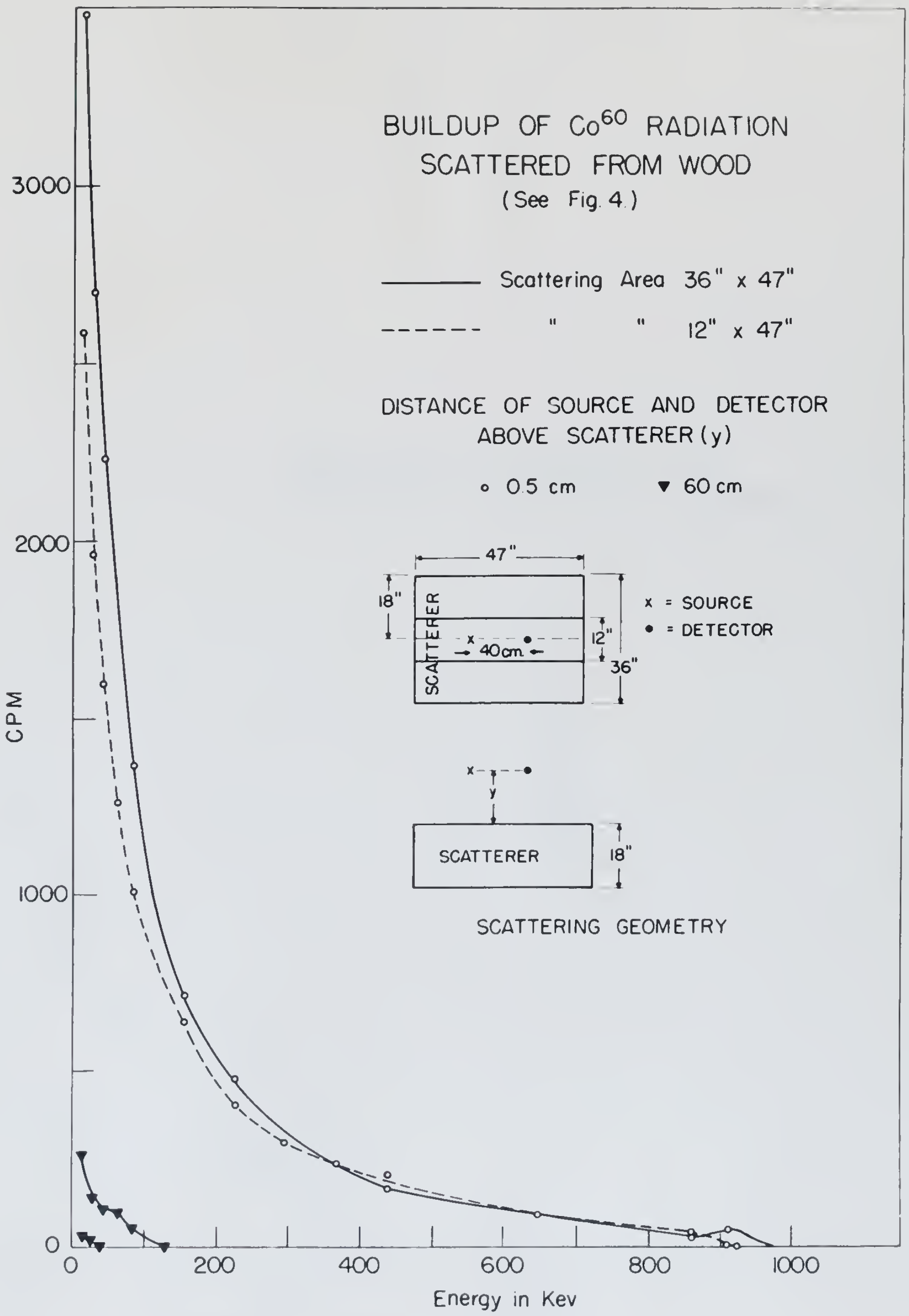
BUILDUP OF Co^{60} RADIATION
SCATTERED FROM WOOD
(See Fig. 4.)
Scattering Area 36" x 47"
" " 12" x 47"
DISTANCE OF SOURCE AND DETECTOR
ABOVE SCATTERER (y)
0.5 cm
60 cm
47"
18"
SCATTERER
x = SOURCE
• = DETECTOR
12"
40 cm
36"
y
SCATTERER
18"
SCATTERING GEOMETRY
CPM
3000
2000
1000
0
0
200
400
600
800
1000
Energy in Kev

Figure 17

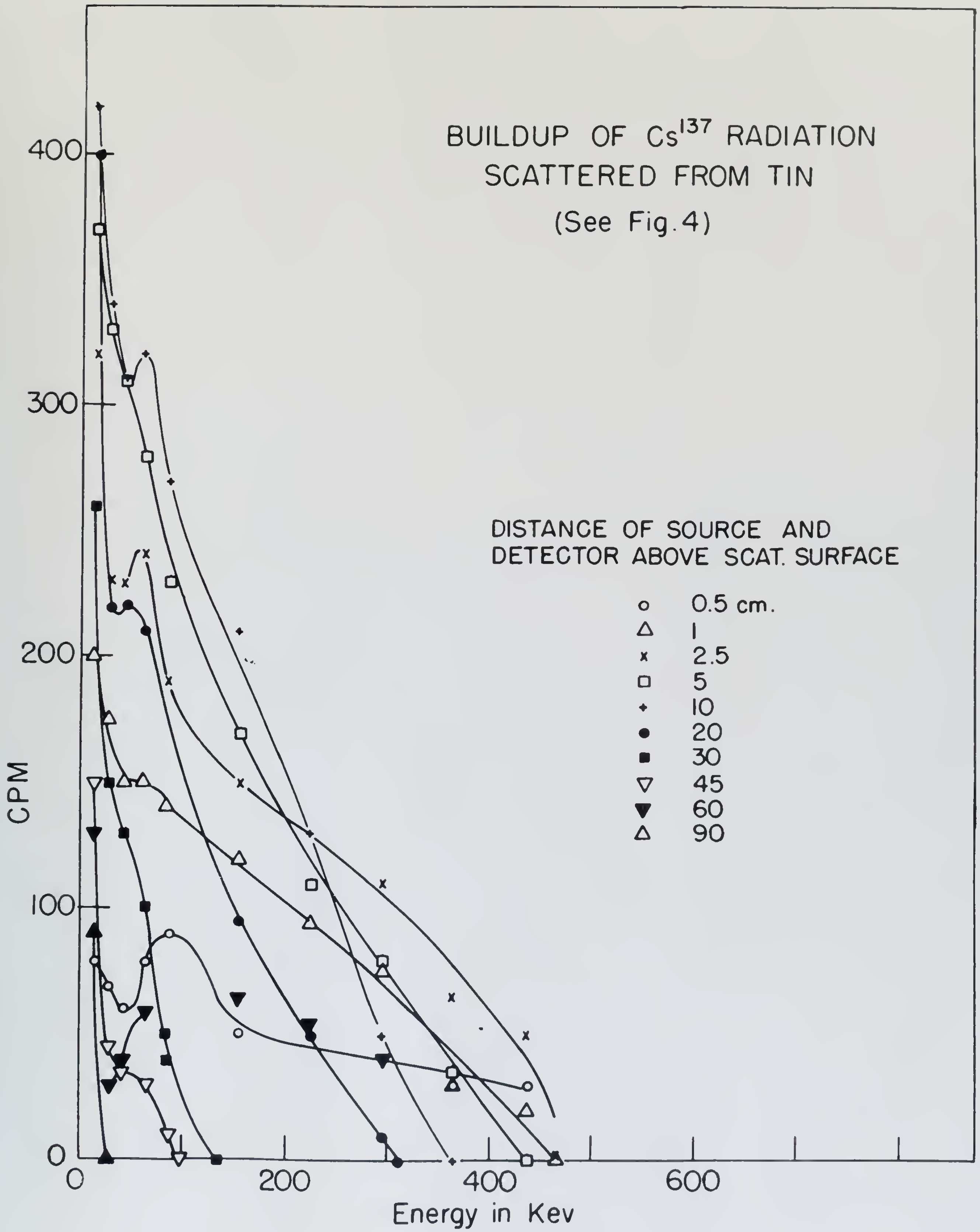
BUILDUP OF Cs137 RADIATION
SCATTERED FROM TIN
(See Fig. 4)
DISTANCE OF SOURCE AND
DETECTOR ABOVE SCAT. SURFACE
0.5 cm.
1
2.5
5
10
20
30
45
60
90
CPM
400
300
200
100
0
0
200
400
600
Energy in Kev

Figure 18

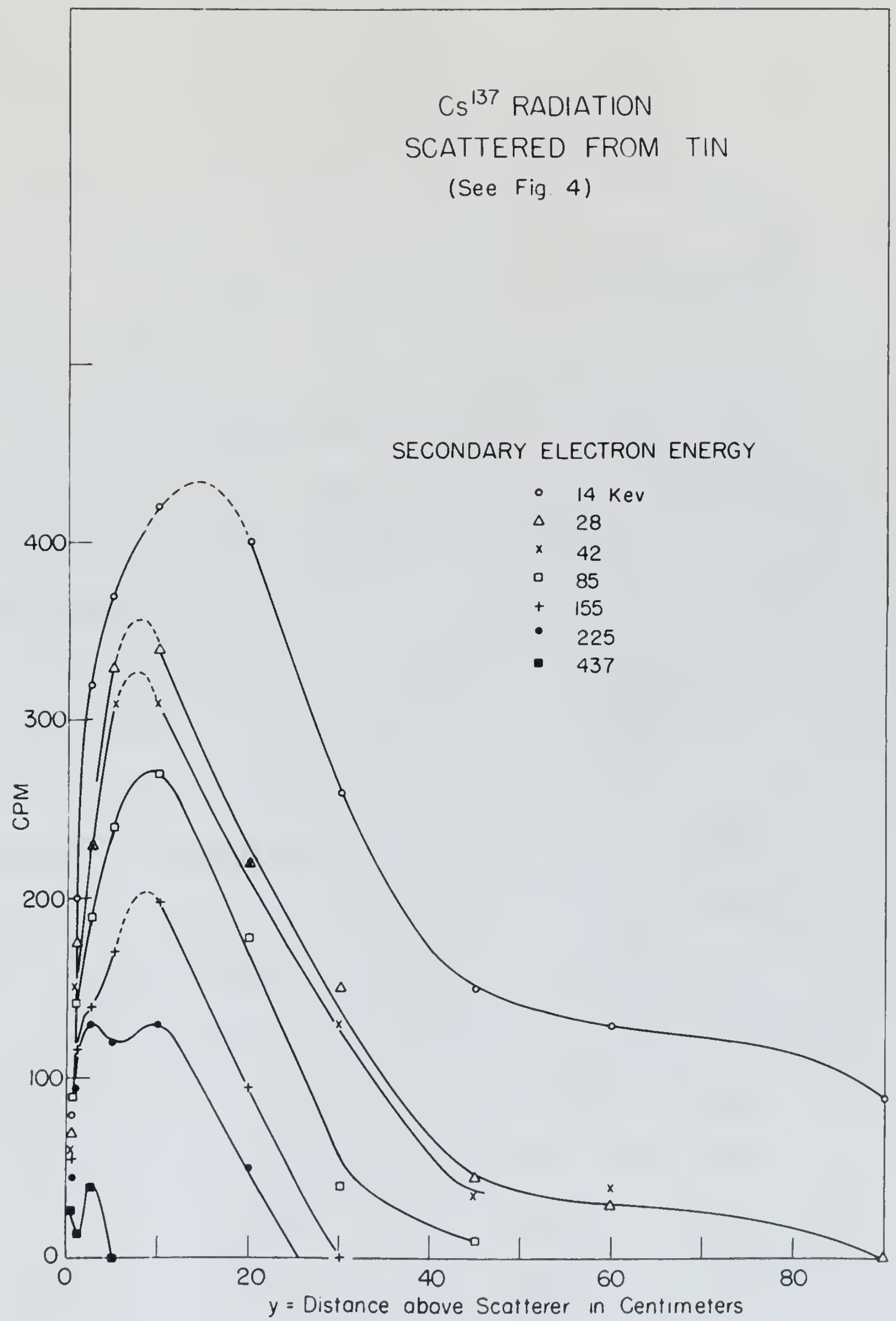
Cs^{137} RADIATION
SCATTERED FROM TIN
(See Fig. 4)
SECONDARY ELECTRON ENERGY
14 Kev
28
42
85
155
225
437
CPM
400
300
200
100
0
0
20
40
60
80
y = Distance above Scatterer in Centimeters

Figure 19

V. SUMMARY AND RECOMMENDATIONS

A. SUMMARY.

1. Co^{60} was used as a radiation source and stilbene as an organic scintillator. They were kept in a horizontal line of constant orientation, 40 cm apart. Both were simultaneously moved vertically towards and away from various scattering materials.

2. The following scattering materials were used: wood, aluminum, iron, tin, and lead. Each was of sufficient thickness to be termed a "semi-infinite" scatterer.

3. Measurements were made as follows: the radiation penetrated the lightshield and stilbene crystal where it ejected Compton secondary electrons. These secondary electrons caused ionization and the emission of light. The light was converted to electrical charge by an RCA 6199 photomultiplier tube. Flow of this charge through a resistor in the input of a linear amplifier caused a voltage drop which triggered a pulse through the amplifier. The amplified pulse was classified as to energy by a differential discriminator of 2 volt window width and with base line continuously shifted by electrically driven scanner. The output of the discriminator fed a counting rate meter which in turn fed an Esterline-Angus recording ammeter which drew the energy spectrum of the secondary electrons in the stilbene.

V. SUMMARY AND RECOMMENDATIONS

A. SUMMARY.

1. Co^{60} was used as a radiation source and stilbene as an organic scintillator. They were kept in a horizontal line of constant orientation, 40 cm apart. Both were simultaneously moved vertically towards and away from various scattering materials.

2. The following scattering materials were used: wood, aluminum, iron, tin, and lead. Each was of sufficient thickness to be termed a 'semi-infinite' scatterer.

3. Measurements were made as follows: the radiation penetrated the lightshield and stilbene crystal where it ejected Compton secondary electrons. These secondary electrons caused ionization and the emission of light. The light was converted to electrical charge by an RCA 6199 photomultiplier tube. Flow of this charge through a resistor in the input of a linear amplifier caused a voltage drop which triggered a pulse through the amplifier. The amplified pulse was classified as to energy by a differential discriminator of 1 volt window width and with base line continuously shifted by electrically driven scanner. The output of the discriminator fed a counting rate meter which in turn fed an Esterline-Angus recording ammeter which drew the energy spectrum of the secondary electrons in the stilbene.

4. A spectrum taken with no scatterer was subtracted from each spectrum taken with a scatterer. The difference was plotted as "Build-up of Co^{60} Radiation Scattered from .." (Figs. 4-8 incl.).

5. These data are also presented by plotting for each of several constant values of secondary electron energy the curve of n vs y where n is the counting rate and y is the distance between the source detector plane and the top surface of the scatterer (Figs. 9-13 incl.).

6. Additional curves were prepared as follows:

a plot of n vs y for a single energy and for 5 different scatterers (Fig. 14),

a comparison of the behaviour of two scattering media of about the same density, iron and tin (Figs. 15 and 16),

a plot of the effect of removing part of the wood scatterer (Fig. 17).

7. A similar experiment was conducted with Cs^{137} as a source and with tin as the scatterer. A curve as described in (4) and one as described in (5) above, were prepared (Figs. 18 and 19 respectively).

8. A qualitative discussion is presented for each figure explaining the maxima, and the variations in intensity, observed, by considering angular distribution shown in Compton-Rayleigh scattering, and taking into account the absorption

of the scattered gammas by photoelectric effect in high Z materials.

9. Most of the observed phenomena were satisfactorily explained on the basis of existing knowledge but a few features will require further observations for verification and clarification.

B. RECOMMENDATIONS FOR FURTHER WORK.

1. The following additional investigation is recommended in this immediate area:

a. Perform, with monoenergetic gamma-ray sources of different energy, the same experiments done here with Co^{60}, particularly to determine to what extent the effects noted are general and to what extent, if any, they are specific to Co^{60}. (This has already been started with Cs^{137}.)

b. Investigate multiple scattering by adding a scattering medium above the source-detector plane. Keeping the source-detector plane parallel to the surfaces of the two scatterers, measure the build-up for various positions between the scatterers and for various separations of the scatterers. (This has already been started for wood with separation of 30 cm with y = 0.5, 10, 15, 20, and 29.5 cm; separation of 10.5 cm with y = 0.5, 5.25, 10 cm; and separation of 1 cm).

c. Extend the multiple scattering experiment for at least one value of the separation to include closing

the gap between the scatterers with vertical scattering material, leaving however a clear channel for the primary radiation.

d. Because of the practical importance of scattering from concrete, so common both as a structural and as a shielding material, make measurements of the build-up of Co^{60} and Cs^{137} radiation scattered from concrete of thickness $\geq$ 2 mfp.

e. For the spectra experimentally obtained in this investigation, determine by the method of Prestwich and Colvin[P3] the average secondary electron energy, the energy absorbed per gram of stilbene, and the dosage. This should be done for the entire spectra and for portions of each spectrum above given energies as this latter will give an approximation of dosage in spite of shielding ("approximation" because of build-up factor in such shielding).

2. The following recommendations are made relative to improving the equipment used in this investigation:

a. Modify the counting rate meter to eliminate the small amount of instability, primarily a sensitivity to changes in line voltage. If feasible, also provide it with integrating circuits of smaller time constant; the higher integration rates now provided will probably never be needed in this laboratory and rate 1 is now defective. The change should be patterned after the most recent counting rate meter

constructed here, which is quite satisfactory.

b. Provide a more stable high voltage supply.

c. Provide stable source of 60 cycle A.C. line voltage between 110 and 115 volts.

APPENDIX A

USE OF THE RCA 6199 PHOTOMULTIPLIER TUBE

It appears appropriate to document the tests made and experience gained with the RCA 6199 Multiplier Phototube.[R5] The significant features of this tube are its smaller size than the 5819, flat end window, more uniform photocathode, and improved signal to noise ratio. It has spectral response S-4 with maximum response at 4000 ± 500Å. The photocathode is circular and semi-transparent with a window of area = 1.2 sq. in., minimum diameter = 1.24", minimum diameter of flat surface 1" and index of refraction 1.51. Its overall length is 4 3/8" ± 3/16", seated length 3 7/8" ± 3/16", maximum diameter 1 9/16", using a duodecal socket.

The rated maximum anode supply voltage is 1250 D.C. or peak A.C.; our experience indicates 1080 volts, where the rated gain is 10^6, is highly satisfactory. Operating it at 1080 volts with no scintillator and with the same rubber glove lightshield as employed for the scattering experiment, no dark current was read at the linear amplifier gain usually used with Co^{60} and the 3/8" diam. × 3/8" long stilbene scintillator. This was true even with the discriminator

base line at 1 volt and operating it as an integral discriminator. This was repeated many times at widely dispersed intervals. No cooling was necessary; the tube operated at normal laboratory temperature (65^{o}-90^{o}F).

The resolution obtained with one tube was tested using anthracene as a scintillator and the internal conversion electrons of Cs^{137} as the source. On the basis of these tests a good circuit was chosen from among several suggested or locally conceived. This circuit (Fig. 20) is one suggested by NRL[F18, H14] and the mounting used designated NRL No. 1, Mod. 1 is one constructed at NRL with features which permit its submersion in water if necessary. Another feature of this mounting is that it presents minimum mass and minimum area so as to reduce any scattering into the detector. No preamplifier is used with it, the capacity of the grounded shielded cable providing a leak which reduces noise in the same ratio as signal. This arrangement led to no noise from the photomultiplier, reasonable gain on the amplifier, and elimination of the preamp, which would otherwise be a source of noise, and a source of scattering placed close to the detector. No dropping resistor was provided at the tube; the one in the input circuit of the model 204-B linear amplifier served this purpose.

The resolution of this, and of all subsequent tubes received was then measured with NaI(Tl) scintillator. At

first a freshly cleaved crystal in mineral oil was used but a canned crystal with MgO reflector was found to be slightly better and was substituted. Still further improvement was obtained by changing from mineral oil to Dow Corning 200 fluid, 10^6 centistokes viscosity. This was later changed to 6×10^5 centistokes viscosity Dow Corning 200 fluid for greater convenience in mounting.

Resolution was measured by taking the energy spectrum of Cs^{137}. The width of the photopeak at half maximum, divided by the position of the photopeak, was used as the primary criterion of the resolution. As a secondary criterion there was also used the ratio of the counting rate at the photo peak to that at the preceding "valley".

Table A-1 shows the results. The average resolution of 10 of the 6199's was less than 11 percent which was the resolution of the best of over 50 5819's tested previously. And of the over 50 5819's only 3 were even comparable with those 10 6199's. (It is understood the 5819 has also been somewhat improved since the above mentioned tests were made.) Two of the 6199's showed 9 1/4 percent resolution as an average of 8 and 12 runs respectively. Hoover,[H14] at NRL, had reported even better resolution and also a distinct dependence of this resolution on voltage; only a slight dependence of this kind was found. In the table under the

W

Tube	Remarks
61A	Defective. Microphonic. Returned to manufacturer.
61B	
	Statistics poor.
	Based on 9 runs.
	Optimum based on 8 runs, shielded on 12 runs.
61C	
	Poor statistics.
61D	Optimum based on 9 runs.
	Poor statistics on determination of optimum.
	Optimum figure based on 12 runs.
	Poor statistics
61E	
	Made 3 separate applications of crystal to verify.
F	
61G	This tube has phenomenal gain but is quite noisy. Not microphonic at 1080v. At 750v resolution was not consistent. Statistics poor on other voltages.
VA1	
VA2	Poor statistics.
	Poor statistics.
VA3	Poor statistics.
VA4	Poor statistics.
VA5	Poor statistics.

f finite series of observations.[E1]

TABLE A- 1

All tests made in NRL No. 1 Mod. 1 with Cs^{137}
Within range of tests, resolution independent of <u>distance</u> and <u>window</u>

Tube	Approx. Voltage	Crystal Matching Agent	Optimum Resolution (percent)	Minimum Resolution (percent)	Resolution with 0.062" μ-metal shield (percent)	Resolution with 0.020" μ-metal shield (percent)	Optimum Resolution ±S.D.*	Resolution with 0.020" μ-metal shield ±S.D.*	Remarks
61A	990	No. 1 Mod. 1 Nujol	16	20					Defective. Microphonic. Returned to manufacturer.
	1080		16						
61B	780	No. 1 Mod. 1 Nujol	10	11					
	990		10						
	1080		10.5						Statistics poor.
	1200		9.5	11					
	1080	No. 3 Nujol	9.5				9.6 ± 0.12		Based on 9 runs.
	1080	No. 3 DC 200 fluid	9.25	10.25		9.75	9.25± 0.25	9.75 ± 0.17	Optimum based on 8 runs, shielded on 12 runs.
61C	1080	No. 1 Mod. 1 Nujol	12.5	15	14				
61D	990	No. 1 Mod. 1 Nujol	10	11.5	11				Poor statistics.
	1080		10.25	11.5	10.5		10.3 ± 0.04		Optimum based on 9 runs.
	1200		10.5	11.5	10.5				Poor statistics on determination of optimum.
	1080	No. 4 DC 200 fluid	9.25	10			9.32 ± 0.21		Optimum figure based on 12 runs.
61E	1080	No. 1 Mod. 1 Nujol	11.5	12					Poor statistics
61F	1080	No. 1 Mod. 1 Nujol	22						Made 3 separate applications of crystal to verify.
61G	750	No. 3 DC 200 fluid	11.5						This tube has phenomenal gain but is quite noisy. Not microphonic at 1080v. At 750v resolution was not consistent. Statistics poor on other voltages.
	900		11						
	1080		11.5						
61VA1	1080	No. 1 Mod. 1 Nujol			13.5				
61VA2	990	No. 1 Mod. 1 Nujol	12.5	13					Poor statistics.
	1080		12						
	[illegible]		12.5	14.5					Poor statistics.
61VA3	1080	No. 4 DC 200 fluid	10.5	12		10.5			Poor statistics.
61VA4	1080	No. 4 DC 200 fluid	10	11		10.5			Poor statistics.
61VA5	1080	No. 4 DC 200 fluid	11	11.5		11.25			Poor statistics.

*S.D. is standard deviation of finite series of observations.

column heading "Crystal; Matching Agent" the term No. 1 Mod. 1 refers to a freshly cleaved crystal of NaI(Tl) in mineral oil (Nujol); No. 3 and No. 4 refer to two Harshaw Chemical Co. canned NaI(Tl) crystals with MgO reflectors. In the "Remarks" column, the statement "Poor Statistics" means only that the number of runs was small so that the data are statistically less reliable. All the scattering tests were subsequently run using 61B.

At first, variations in gain were found, even for a single tube and a single crystal. This was determined to be due to rotating the tube a little between such runs. The point then closest to the supporting aluminum tube was marked and the angular position of the tube varied by rotating about the long axis of the tube envelope which was vertical (see Fig. 1). The angle recorded as θ is the angle from the original position measured counter-clockwise looking down along the tube axis. Table A-2 gives some of the results. For every tube tested the maximum gain and smallest (best) resolution was obtained consistently in the vicinity of one position. For most of the tubes this was approximately 0°; for the remainder it was 180°. In every case the lowest gain and poorest resolution was obtained at a point 180° from the position giving the highest gain and best resolution.

Table A-2

Angular Dependence of Gain and Resolution

	of 204B	Peak Position	Peak Height	Valley Height	Peak Height / Valley Height	Half Breadth	Half Breadth / Peak Position
61B run at 1200 volts with channel width = 1.00 volts (no shield)							
0°	4 × 0.675	71.5	104	5.5	19	6.7	0.093
45°	4 × 0.675	70	106	5.5	19.5	6.9	0.099
90°	4 × 0.675	67.5	104	6.5	16	7.2	0.107
180°	4 × 0.675	64.5	105	7.0	17.5	7.2	0.112
270°	4 × 0.675	68	107	6.5	16.5	7.1	0.104
315°	4 × 0.675	68.5	109	6.0	18	7.2	0.105
61D run at 1080 volts with channel width = 1.00 volts (no shield)							
180°	16 × 0.6	67.5	88	6.0	14.5	7.8	0.116
90°	16 × 0.6	71.2	84.5	5.8	14.5	7.9	0.111
0°	16 × 0.6	76.5	86	4.5	19	7.9	0.103
Same but with 0.020 μ-metal shield							
0°	16 × 0.6	71.8	89	6.0	14.8	7.7	0.107
180°	16 × 0.6	72.3	90	6.0	15.0	7.7	0.106

Resolution = $\frac{\text{Half Breadth}}{\text{Peak Position}}$. $\frac{\text{Peak Height}}{\text{Valley Height}}$ is additional indication but is rather unreliable because minor counting rate meter instability mentioned previously could affect Valley Height by 1.0 and so could the occasional distortion in the printing of the Esterline-Angus chart paper.

when tested with a 0.062" μ-metal shield (which was designed for a 5819 and hence was too large) the results were independent of θ and were approximately equal to those obtained at $\theta = 90^{\circ}$ and $\theta = 270^{\circ}$ with no shield. When tested with a properly fitting 0.020" μ-metal shield a little less consistency was found but enough runs were not made to place reliance on this; however with this shield the reproducible angular dependence was certainly eliminated. There seemed no advantage to using the shield and several possible disadvantages so 61B was taped to its stand at $\theta = 0^{\circ}$ for the scattering runs.

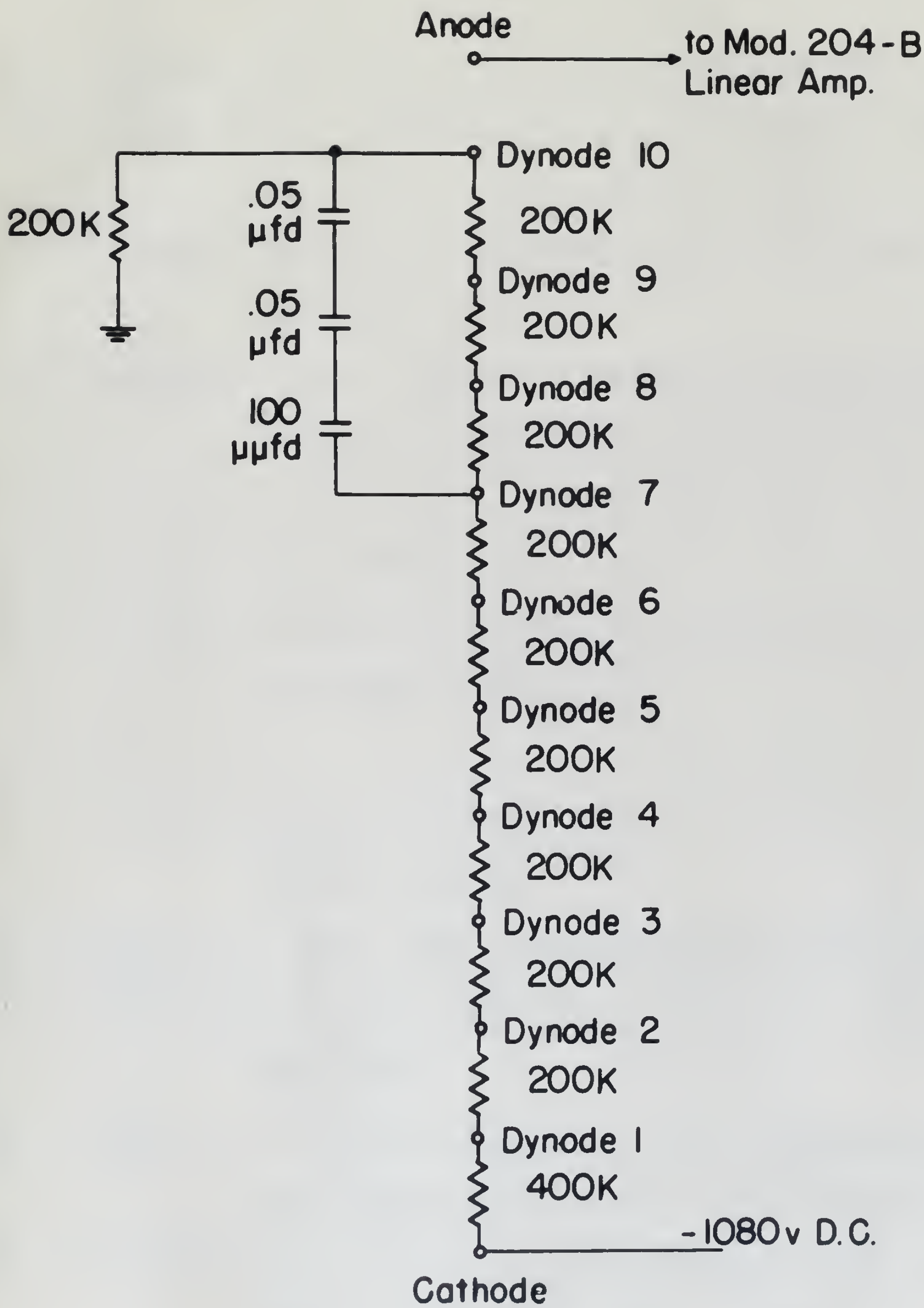
Anode
to Mod. 204-B
Linear Amp.
200K
.05
μfd
.05
μfd
100
μμfd
Dynode 10
200K
Dynode 9
200K
Dynode 8
200K
Dynode 7
200K
Dynode 6
200K
Dynode 5
200K
Dynode 4
200K
Dynode 3
200K
Dynode 2
200K
Dynode 1
400K
-1080 v D.C.
Cathode

Figure 20

BIBLIOGRAPHY

A1 Allen, J. S.: Rev. Sci. Instr. **18**, 739-749 (1947).

A2 Allen, J. S.: Proc. I. R. E. **38**, 346-358 (1950).

B1 Blizard, E.P. and DeBenedetti, S.: Rev. Sci. Instr. **20**, 81(L) (1949).

B2 Brucker, G. J.: "Energy Dependence of Scintillating Crystals", Nucleonics **10**, No. 11, 72-74 (1952).

B3 Bell, P. R. and Davis, R. C.: AECD-1889.

B4 Bell, P. R.: AECD-1854.

B5 British Journal of Radiology, Supplement No. 1, 1947 (numberous authors).

C1 Corson, D. R. and Wilson, R. R.: Rev. Sci. Instr. **19**, 207-233 (1948).

C2 Coltman, J. W.: Proc. I.R.E. **37**, 671-682 (1949).

C3 Coltman, J. W. and Marshall, F. H.: Phys. Rev. **72**, 529 (1947).

C4 Compton, A. H. and Allison, S. K.: "X-rays in Theory and Experiment", D. Van Nostrand,1948.

C5 Curran, S. C.: "Luminescence and the Scintillation Counter", Academic Press, 1953.

D1 Davisson, C. M. and Evans, R. D.: Phys. Rev. **81**, 404-411 (1951).

BIBLIOGRAPHY

A1 Allen, J. S.: Rev. Sci. Instr. 18, 739-749 (1947).

A2 Allen, J. S.: Proc. I. R. E. 38, 346-358 (1950).

B1 Blizard, E.P. and DeBenedetti, S.: Rev. Sci. Instr. 20, 81(L) (1949).

B2 Brucker, G. J.: "Energy Dependence of Scintillating Crystals", Nucleonics 10, No. 11, 72-74 (1952).

B3 Bell, P. R. and Davis, R. C.: AECD-1659.

B4 Bell, P. R.: AECD-1686.

B5 British Journal of Radiology, Supplement No. 1, 1947 (numberous authors).

C1 Corson, D. R. and Wilson, R. R.: Rev. Sci. Instr. 19, 207-233 (1948).

C2 Coltman, J. W.: Proc. I.R.E. 37, 671-682 (1949).

C3 Coltman, J. W. and Marshall, F. H.: Phys. Rev. 72, 528 (1947).

C4 Compton, A. H. and Allison, S. K.: "X-rays in Theory and Experiment", D. Van Nostrand, 1946.

C5 Curran, S. C.: "Luminescence and the Scintillation Counter", Academic Press, 1953.

D1 Davisson, C. M. and Evans, R. D.: Phys. Rev. 81, 404-411 (1951).

D2 Davisson, C. M. and Evans, R. D.: Revs. Modern Phys. 24, 79-107 (1952).

D3 Deutsch, M.: Nucleonics 2, 58 (1948).

D4 Dixon, W. R. et al: "Room Protection Measurements for Cobalt-60 Therapy Units", Nucleonics 10, No. 3, 42-45 (1952).

E1 Evans, R. D.: "Introduction to the Atomic Nucleus", (in preparation for publication).

E2 Engstrom, R. W.: Rev. Sci. Instr. 18, 587-588 (1947).

E3 Elliot, J. O. et al: Rev. Sci. Instr. 21, 631-633 (1950).

E4 Evans, R. D. and Evans, R. O.: Revs. Modern Phys. 20, 305-326 (1948).

E5 Elmore, W. C. and Sands, M.: "Electronics", McGraw-Hill Book Co., 1949.

F1 Fano, U.: "Gamma-Ray Attenuation", Nucleonics 11, No. 8, 8-12 (1953)(this material contained also in F8).

F2 Fermi, E.: "Nuclear Physics", Univ. of Chicago Press, p.38-49, 1951.

F3 Frazell, C. E. and Smith, C. D.: Rev. Sci. Instr. 19, 817-818 (1948).

F4 Fano, U.: Phys. Rev. 76, 739 (1949).

F5 Fano, U., Hurwitz, and Spencer, L. V.: Phys. Rev. 77, 425 (1950).

F6 Faust, W. R.: "Penetration of γ-Radiation Through Thick Targets", NRL Rep. 3613, 1/19/50.

F7 Francis, Bell, and Gundlach: Rev. Sci. Instr. 22, 133 (1951).

F8 Fano, U. et al: "Gamma-Ray Attenuation", NBS Rep. 2222.

F9 Farmer, E. C. and Berstein, I. A.: "Molded Multi-Crystalline Stilbene for Scintillation Counting", Nucleonics 10, No. 2, 54-56 (1952).

F10 Faust, W. R. and Johnson, M. H.: Phys. Rev. 75, 467 (1949).

F11 Fano, U.: Private communication to Dr. G. J. Hine, 1953.

F12 Faust, W. R. and associates: Private communication.

F13 Faust, W. R.: Phys. Rev. 77, 227 (1950).

G1 Gillette, R. H.: Rev. Sci. Instr. 21, 294-301 (1950).

G2 Graves, J. D. and Kuch, G. E.: Rev. Sci. Instr. 21, 304-307 (1950).

G3 Gray, L. H.: Proc. Roy. Soc. (London) A159, 263-293 (1937).

G4 Goodman, C.: "The Science and Engineering of Nuclear Power", Vol. I, Addison-Wesley Press, 1947; Vol. II, Addison-Wesley Press, 1949.

H1 Heitler, W.: "The Quantum Theory of Radiation", 2nd ed., Oxford Press, 1949.

H2 Hall, H.: Phys. Rev. 45, 620-627 (1934).

H3 Hall, H.: Phys. Rev. 84, 167 (1951).

H4 Hall, H.: Revs. Modern Phys. 8, 358 (1936).

H5 Hulme, McDougall, Buckingham, and Fowler: Proc. Roy. Soc. (London) 149A, 131 (1935).

H6 Hanan, G. C. and Pontecorvo, B.: Phys. Rev. 75, 983 (1949).

H7 Hoyt, R. C.: Rev. Sci. Instr. 20, 178-180 (1949).

H8 Hopkins, J. I.: Revs. Sci. Instr. 21, 29 (1950).

H9 Hofstadter, R.: Proc. I.R.E. 38, 726-740 (1949),

H10 Hayward, E.: Phys. Rev. 86, 493-495 (1952).

H11 Hine, G. J.: "Secondary Electron Emission and Effective Atomic Numbers", Nucleonics 10, No. 1, 9-15 (1952).

H12 Hayward, E. and Hubbel, J. H.: "An Experiment on Gamma-Ray Backscattering", NBS Report No. 2264.

H13 Hine, G. J.: Backscattering experiments to be published.

H14 Hoover: Private communication, 1952.

H15 Hirschfelder, J. E. et al: Phys. Rev. 73, 852-862 (1948); Phys. Rev. 73, 863-868 (1948).

I1 Ittner, W. B. and Ter-Pogossian, M.: "Air Equivalence of Scintillation Materials", Nucleonics 10, No. 2, 48 (1952).

J1 Jordan, N. H. and Bell, R. P.: "Scintillation Counters", Nucleonics 5, 30-41 (1949).

J2 Jordan, W. H.: "Scintillation Counter Symposium, June 1949", AECU-583, 10/21/49.

K1 Kallman, H.: Phys. Rev. 75, 623 (1949).

K2 Kallman, et al: "Scintillation Counting Techniques", Nucleonics 10, No. 9, 15-17 (1952).

K3 Kelley, G. G.: "Pulse Amplitude Analyzers for Spectrometry", Nucleonics 10, No. 4, 34-37 (1952).

K4 Klein, O. and Nishina, Y.: Z. Physik. 52, 853 (1929).

K5 Kallman, H. and Furst, M.: Nucleonics 8, No. 3, 32 (1951).

L1 Latyshev, G. D.: Revs. Modern Phys. 19, 132-145 (1947).

L2 Lea, D. E.: "Actions of Radiations on Living Cells", Cambridge Univ. Press, 1947.

L3 Liebson, S. H.: "Temperature Effects in Organic Fluors", Nucleonics 10, No. 7, 41-45 (1952).

L4 Liebson, S. H.: "Organic Scintillators", NRL Report No. 3723, 8/21/50.

L5 Lamerton, L. F.: Brit. J. Radiol. 21, 276-286 (1948).

M1 Marshall, F., Coltman, J. W., and Hunter, L. P.: Rev. Sci. Instr. 18, 504-513 (1947).

M2 Marshall, F. et al: Rev. Sci. Instr. 19, 744-770 (1948).

M3 Morton, G. A.: RCA Review, Vol. X, 525 (1949).

N1 Nickson, J. J.: "Symposium on Radiobiology (1950)", John Wiley and Son, 1952.

N2 Norman, A. G.: "Biochemistry of Cellulose, the Polyuronides, Lignin, etc.", Clarendon Press, 1937.

N3 Nucleonics: "Latest Developments in Scintillation Counting", Nucleonics 10, No. 3, 32-41 (1952).

N4 Nucleonics: "Properties of Scintillation Materials", Nucleonics 6, No. 5, 70-73 (1950).

O1 O'Rourke, R. C.: Phys. Rev. 85, 881-888 (1952).

P1 Papp, G.: Rev. Sci. Instr. 19, 568 (1948).

P2 Pringle, R. W. et al: Rev. Sci. Instr. 21, 216-218 (1950).

P3 Prestwich, G. D. and Colvin, T. H.: "Gamma Ray Dosimetry with a Scintillation Counter", Thesis-1952).

P4 Peebles, G. H. "Gamma-Ray Transmission Through Finite Slabs. Part I.", R.M.653 (Rand).

R1 Rasetti, F.: "Elements of Nuclear Physics", Prentice-Hall, 1946, pp. 66-98.

R2 Reiffel, L. and Burgwald, G.: Rev. Sci. Instr. 20, 711-715 (1949).

R3 Richtmyer, F. K. and Kennard, E. H.: "Introduction to Modern Physics", McGraw-Hill Book Co., 1947.

R4 Reynolds, G. T.: "Solid and Liquid Scintillation Counters", Nucleonics 10, No. 7, 46-52 (1952).

R5 RCA Tube Handbook, HB-3, Vols. 5 and 6.

S1 Stobbe, M.: Ann. d. Phys. 7, 661 (1930).

S2 Sauter, F.: Ann. d. Phys. 9, 217 (1931).

S3 Sauter, F.: Ann. d. Phys. 11, 454 (1931).

S4 Spencer, L. V. and Fano, U.: J. Res. NBS 46, 446 (1951).

S5 Spencer, L. V. and Fano, U.: Phys. Rev. 81, 464 (1951).

S6 Spencer, L. V. and Stinson: Phys. Rev. 86, 662 (1952).

S7 Stoddart, H.: "Report on an Electron Multiplier", AECU-564.

S8 Seitz, F. and Mueller, D. W.: "On the Statistics of Luminescent Counter Systems", AECU-715.

S9 Sangster, R. C.: "A Study of Organic Scintillators", ONR Tech. Report No. 55, 1/1/52.

S10 Spencer, L. V.: Phys. Rev. 88, 794 (1952).

S11 Spiers, F. W.: Brit. J. Radiol. 19, 52-63 (1946).

S12 Schorger, A. W.: "Chemistry of Cellulose and Wood", McGraw-Hill Book Co., 1926.

T1 Taschek, R. F.: "Relative Sensitivities of Some Organic Compounds for Scintillation Counters", AECD-2353.

T2 Taylor, C. J. et al: Phys. Rev. 84, 1034-1043 (1953).

T3 Timmerhaus, K. D. et al: Nucleonics 6, No. 6, 37-41 (1950).

V1 Van Dilla, M. A.: "The Dosimetry of X- and Gamma-Rays with Liquid-Filled Ion Chambers", Thesis-1951.

V2 Van Dilla, M. A. and Hine, G. J.: "Gamma-Ray Diffusion Experiments in Water", Nucleonics 10, No. 7, 54-58 (1952).

V3 Van Rennes, A. B.: "Pulse-Amplitude Analysis in Nuclear Research", Nucleonics 10, Nos. 7, 8, 9, and 10 (1952)(especially Part II, Nucleonics 10, No. 8, 22-28 (1952)).

V4 Vinti, J. P.: Phys. Rev. 91, 345-348 (1953).

W1 White, G. R.: Phys. Rev. 80, 154 (1950).

W2 White, G. R.: "X-ray Attenuation Coefficients", NBS Report No. 1003 (1952).

W3 White, N. E. and Henderson, W. B.: "Measurements of Gamma-Ray Scattering Using a Liquid-Filled Ion Chamber",(Thesis-1952).

W4 Wouters, L. F.: "Solid Counters: Scintillation Counters", AECD-2203.

W5 Whitcher, S. L.: "Energy Absorption by Externally Irradiated Liquids", Nucleonics 10, No. 4, 47-51 (1952; Nucleonics 10, No. 5, 54-58 (1952).

W6 Wouters, L. F.: Nucleonics 10, No. 8, 48-53 (1952).

21550
Thesis
B369
Bennett
Some measurements of gamma ray
scattering.

QUASI-STATIC STABILITY CONCEPTS AND APPLICATION TO THE LONGITUDINAL MOTION OF AN AIRCRAFT

William Charles Bergstedt
Lieutenant, United States Navy

12 June, 1952

University of Michigan

Thesis (MS)

This paper, an expansion and discussion of a series of lectures given by Dr. F. N. Scheubel of the Technical Institute, Darmstadt, Germany, was undertaken by the writer as a thesis project while working for the degree of Master of Science in Aeronautical Engineering at the University of Michigan, Ann Arbor, Michigan. These lectures were given at the University of Michigan during the fall of 1951 while Dr. Scheubel was visiting the University at the invitation of Dr. E. W. Conlon of the Aeronautical Engineering Department.

Dr. Scheubel presented the material in six lectures, the first three devoted to quasi-static stability concepts, the last three to their use in the solution of the equations of motion. His limited time prevented a detailed accounting of the assumptions involved as well as minute explanations of the approximations made. It is the purpose here to verify and expand on his presentation to a degree consistent with the limited scope of such a paper.

Briefly, his material covered the following. His lectures were restricted to symmetric or longitudinal motion. He developed the longitudinal equations of motion and the quasi-static stability criteria at equilibrium and at constant speed. He solved the equations using these quasi-static stability concepts for both the phugoid and short period modes for the stick-fixed case. An amplitude-phase relation for the two variables applicable to the modes was discussed. He then introduced the degree of freedom about the elevator hinge line and solved for the stick-free case. Finally the effects of an elevator impulse were discussed.

This approach to dynamic longitudinal motion differs from standard methods mainly in the quasi-static stability concepts as regards their insertion in the solutions to the equations of motion. In this respect, the method may, as illustrated, be safely applied only to conventional aircraft, i.e., a rigid body, where the number of degrees of freedom and thus the complexity of solution is restricted. The analysis of the motion assuming a phygoid and a short period oscillation serves only to illustrate the handling of the quasi-static concepts. The limitation of the method in respect to acceptable separation of the motion into these modes was

The equations of motion as established by the standard approach of reference 1 are relegated to the flight path direction or wind axes in order that the further discussion will be based on common assumptions and approximations. Dr. Scheubel's equations as developed for a system relative to the flight path will then be compared term by term with the standard equations. From this point onward, i.e., beginning with non-dimensionalizing the equations, the presentation is as Dr. Scheubel developed it.

$m = W/g$	mass of the aircraft
U_1, W_1	initial velocities along x and z body axis
u', w	perturbation velocities along x and z body axis
q	angular velocity about y axis (body or wind)
X, Z, M	air forces and moments
θ, γ, α or $\Delta\theta$, $\Delta\gamma$, $\Delta\alpha$	perturbation of attitude angle, flight path angle, and angle of attack
Θ_1	initial attitude angle
i_y^2	aircraft radius of gyration about y axis
$I_{yy} = mi_y^2$	moment of inertia about y axis
$V_o = w_1^2 + U_1^2$	initial flight path velocity
ΔV	velocity perturbation along flight path
$V = V_o + \Delta V$	velocity along flight path following perturbation
L, D, M	lift, drag and air moment
W	aircraft weight
T_o, D_o	initial thrust and drag
δ	elevator deflection
C_L	lift coefficient for aircraft
ρ	air density
S	wing area
C_D	aircraft drag coefficient
$u = \Delta V/V$	non-dimensional velocity perturbation, ratio of perturbation to total flight path velocity

$\mu = \frac{2W}{g\ S^{3/2}}$	mass density (See Appendix A)
$\tau = t/t_s$	non-dimensional time
M_o	initial moment about y axis
r_h	tail length, distance from aircraft c.g. to center of pressure of horizontal tail
$z = R \pm iI$	conjugate complex root of characteristic equation. R is real part, I is imaginary part
$k_y^2 = S/i_y^2$	
a_1, a_2 ...... or A_1, A_2	constant coefficients of equations
x	position of aircraft center of gravity from most forward part of aircraft in percent of wing chords
x_n	position of neutral point of aircraft from most forward part of aircraft in percent of wind chords
α_h	angle of attack of horizontal tail
C_{Lh}	lift coefficient of horizontal tail
S_h	area of horizontal tail
ω	angular frequency of mode of motion
T_p, T_r	periods of phygoid (p) and rotary (r) modes of motion
$\bar{L}_p$	wave length of phygoid
ρ_e	distance between the hinge line and center of gravity of the elevator
m_e	mass of the elevator
i_e^2	radius of gyration of the elevator
C_h	hinge moment coefficient of elevator
c_h	mean aerodynamic chord of the horizontal tail

h altitude change

Subscript ∞ indicates steady state values in the response discussion. Any other symbols used are either obvious or are locally defined for ease in handling equations.

The standard development in a perfectly general way as accomplished in reference 1 result in the equations of longitudinal motion of the form,

A.1 $m(\dot{u}' + W_1 q) = X_{u'} u' + X_w w + X_q q - mg \cos \Theta_1 \theta$.

A.2 $m(\dot{w} - U_1 q) = Z_{u'} u' + Z_w w + Z_q q - mg \sin \Theta_1 \theta$.

A.3 $m\, i_y^2\, \dot{q} = I_{yy} \dot{q} = M_u\, u' + M_w w + M_q q$.

These equations are relative to body axes and contain the following assumptions and approximations:

(a) Initial symmetric steady motion is assumed.

(b) The air reactions do not depend on the rates of change of the variables, U, V and W, or their integrals.

(c) Second order and higher terms of the air reactions are neglected, i.e., only infinitesimal disturbances from an initial steady motion are treated.

(d) The aircraft has a plane of symmetey and the steady motion about which the disturbances occur is symmetrical with regard to that plane.

(e) The disturbance initially imposed on the system is unenforced and the controls are locked. This rules out an initial couple, M_o, and the variation of M with δ.

The variables are seen to be u, w and q. These are illustrated in Figure 1. The relation between the body axes and the wind axes is shown in Figure 2. The body axes are primed. Angles are measured positive counterclockwise from the horizontal reference for γ and Θ_1, from the wind line for α.

In regard to these figures it is seen that,

(a) Since q is a velocity and θ a displacement, $\theta = \int q\, dt = \Delta \alpha + \Delta \gamma$

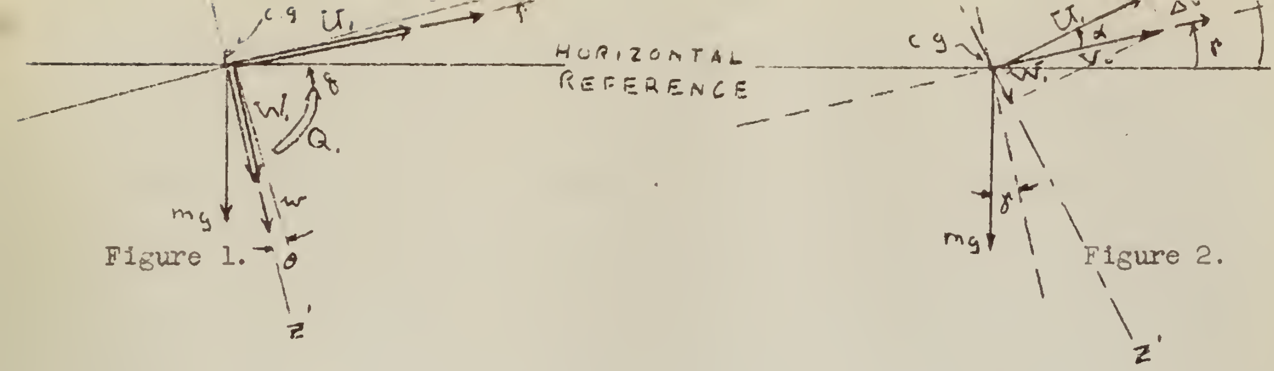

Figure 1. Figure 2.

(b) V_o is the steady state velocity and, $V_o^2 = W_1^2 + U_1^2$.

Then there is the definition, $V = V_o + \Delta V$

$$\text{also,} \quad \frac{dV}{dt} = \frac{d(\Delta V)}{dt}$$

(c) In essence u is now ΔV, and w does not exist.

The inertia terms of the equations of motion parallel and perpendicular to the wind direction and about the center of gravity become, neglecting the inertia force due to linear acceleration perpendicular to the wind direction,

for A.1: $\quad m \dfrac{d(\Delta V)}{dt}$

for A.2: $\quad m V \dfrac{d\gamma}{dt}$

for A.3: $\quad I_{yy} \dfrac{d^2(\alpha + \gamma)}{dt^2}$.

The weight components relative to the wind axes become,

along x: $\quad mg \sin \gamma$

along z: $\quad -mg \cos \gamma$

and these are only affected by $\Delta \gamma$.

There remains only the air reaction derivatives. The force created on the tail due to q is the largest resulting from this disturbance and from experience it is known to be small along the wind axes so X_q and Z_q are neglected.

bations existed along both axes. Using wind axes, only the velocity perturbation, ΔV, now exists. Any sinking velocity along the z wind axis is merely a change in angle of attack. The air reactions along x consist only of the drag in its entirety, neglecting variations of thrust. The drag varies with both α and V. The air reactions along z consist only of the lift in its entirety and is affected by the same quantities. A pure rotary perturbation about the center of gravity changes both α and γ but only α affects the linear forces. The same applies to the air moments. The variations with α are found by wind tunnel tests and any rotation of the model about the center of gravity is considered pure α . This does not hold for the case of the effect on M of both $\Delta\dot{\alpha}$ and $\Delta\dot{\gamma}$. These two perturbations make up θ, which, when multiplied by the tail length, gives the effective sinking velocity of the horizontal tail. This sinking velocity in turn is felt as a change in angle of attack of the tail.

Thus the external forces for A.1 become,

$$\frac{\partial D}{\partial \alpha}\Delta\alpha + \frac{\partial D}{\partial V}\Delta V + \frac{\partial}{\partial \gamma}(mg \sin \gamma)\Delta\gamma$$

and equation A.1 is,

$$m\frac{d(\Delta V)}{dt} = \frac{\partial D}{\partial \alpha}\Delta\alpha + \frac{\partial D}{\partial V}\Delta V + mg \cos \gamma \Delta\gamma .$$

Equation A.2 is,

$$m V \frac{d\gamma}{dt} = \frac{\partial L}{\partial \alpha}\Delta\alpha + \frac{\partial L}{\partial V}\Delta V + mg \sin \gamma \Delta\gamma .$$

Equation A.3 becomes,

$$I_{yy}\frac{d^2(\alpha + \gamma)}{dt^2} = \frac{\partial M}{\partial \alpha}\Delta\alpha + \frac{\partial M}{\partial V}\Delta V + \frac{\partial M}{\partial \dot{\alpha}}\Delta\dot{\alpha} + \frac{\partial M}{\partial \dot{\gamma}}\Delta\dot{\gamma} .$$

The use of the wind axes then has the advantage of the aircraft's forward motion being along the x axis so that the lift and drag forces always

made along the axis of perpendicularity which is the case if the forces are resolved along the body axes. The disadvantage is that these axes change continuously so that the moments and products of inertia change. For small disturbances from initial horizontal flight these discrepancies are considered negligible. Also the thrust does not act along the wind axes for all aircraft and, for an individual aircraft, at all times.

The continuity of this paper and the advantage of physical "feel" that is had from the development of the equations of motion from initial supposition of wind axes can be best maintained by including such a development in its entirety at this point. This is the method used by Dr. Scheubel and appears to be in general use in Germany. See Reference 2.

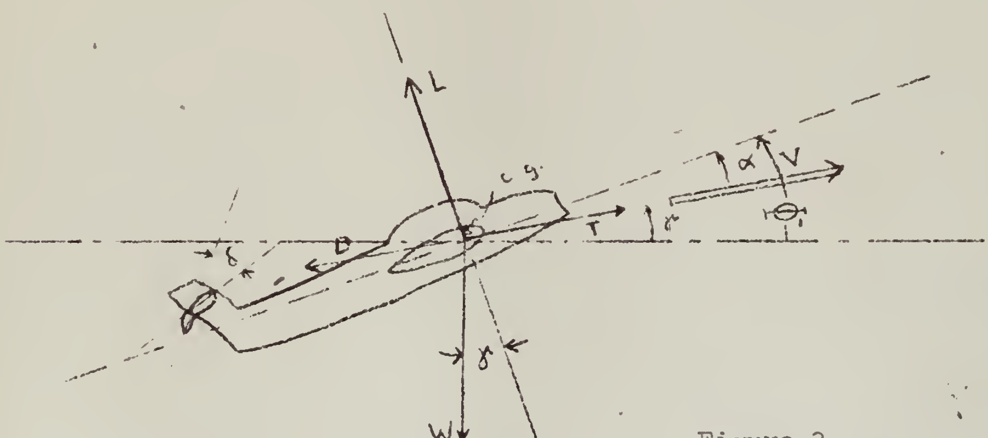

Figure 3.

With the aircraft in an attitude and with the external forces as shown in Figure 3, the external forces are equated to the time rate of change of momentum in the direction of the wind axis, i.e., along V, and one equation of equilibrium follows.

$$\frac{W}{g}\frac{dV}{dt} = T - D - W \sin \gamma .$$

then, following a small disturbance, are the initial values plus the increments due to the changes,

$$\frac{W}{g}\ \frac{dV}{dt} = T_o - D_o - W \sin \gamma_o + \frac{\partial T}{\partial V}\Delta V - \frac{\partial D}{\partial V}\Delta V - \frac{\partial D}{\partial \alpha}\Delta \alpha - W \cos \gamma \Delta \gamma \ .$$

This is the result of a Taylor Series expansion of the quantities T, D and W as functions of α, V, γ and δ in which second order terms and above are neglected under the assumption that the changes are small. Assuming an initial condition of equilibrium, it is seen that this equation is comparable to equation A.1 with one exception. Thus all the assumptions previously enumerated hold. The exception is the thrust term. It is easily seen that thrust is not affected by changes in α, γ, or δ. The stick-fixed case is considered here also. Thus all terms involving δ are neglected.

This first equation is now manipulated into a form necessary for subsequent solution. Initial equilibrium and assuming γ small gives,

$$T_o - D_o - W \sin \gamma_o = 0 \quad \text{and,} \quad \cos \gamma = 1 \quad \text{or} \quad W = L$$

$$\text{also,} \quad L = C_L \tfrac{1}{2} \rho V^2 S \quad \text{and,} \quad D = C_D \tfrac{1}{2} \rho V^2 S \ .$$

Multiplying terms in T by $\frac{T_o}{T_o}$ and $\frac{V}{V}$, and terms in D by $\frac{D_o}{D_o}$ and $\frac{V}{V}$ there is

$$\frac{W}{g}\ \frac{dV}{dt} = T_o \frac{V}{T_o}\ \frac{\partial T}{\partial V}\ \frac{\Delta V}{V} - D_o \frac{V}{D_o}\ \frac{\partial D}{\partial V}\ \frac{\Delta V}{V} - \frac{\partial D}{\partial \alpha}\Delta\alpha - L \Delta \gamma \ .$$

Now,

$$\frac{V}{T_o}\ \frac{\partial T}{\partial V} = \frac{\partial \ln T}{\partial \ln V} \ ; \ \frac{V}{D_o}\ \frac{\partial D}{\partial V} = \frac{\partial \ln D}{\partial \ln V} \quad \text{and letting} \quad \frac{\Delta V}{V} = u$$

there is,

$$\frac{W}{g}\ \frac{dV}{dt} = \frac{W}{g}\ \frac{d(V_o + \Delta V)}{dt} = \frac{W}{g}\ \frac{d(\Delta V)}{dt}$$

$$= C_D \rho \frac{V^2}{2} S \left(\frac{T_o}{D_o}\ \frac{\partial \ln T}{\partial \ln V} - \frac{\partial \ln D}{\partial \ln V}\right) u - \left(\frac{\partial C_D}{\partial \alpha}\Delta\alpha - C_L \Delta \gamma\right) \rho \frac{V^2}{2} S \ .$$

Using the standard notation, $\frac{\partial C_D}{\partial \alpha} = C_{D\alpha}$ and dividing by $\rho \frac{V^2}{2}$ S, there is

This equation is non-dimensionalized in the usual manner. The right side of the equation is non-dimensional as it stands. Considering the left side, multiplying numerator by V/V and the denominator by t_s/t_s,

$$\frac{W}{g} \frac{2}{\rho V^2 S} \frac{V}{t_s} \frac{d(\Delta V/V)}{d(t/t_s)} \quad .$$

A time unit, t_s, is adopted by letting, $\frac{W}{g} \frac{2}{\rho V^2 S} \frac{V}{t_s} = 1$ then,

$t_s = \frac{2WS^{1/2}}{g\rho V S^{3/2}} = \mu \frac{S^{1/2}}{V} = C_L \frac{V}{g}$ where the mass number, μ , is given by,

$\mu = \frac{2W}{g\rho S^{3/2}} = \frac{2}{g\rho} (\frac{W}{S})^{3/2} \frac{1}{W^{1/2}}$. This mass number, or density factor, is discussed in Appendix A. Now the non-dimensional time is given by, $t/t_s = \tau$ so that, $d(\frac{t}{t_s}) = d\,\tau$ and the variable ΔV is transformed as, $\frac{\Delta V}{V} = u$.

The first equation of motion then becomes,

A.4 $$\frac{du}{d\tau} = \dot{u} = - C_{L_\alpha} \Delta\alpha - C_L \Delta\gamma - C_D \left(\frac{\partial \ln D}{\partial \ln V} - \frac{T_o}{D_o} \frac{\partial \ln T}{\partial \ln V}\right) u \quad ..$$

Again referring to Figure 3, the external forces perpendicular to the wind line are equated to the centrifugal force or mass times the centrifugal acceleration. $\frac{W}{g} V \frac{d\theta}{dt} = \frac{W}{g} V \frac{d\gamma}{dt} = L - W \cos\gamma$ since, $\frac{W}{g} V \frac{d\alpha}{dt} = 0$, because $V \frac{d\alpha}{dt}$ results in no change in velocity perpendicular to the flight path and the linear acceleration in this direction is neglected. If a small disturbance is introduced, and, since lift does not vary with γ and the stick-fixed case is assumed,

$$\frac{W}{g} V \frac{d\gamma}{dt} = L_o - W \cos\gamma_o + \frac{\partial L}{\partial\alpha}\Delta\alpha + \frac{\partial L}{\partial V}\Delta V + W \sin\gamma\,\Delta\gamma \, .$$

With the same assumption as before, that of initial equilibrium, this equation is seen to be the same as equation A.2 and so the same assumptions and approximations are implied. Expanding the derivatives,

and

$$\frac{\partial}{\partial V}\left(C_L \rho \frac{V^2}{2} S\right) = \frac{\partial C_L}{\partial V} \rho \frac{V^2}{2} S + C_L 2 \rho \frac{V^2}{2} \frac{V}{V} = \rho \frac{V^2}{2} S \left(\frac{C_L}{C_L} \frac{V}{V} \frac{\partial C_L}{\partial V} + \frac{2C_L}{V}\right)$$

so

$$\Delta L = \rho \frac{V^2}{2} S \left(C_{L\alpha} \Delta\alpha + C_L \left(2 + \frac{\partial \ln C_L}{\partial \ln V}\right) u \right)$$

also, $W \sin \gamma \Delta \gamma = C_L \sin \gamma \rho \frac{V^2}{2} S \Delta \gamma$, so that the entire equation becomes,

$$\frac{W}{g} \frac{2}{\rho V^2 S} V \frac{d\gamma}{dt} = C_{L\alpha} \Delta\alpha + C_L \left(2 + \frac{\partial \ln C_L}{\partial \ln V}\right) u + C_L \sin \gamma \Delta \gamma .$$

The left side is non-dimensionalized as before. Dividing the denominator by t_s/t_s, there is,

$$\frac{W}{g} \frac{2}{\rho V^2 S} \frac{V}{t_s} \frac{d\gamma}{d(\frac{t}{t_s})} = \frac{d\gamma}{d\tau} = \dot{\gamma} .$$

So finally there is the second equation of motion,

A.5 $$\dot{\gamma} - C_L \left(2 + \frac{\partial \ln C_L}{\partial \ln V}\right) u - C_{L\alpha} \Delta\alpha - C_L \sin \gamma \Delta \gamma = 0$$

The final equation of the longitudinal motion is obtained by equating the moments to the moment of momentum about the center of gravity of the aircraft. Considering Figure 3 again, this is,

$$\frac{W}{g} i_y^2 \frac{d^2(\alpha + \gamma)}{dt^2} = M_o + \Delta M$$

where, $\frac{W}{g} i_y^2$ is the moment of inertia and i_y^2 is the radius of gyration. Since M is a function of lift and drag which in turn are not affected by γ, neglecting the influence of $\dot{V}$, and with the stick-fixed assumption, there is,

$$\frac{W}{g} i_y^2 \frac{d^2(\alpha + \gamma)}{dt^2} = I_{yy} \frac{d^2(\alpha + \gamma)}{dt^2}$$

$$= M_o + \frac{\partial M}{\partial \alpha} \Delta\alpha + \frac{\partial M}{\partial V} \Delta V + \frac{\partial M}{\partial \dot{\alpha}} \Delta\dot{\alpha} + \frac{\partial M}{\partial \dot{\gamma}} \Delta\dot{\gamma} .$$

This is seen to be the same as equation A.3 assuming initial equilibrium.

$$\Delta M = \frac{\partial C_M}{\partial \alpha} \rho \frac{V^2}{2} S^{3/2} \Delta \alpha + V \frac{\partial C_M}{\partial V} \rho \frac{V^2}{2} S^{3/2} \frac{\Delta V}{V} + \frac{\partial C_M}{\partial (\frac{d\theta}{dt})} \rho \frac{V^2}{2} S^{3/2} \frac{d\theta}{dt}$$

since, $\Delta \dot{\alpha} + \Delta \dot{\gamma} = \frac{d(\alpha + \gamma)}{dt} = \frac{d\theta}{dt}$.

An important point to note here is the German use of the square root of the wing area as the additional length term when converting moments to coefficient form. The reasoning is that this quantity is more easily definable for the variegated types of wings now in existence whereas the man aerodynamic chord is somewhat nebulous in definition in the literature. Another reason is the fact that the quantity $r_h/S^{1/2}$ ranges from 0.8 to 1.10 and this facilitates its approximation to unity where it appears.

Considering the last term and non-dimensionalizing the derivative by letting, $q = \frac{d\theta}{dt} \frac{S^{1/2}}{V}$,

$$\frac{\partial C_M}{\partial (\frac{d\theta}{dt})} \rho \frac{V^2}{2} S^{3/2} \frac{d\theta}{dt} = \frac{\partial C_M}{\partial q} \rho \frac{V^2}{2} S^{3/2} \frac{d\theta}{dt} \frac{S^{1/2}}{V} .$$

Then non-dimensionalizing the entire term,

$$\frac{\partial C_M}{\partial q} \rho \frac{V^2}{2} S^{3/2} \frac{d(\alpha + \gamma)}{d(t/t_s)} \frac{V}{S^{1/2}} \frac{1}{\mu} \frac{S^{1/2}}{V} = C_{M_q} \rho \frac{V^2}{2} \frac{S^{1/2}}{\mu} (\dot{\alpha} + \dot{\gamma}) .$$

Now non-dimensionalizing the left side of the equation, after dividing by $\rho \frac{V^2}{2} S^{3/2}$,

$$\frac{W}{g} i_y^2 \frac{2}{\rho V^2 S^{3/2}} \frac{1}{t_s^2} \frac{d^2(\alpha + \gamma)}{d(t/t_s)^2} = \mu i_y^2 \frac{1}{V^2} \frac{V^2}{S\mu^2} (\ddot{\alpha} + \ddot{\gamma})$$

$$= (\ddot{\alpha} + \ddot{\gamma}) \frac{i_y^2}{S} \frac{1}{\mu} = \Delta M .$$

This equation may be rewritten in the more concise form,

$$A.6 \quad \ddot{\alpha} - C_{M_q} \frac{S}{i_y^2} \dot{\alpha} - C_{M_\alpha} \frac{S}{i_y^2} \mu \Delta \alpha + \ddot{\gamma} - C_{M_q} \frac{S}{i_y^2} \dot{\gamma} - \frac{\partial C_M}{\partial V} \frac{S}{i_y^2} \mu u = 0$$

There are then, the longitudinal equations of motion in non-dimensional form

A.5 $$\dot{\gamma} - C_L \left(2 + \frac{\partial \ln C_L}{\partial \ln V}\right) u - C_{L_\alpha} \Delta\alpha - C_L \sin\gamma \Delta\gamma = 0$$

A.6 $$\ddot{\alpha} - C_{m_q} \frac{S}{i_y^2} \dot{\alpha} - C_{m_\alpha} \frac{S}{i_y^2} \mu \Delta\alpha + \ddot{\gamma} - C_{m_q} \frac{S}{i_y^2} \dot{\gamma} - \frac{\partial C_m}{\partial \ln V} \frac{S}{i_y^2} \mu u = 0$$

These equations have been seen to compare term by term, except for the inclusion of variation of thrust with velocity, with these developed in a more general sense. The assumptions and approximations have been cited. The dependent variables are u, α and γ.

A more general case would be that of assuming, instead of the homogeneous set above, the equating of the quantities above to forcing functions of the elevator displacement, δ . This would require, in addition, an equation of motion involving moments about the elevator hinge line. This would be the case of stick-free stability and motion.

It is noted that a striking difference between these equations and those more familiar to most students is the form in which the stability derivatives have resulted. Since the problem is now ready for analysis of modes of motion, damping factors and associated desired results, the question arises as to why this form of the derivatives and how they are to be evaluated.

The usual procedure is the separate evaluation of each derivative by similarity to previous determinations or by wind tunnel or flight testing. It is seen that certain of the derivatives in the three equations above are in combination. For a special but usual case of the solution of the equations of motion further combinations of these derivatives appear. A discussion of both the general case and this special one of the solution follows.

comes quite involved in that the solution is carried to the determination of an equation for each variable composed of both the complimentary function and particular integral. See Reference 1. If the equations are restrictid to the stick-fixed case and the motion is assumed resulting in the absence of an applied forcing function, the equations will be homogeneous and the solution resulting will be the complimentary function only.

The discussion here will be further restricted in that the equations in terms of the variables will not be the end result This would merely give the particular motion resulting from certain initial conditions.

The characteristic equation which results from the solution of the differential equations being of the form, $x = x_o e^{z\tau}$, will be analyzed for its roots and information relative to inspection of these roots. This will show the character of the motion as regards stability, periodicity and demping.

The nature of the characteristic equation, or stability quartic, will be set down from the determinant resulting from the solution, $x = x_o e^{z\tau}$ Experience has shown that the two sets of roots that form the solution are usually of such widely separate magnitude that they may be separated. The special case mentioned is based on this fact

Since Scheubel's solutions employing the quasi-static stability concepts are based on the premise that the roots are separable, the general characteristic equation will be set down without further comment and the special case will be stressed in preparation for the solution by his quasi-static stability concepts. The errors involved in this approximation to the roots, especially as it increases with angle of attack, is discussed at length in Reference 1 It is shown that it is a good approximation for low angles of attack, i.e., 3°, but becomes unacceptable for angles of attack near 10° especially for neutral

Assuming a solution of the form, $x = x_o e^{z\tau}$, where z is a real or comples constant, the indicated operations on the variables are then carried out. The stability quartic results from an expansion of the following determinant that follows from the fact that the equations are consistent if the determinant of their coefficients vanishes.

Rearranging the equations by variables,

$$
\begin{array}{llll}
 & u & & \\
\text{A.4} & \dot{u} + C_D\left(\frac{\partial \ln D}{\partial \ln V} - \frac{T_o}{D_o}\frac{\partial \ln T}{\partial \ln V}\right)u & C_L \gamma & C_{D_\alpha}\alpha = 0 \\
\text{A.5} & -C_L\left(2 + \frac{\partial \ln C_L}{\partial \ln V}\right)u & \dot{\gamma} - C_L \sin\gamma\cdot\gamma & -C_{L_\alpha}\alpha = 0 \\
\text{A.6} & -\frac{\partial C_m}{\partial \ln V}\frac{S}{i_y^2}\mu u & \ddot{\gamma} - C_{m_q}\frac{S}{i_y^2}\dot{\gamma} & \ddot{\alpha} - C_{m_q}\frac{S}{i_y^2}\dot{\alpha} - C_{m_\alpha}\frac{S}{i_y^2}\mu\cdot\alpha = 0
\end{array}
$$

The assumptions are made that $C_L \sin\gamma\cdot\gamma$ is negligible since near horizontal flight is assumed, and that approximately, $T_o = D_o$.

The determinant of the coefficients is then, using $k_y^2 = S/i_y^2$

$$
\begin{vmatrix}
z + C_D\left(\frac{\partial \ln D}{\partial \ln V} - \frac{\partial \ln T}{\partial \ln V}\right) & C_L & C_{L_\alpha} \\
-C_L\left(2 + \frac{\partial \ln C_L}{\partial \ln V}\right) & z & -C_{L_\alpha} \\
-\frac{\partial C_m}{\partial \ln V} k_y^2 \mu & z^2 - C_{m_q} k_y^2 z & z^2 - C_{m_q} k_y^2 z - C_{m_\alpha} k_y^2 \mu
\end{vmatrix}
$$

The quartic becomes,

$$\text{B.1} \qquad z^4 + a_3 z^3 + a_2 z^2 + a_1 z + a_o = 0$$

where,

$$a_2 = -\left(C_{m_\alpha} + C_{m_q}\frac{C_{L_\alpha}}{\mu}\right) k_y^2 \mu + C_D \left(\frac{\partial \ln D}{\partial \ln V} - \frac{\partial \ln T}{\partial \ln V}\right)\left(C_{L_\alpha} - C_{m_q} k_y^2\right)$$

$$+ \left(C_L - C_{D_\alpha}\right)\left[C_L\left(2 + \frac{\partial \ln C_L}{\partial \ln V}\right)\right]$$

$$a_1 = -\left(C_{m_\alpha} + C_{m_q}\frac{C_{L_\alpha}}{\mu}\right) k_y^2 \mu \cdot C_D \left(\frac{\partial \ln D}{\partial \ln V} - \frac{\partial \ln T}{\partial \ln V}\right)$$

$$- \left[C_{m_\alpha} - \frac{\partial C_m}{\partial \ln V}\;\frac{C_{L_\alpha}}{C_L\left(2 + \frac{\partial \ln C_L}{\partial \ln V}\right)}\right] k_y^2 \mu \cdot \frac{C_{D_\alpha} \cdot C_L\left(2 + \frac{\partial \ln C_L}{\partial \ln V}\right)}{C_{L_\alpha}}$$

$$+ \left(C_{m_\alpha} + C_{m_q}\frac{C_{L_\alpha}}{\mu}\right) k_y^2 \mu \cdot \frac{C_{D_\alpha} C_L\left(2 + \frac{\partial \ln C_L}{\partial \ln V}\right)}{C_{L_\alpha}}$$

$$- C_{m_q} k_y^2 \left[C_L^2\left(2 + \frac{\partial \ln C_L}{\partial \ln V}\right)\right]$$

$$a_o = - C_L^2\left(2 + \frac{\partial \ln C_L}{\partial \ln V}\right)\left[C_{m_\alpha} - \frac{\partial C_m}{\partial \ln V}\;\frac{C_{L_\alpha}}{C_L\left(2 + \frac{\partial \ln C_L}{\partial \ln V}\right)}\right] k_y^2 \mu .$$

The usual methods for the solution of quartics may be employed to solve this equation as it stands. The constants have been arranged in the particular fashion shown for reasons to be mentioned later.

2. The Case of Distinct Sets of Roots.

Experience has shown that the usual motion in flight consists of a long period, low frequency, lightly damped motion, called the phygoid or flight path oscillation, and a short period, heavily damped motion, called the rotary oscillation. This suggests the factoring of the characteristic equation into two quadratic equations.

The length of the period of the rotary oscillation has been found to be at most of 1-5 seconds while that of the phygoid usually is of the order of 30-60 seconds for most conventional planes. This suggests that, due to the

stant. Thus this mode is governed by equations A.5 and A.6 with the terms in u eliminated. The solution for the phygoid can neither ignore the change in velocity or angle of attack. However, consideration of equation A.6 shows that, due to the large magnitude of the factor μ discussed in Appendix A, an approximation may be made that the terms containing this item are large compared to the other terms. Solving this equation for α, the terms in α in equations A.4 and A.5 are then expressed by a term in u. The phygoid will be solved for, as regards the information mentioned previously, by consideration of the equations enclosed by the dashed lines in the equation array modified by the approximation discussed above. The rotary oscillation will be concerned by the equations enclosed by the dotted lines in the array.

a. The Phugoid.

Equation A.6 becomes, nelgecting terms not involving μ,

$$-\frac{\partial C_m}{\partial \ln V} k_y^2/\mu\, u - C_{m_\alpha} k_y^2/\mu\, \alpha = 0$$

or,

$$\alpha = -\left(\frac{\partial C_m}{\partial \ln V}/C_{m_\alpha}\right)u \quad .$$

Equations A.4 and A.5 in coefficient form are now, assuming a solution of the form, $x = x_o e^{z\tau}$,

$$Z + C_D\left(\frac{\partial \ln D}{\partial \ln V} - \frac{\partial \ln T}{\partial \ln V}\right) - C_D\left(\frac{\frac{\partial C_m}{\partial \ln V}}{C_{m_\alpha}}\right) + C_L = 0$$

$$-C_L\left(2 + \frac{\partial \ln C_L}{\partial \ln V}\right) + C_{L_\alpha}\left(\frac{\frac{\partial C_m}{\partial \ln V}}{C_{m_\alpha}}\right) \quad Z = 0$$

which gives the quadratic,

B.2 $$Z^2 + a_1 Z + a_o = 0$$

where

and,

$$a_o = C_L^2\left(2 + \frac{\partial \ln C_L}{\partial \ln V}\right) + C_L C_{L\alpha}\left(\frac{\frac{\partial C_m}{\partial \ln V}}{C_{m\alpha}}\right)$$

$$= \frac{C_L^2\left(2 + \frac{\partial \ln C_L}{\partial \ln V}\right)}{C_{m\alpha}}\left[C_{m\alpha} - \frac{\partial C_m}{\partial \ln V} \quad \frac{C_{L\alpha}}{C_L\left(2 + \frac{\partial \ln C_L}{\partial \ln V}\right)}\right]$$

The quadratic has the roots,

$$z = \frac{-a_1 \pm \sqrt{a_1^2 - 4a_o}}{2} = R_1 \pm i I_1 \quad .$$

Where the damping factor, R_1, is, $R_1 = -\frac{a_1}{2}$ the frequency or period factor is, $I_1 = \sqrt{a_o - \frac{1}{4} a_1^2}$.

b. The Short Period Oscillation.

Neglecting the velocity terms, and equation A.4 in its entirety, equations A.5 and A.6 become, in coefficient form,

$$\begin{vmatrix} z & -C_{L\alpha} \\ z^2 - C_{m_q} k_y^2 z & z^2 - C_{m_q} k_y^2 z - C_{m\alpha} k_y^2 \mu \end{vmatrix} = 0$$

which gives, $z^3 + A_1 z^2 + A_o = 0$ B.3

where, $A_1 = (C_{L\alpha} - C_{m_q} k_y^2)$ and, $A_o = (C_{m\alpha} - C_{m_q} \frac{C_{L\alpha}}{\mu}) k_y^2 \mu$. One root is, $z = 0$, the others are, $z = R_2 + iI_2$ and the damping factor is, $R_2 = -\frac{A_1}{2}$, the frequency factor, $I_2 = \sqrt{A_o - \frac{1}{4} A_1^2}$.

Before any further evaluation of the quantities determined up to this point, the quasi-static stability criteria are developed.

Before proceeding with the quasi-static stability development, it may be helpful if a reiteration be made of the specialization assumed leading to this development compared with methods of a more general nature as in references 1 and 4. Both of these references discuss the special case of the approximation to the roots resulting from the assumption that the solution consists of two pairs of complex roots sufficiently separated in magnitude to warrant a factoring of the characteristics quartic. This facile solution is usual in most cases but may not be sound for unconventional aircraft or even conventional aircraft where additional facts must be considered. These are, flexing of the component parts such as wings and tail surfaces of the aircraft, which would entail additional degrees of freedom, large changes in the coefficients of the equations due to rapid depletion of a large fuel supply and its effect on the derivatives. Many of these latter considerations are undergoing exhaustive study at present and do not lend themselves to any concise generalizations. From, say, a project engineer's point of view, especially in the initial stages of design, concern is given to information available from the most rapid and inexpensive data available. This is especially true at present since specifications, the military in particular, require employment of the finished design throughout large ranges in altitude, speed and weight. The assumption of the presence of two quite widely separated modes, however, is sound for most conventional aircraft and for unconventional aircraft at certain phases of their flight history. The conditions that hold for the phugoid were seen to be a slow oscillation of long period and wave length and relatively light damping. The rotary oscillation is a short, heavily damped oscillation.

In regard to standard methods, the coefficients needed to determine the constants for the final solutions of the equations of motion are obtained primarily from static wind tunnel tests. This is the rule for the values of

ents are found by static stability considerations for the variation of the moment with α . See reference 5. A dynamic wind tunnel test is used to find C_{m_q} . See references 1, 4 and 6.

The coefficients as they have been developed in this paper will be evaluated in much the same manner as regards those concerned with linear forces. However, the method of evaluation of the logarithmic derivatives will be illustrated. As for the moment derivatives, the determination of C_{m_q} will not be discussed assuming that it may be found by the usual methods. The static longitudinal stability criterion, C_{m_α} , is the quanitity that the next few pages will be concerned with. This quantity Dr. Schéubel determines in a quasi-static way. Qausi-static in that it is developed from assumptions made on the dynamic motion of the aircraft. The two concepts, quasi-static stability at equilibrium and at constant speed, follow from the fact that an aircraft has two distinct phases of motion following a disturbance.

Quasi-static stability at equilibrium of forces is essentially a consideration of the equilibrium conditions reached at a time in the flight history following a disturbance at which the new velocity is obtained. This new velocity is the initial value plus the incremental increase due to the perturbation. The quasi-static stability at constant speed development holds for the relatively short period following the disturbance in which the velocity is assumed not to have reaches its final value.

The dynamic response to an elevator deflection is disected, so to speak, to give these two quasi-static concepts. The aircraft is initially in steady, nearly horizontal straight flight. Starting from this steady straight flight, we assume that the elevator angle, δ , has been changed suddenly by a certain amount, $d\,\delta$, and we ask what will happen.

tudinal moment and a small change in lift. This latter change is so small it is neglected. The change in moment disturbing the equilibrium gives an angular velocity about the lateral axis, and, due to this, the angle of attack is changed too. A change in the angle of attack gives rise to a change of the lift coefficient and by it a change in lift. So the equilibrium of forces perpendicular to the direction of flight is disturbed too. All these effects hold during the initial portion of the period following the disturbance, i.e., during the first few seconds. In addition, it is assumed that the speed remains essentially constant during this period.

This then is the situation maintaining for quasi-static stability at constant speed and considers the change in force perpendiicular to the flight path caused by the initial curvature of the flight path and the change in moments resulting from the disturbance.

Eventually the change in elevator causing the change in angle of attack thereby the lift coefficient results in the aircraft attaining a new steady state, that is a new point of equilibrium of forces and moments at a certain speed, V + dV, which is different from the initial one by dV. Quasi-static stability at equilibrium concerns itself with this portion of the flight history. From experience it is known that it takes an aircraft an appreciable time, normally several minutes, for the speed to adjust itself to a changed elevator displacement.

1. Quasi-static Stability at Equilibrium.

The implication of an initial steady state of motion necessitates equilibrium of forces and of moments. From Figure 4 this is seen to be,

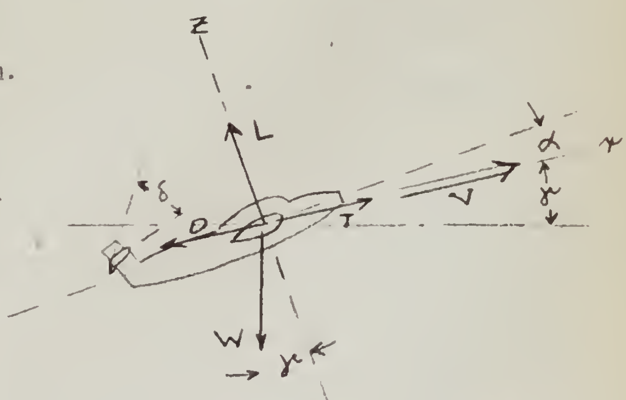

Figure 4.

$$\Sigma F_z : \quad L - W \cos \gamma = 0$$

$$\Sigma M : \quad M = 0$$

$$\Sigma M_\delta : \quad M_\delta = 0 \ .$$

Having started from nearly horizontal flight the flight path will remain nearly horizontal for sufficiently small changes so that the component of the weight perpendicular to the path remains almost unchanged. From the second equation, that of equilibrium of forces perpendicular to the path of flight, then,

$$d(L - W \cos \gamma) = dL = 0, \text{ since, as before } \sin \gamma = \gamma = 0.$$

$$dL = dC_L \rho \frac{V^2}{2} S + 2C_L \rho \frac{V^2}{2} S \frac{dV}{V} = 0$$

now,

$$dC_L = \frac{\partial C_L}{\partial \alpha} d\alpha + \frac{\partial C_L}{\partial V} dV \frac{VC_L}{VC_L}$$

so that,

$$\left[\frac{\partial C_L}{\partial \alpha} d\alpha + C_L \left(\frac{\partial \ln C_L}{\partial \ln V} + 2 \right) \frac{dV}{V} \right] \rho \frac{V^2}{2} S = 0$$

or,

$$\frac{dV}{V} = d \ln V = - \frac{\dfrac{\partial C_L}{\partial \alpha}}{C_L \left(2 + \dfrac{\partial \ln C_L}{\partial \ln V} \right)} \cdot d\alpha$$

then finally,

C.1 $$\left. \frac{d \ln V}{d \alpha} \right|_E = - \frac{\dfrac{\partial C_L}{\partial \alpha}}{C_L \left(2 + \dfrac{\partial \ln C_L}{\partial \ln V} \right)}$$

where the subscript E indicates an equilibrium consideration with the assumptions implies above. This equation is neither a partial nor a total derivative from a mathematical point of view and caution must be exercised in handling it.

If the new state of motion is a steady one, which it must be, $dC_M = M - M_o = 0$. The moment coefficient depends on α , V, δ , and the angular velocity, $\frac{d\theta}{dt}$. Since, however, it is assumed that the flight path has no curvature at the new steady state, and, indeed, in actuality such would be the case, the angular velocity is zero. Thus the quantity, q, does not appear.

$$\Sigma F_z : \quad L - W \cos \gamma = 0$$

$$\Sigma M : \quad M = 0$$

$$\Sigma M_\delta : \quad M_\delta = 0 \, .$$

Having started from nearly horizontal flight the flight path will remain nearly horizontal for sufficiently small changes so that the component of the weight perpendicular to the path remains almost unchanged. From the second equation, that of equilibrium of forces perpendicular to the path of flight, then,

$$d(L - W \cos \gamma) = dL = 0, \text{ since, as before } \sin \gamma = \gamma = 0.$$

now,

$$dL = dC_L \rho \frac{V^2}{2} S + 2C_L \rho \frac{V^2}{2} S \frac{dV}{V} = 0$$

$$dC_L = \frac{\partial C_L}{\partial \alpha} d\alpha + \frac{\partial C_L}{\partial V} dV \frac{VC_L}{VC_L}$$

so that,

$$\left[\frac{\partial C_L}{\partial \alpha} d\alpha + C_L \left(\frac{\partial \ln C_L}{\partial \ln V} + 2\right) \frac{dV}{V}\right] \rho \frac{V^2}{2} S = C$$

or,

$$\frac{dV}{V} = d \ln V = - \frac{\dfrac{\partial C_L}{\partial \alpha}}{C_L\left(2 + \dfrac{\partial \ln C_L}{\partial \ln V}\right)} \cdot d\alpha$$

then finally,

C.1
$$\left.\frac{d \ln V}{d \alpha}\right|_E = - \frac{\dfrac{\partial C_L}{\partial \alpha}}{C_L\left(2 + \dfrac{\partial \ln C_L}{\partial \ln V}\right)}$$

where the subscript E indicates an equilibrium consideration with the assumptions implies above. This equation is neither a partial nor a total derivative from a mathematical point of view and caution must be exercised in handling it.

If the new state of motion is a steady one, which it must be, $dC_M = M - M_o = 0$. The moment coefficient depends on α, V, δ, and the angular velocity, $\frac{d\theta}{dt}$. Since, however, it is assumed that the flight path has no curvature at the new steady state, and, indeed, in actuality such would be the case, the angular velocity is zero. Thus the quantity, q, does not appear.

$$dC_M = \frac{\partial C_M}{\partial \alpha} d\alpha + \frac{\partial C_M}{\partial \delta} d\delta + \frac{\partial C_M}{\partial \ln V} d \ln V = 0$$

or

$$d\alpha \left(\frac{\partial C_M}{\partial \alpha} + \frac{\partial C_M}{\partial \ln V} \frac{d \ln V}{d\alpha}\right) = - \frac{\partial C_M}{\partial \delta} d\delta$$

thus,

$$\left.\frac{d\alpha}{d\delta}\right|_E = - \frac{\dfrac{\partial C_M}{\partial \delta}}{\dfrac{\partial C_M}{\partial \alpha} + \dfrac{\partial C_M}{\partial \ln V} \left.\dfrac{d \ln V}{d\alpha}\right|_E} = - \frac{\dfrac{\partial C_M}{\partial \delta}}{\left.\dfrac{dC_M}{d\alpha}\right|_E}$$

where,

C.2 $$\left.\frac{dC_M}{d\alpha}\right|_E = \frac{\partial C_M}{\partial \alpha} + \frac{\partial C_M}{\partial \ln V} \left.\frac{d \ln V}{d\alpha}\right|_E .$$

This then, is a new stability requirement that applies to that phase of the longitudinal motion described and implied from the previous discussion. This requirement certainly is sound. For an aircraft which does not have this quasi-static stability will be unstable in as much as for any disturbed state of motion, enforced by an elevator displacement, will show the tendency to move its elevator further in this direction, so increasing the deviation from its initial state.

The usual static stability criterion, $\frac{dC_M}{d\alpha}$, is considered either, $-\frac{dC_M}{dC_L} \frac{dC_L}{d\alpha}$ or, $-\frac{dC_L}{d\alpha}(x - x_N)$. The quantity, $\frac{dC_L}{d\alpha}$, in either of the above is a constant throughout the usual range of normal flight, i.e, unstalled flight. The value of $x - x_N$ can be found graphiclly from wind tunnel data of C_M vs. C_L as explained in reference 5. This is the more informative quantity since a shift in the center of gravity is more readily determined throughout the flight history.

The first term in equation C.2 is very similar to the static stability criterion above. However for comparison, equation C.2 is written in its entirety as,

where $x_N|_E$ is a new neutral point that takes into account variation of the neutral point with velocity, i.e., compressibility effects. First, it is noted that variation of lift coefficient with angle of attack differs between the two. This is due to the fact that the ordinary determination of the change of lift coefficient with angle of attack is accomplished in wind tunnel tests where the stream velocity is kept constant. The results are then based on a constant dynamic pressure, whereas the present development is not. The difference between the two is about 1-3o/o and is sumed negligible. The quantity $x_N|_E$ moves with respect to velocity, dynamic pressure, deflection of the fuselage, twist of the wings and horizontal stabilizer. A comparison with the movement of the usual static stability neutral point will be made only with respect to variation with velocity and dynamic pressure. Figure 5 shows the variation with velocity of three different aspects of stability at sea level. These are: (a) static stability only, (b) quasi-static stability assuming the zero lift moment coefficient, $C_{M_{L_o}}$, to be -0.02, and (c) quasi-static stability with zero lift coefficient assumed zero. Figure 6 shows the comparison of the same quantities at altitude. Here the decrease in the stability margin

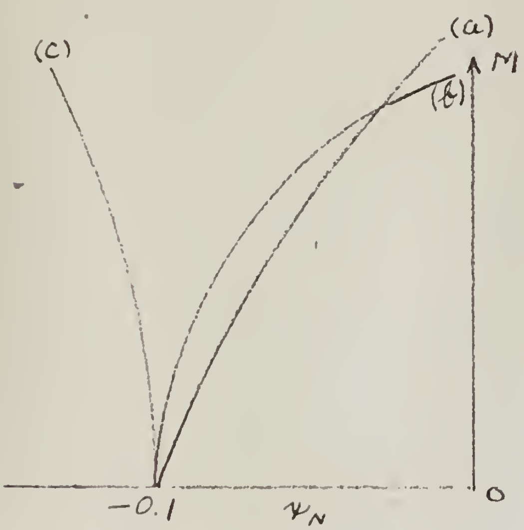

H = Sea Level

Figure 5

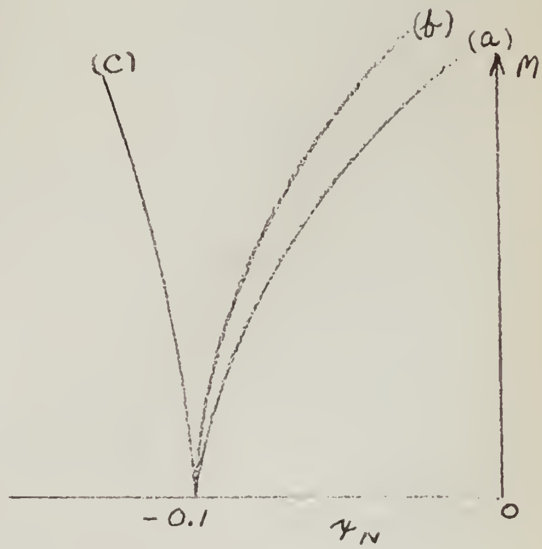

H = 40,000 ft.

Figure 6

the dynamic pressure in the denominator of the additional term, i.e., C_L in $\left.\frac{d \ln V}{d\alpha}\right|_E$.

2. Quasi-Static Stability at Constant Speed.

Recalling the discussion of the conditions holding following the imposing of a small elevator deflection on the steady state, it was seen that in the first small interval following the change the speed does not change appreciably. Thus the quasi-static stability at equilibrium concept does not hold for this phase of the disturbed motion. It was further seen that the equilibrium of forces perpendicular to the direction of flight is disturbed too. The equation of motion for this direction shows what happens.

If a force is exerted on a body moving in a certain direction, its path will be curved. See Figure 7. If an aircraft, the motion may become rather complicated, for, due to the curvature of the flight path in a vertical plane, the component force of the weight perpendicular to the path changes too. Restriction to small disturbances close to horizontal flight allows neglecting the changes in the weight component.

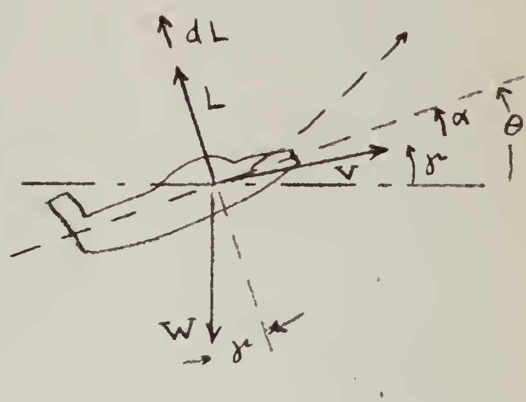

Figure 7.

For instance, a change in angle of flight path of 15° gives only 3 o/o change. The centripetal acceleration is $V \frac{d\gamma}{dt}$. The equation of motion is therefore,

$$\frac{W}{g} V \frac{d\theta}{dt} = d(L - W \cos \gamma) = dL$$

and

$$dL = \left[\frac{\partial C_L}{\partial \alpha} d\alpha + \frac{\partial C_L}{\partial (\frac{d\theta}{dt})} \frac{d\theta}{dt}\right] \rho \frac{V^2}{2} S$$

$$= \left(\frac{\partial C_L}{\partial \alpha} d\alpha + \frac{\partial C_L}{\partial q} dq\right) \rho \frac{V^2}{2} S \quad ,$$

and, multiplying by $\frac{S^{1/2}}{V}$ and noting that $\frac{1}{\mu} = \rho \frac{V^2 S^{3/2}}{2m}$, there is

$$\mu \, dq \left(1 - \frac{\frac{\partial C_L}{\delta q}}{\mu}\right) = \frac{\partial C_L}{\delta \alpha} \, d\alpha$$

or,

C.3 $$\left.\frac{dq}{d\alpha}\right|_V = \frac{\frac{\partial C_L}{\delta \alpha}}{1 - \frac{\frac{\partial C_L}{\delta q}}{\mu}} \cdot \frac{1}{\mu} \; .$$

The term, $\frac{\partial C_L/\partial q}{\mu}$, may be neglected since $\frac{\partial C_L}{\delta q}$ is small compared to $\frac{\partial C_L}{\delta \alpha}$ and, also, the usually large magnitude of μ makes it negligible compared to unity. This is also the common approximation as seen by the neglecting of X_q and Z_q in references 1, 3 and 4.

Thus there is the relation, $\left.\frac{dq}{d\alpha}\right|_V = \frac{\partial C_L}{\delta \alpha} \frac{1}{\mu}$, resulting from a consideration of the forces perpendicular to that of flight in the first instant following a disturbance.

This curvature of the flight path or angular velocity has an influence on the equilibrium of moment about the lateral axis. So a consideration of the equilibrium of moments along this curved flight path involves the change in elevator deflection, the change in angle of attack and this angular velocity. The effect of velocity is omitted because of the assumptions of this phase of the motion. There is then,

$$dC_M = \frac{\partial C_M}{\delta \alpha} d\alpha + \frac{\partial C_M}{\delta q} \left.\frac{dq}{d\alpha}\right|_V d\alpha + \frac{\partial C_M}{\delta \delta} d\delta = 0$$

or,

$$d\alpha = - \frac{\frac{\partial C_M}{\delta \delta}}{\frac{\partial C_M}{\delta \alpha} + \frac{\partial C_M}{\delta q} \left.\frac{dq}{d\alpha}\right|_V} \, d\delta \; .$$

This expression is similar to the one found for the equilibrium of a steady state of flight enforces by a certain elevator displacement. It contains the

$$d\alpha\,\Big|_V \qquad \partial\alpha \qquad \partial q \qquad d\alpha\,\Big|_V$$

called "quasi-static stability at constant speed". A comparison of this quantity with the usual static stability is seen following a further evaluation.

The angular velocity causes the angle of attack of the horizontal tail plain, α_h, to change by the amount,

$$d\,\alpha_h = \frac{\frac{d\theta}{dt}\, r_h}{V} \qquad \text{but,} \qquad \frac{d\theta}{dt} = dq\,\frac{V}{S^{1/2}}$$

therefore,

$$\frac{d\alpha_h}{dq} = \frac{r_h}{S^{1/2}} \quad .$$

This change in tail angle of attack gives rise to an increase in lift coefficient of the horizontal tail plane, C_{L_h}, and by it a decrease in moment about the lateral axis,

$$dC_M = -\,dC_{L_h}\,\frac{S_h\, r_h}{S^{3/2}}$$

and, having noted its dependence on angular velocity, there is,

$$\frac{dC_M}{dq} = -\,\frac{\partial C_{L_h}}{\partial \alpha_h}\,\frac{S_h\, r_h}{S^{3/2}}\,\frac{\partial \alpha_h}{dq} = -\,\frac{\partial C_{L_h}}{\partial \alpha_h}\, S_h \left(\frac{r_h}{S}\right)^2 \quad .$$

This quantity, C_{M_q}, may be determined by a dymanic wind tunnel test described in reference 1, or by use of the curved-flow technique referred to in reference 6.

The term, $\frac{\partial C_M}{\partial q}\,\frac{dq}{d\alpha}\Big|_V$, added to the static stability is always negative, since C_{M_q} is a damping derivative. Thus this is an increase in static stability and the neutral point corresponding to this quasi-static stability is behind the one for static stability by about, $\frac{K}{\mu}$, where, $K = C_M \;\; C_{L_\alpha}$.

This apparent improvement over wind tunnel static stability is seen to be larger for an aircraft of small wing loading at low altitude than for one of the high wing loading at high altitude.